Electrochemical Biosensors for On-line Monitoring of Cell Culture Metabolism

THÈSE N^{O} 5568 (2012)

PRÉSENTÉE LE 23 NOVEMBRE 2012

À LA FACULTÉ INFORMATIQUE ET COMMUNICATIONS

LABORATOIRE DES SYSTÈMES INTÉGRÉS (IC/STI)

PROGRAMME DOCTORAL EN MICROSYSTÈMES ET MICROÉLECTRONIQUE

ÉCOLE POLYTECHNIQUE FÉDÉRALE DE LAUSANNE

POUR L'OBTENTION DU GRADE DE DOCTEUR ÈS SCIENCES

PAR

Cristina BOERO

acceptée sur proposition du jury:

Prof. N. de Rooij, président du jury
Prof. G. De Micheli, Dr S. Carrara, directeurs de thèse
Dr T. Bachmann, rapporteur
Prof. M. Gijs, rapporteur
Prof. T. Sverre Lande, rapporteur

ÉCOLE POLYTECHNIQUE
FÉDÉRALE DE LAUSANNE

Suisse
2012

Abstract

Current research in the biotechnological field is hampered by the lack of available technologies dedicated to cell monitoring. While on the one hand physicochemical parameters, such as pH, temperature, cell density and adhesion, can be monitored quite easily with automated systems, on the other the variation of cell metabolism is still challenging. Indeed, the real-time detection of metabolites can noticeably extend the knowledge of the molecular biology for therapeutic purposes, as well as for the investigation of several types of diseases. Electrochemical biosensors are the ideal candidates for cell monitoring, since they can be integrated with the electronic portion of the system, leading to high-density arrays of biosensors with better performance in terms of signal-to-noise ratio, sensor response, and sample volumes.
The present research covers the design, the fabrication, the characterization, and the validation of a minimally-invasive system for the real-time monitoring of different metabolites in a cell culture. The electrochemical biosensor consists of an array of gold working electrodes accomplished by standard microfabrication processes. The deposition of carbon nanotubes and the selective modification with enzymes onto metallic electrodes is performed by adapting an ultra-low volume dispensing system for DNA and protein drop cast. The biological sensing element ensures high selectivity for the target molecule to detect, while nanomaterials confer superior performance (e.g. sensitivity) with respect to standard immobilization strategies. The *on-line* detection of glucose, lactate, and glutamate is achieved with an *ad hoc* fluidic system. The use of a microdialysis probe in direct contact with the cell culture avoids contamination problems and dilution steps for metabolite measurements. Carbon nanotube-based biosensors and the system for real-time measurements are validated on two cell lines under different experimental conditions. The electronic system for electrochemical measurements is also designed and realized with discrete components to be interfaced with the platform. The adopted architecture is able to optimally record the current ranges involved in the electrochemical cell, while the wireless communication between the electronic system and the remote station ensures minimally invasiveness and high portability of the device. Existing technologies and materials are used in an original manner to achieve the *on-line* monitoring of metabolites in stem cell-like cultures, paving the way for the development of miniaturized, high-sensitive, and inexpensive devices for continuous cell monitoring.

Keywords: amperometric biosensor, carbon nanotube, real-time monitoring, cell metabolism, oxidase, potentiostat.

Résumé

La recherche dans le domaine des biotechnologies est actuellement entravée par l'absence de technologies adaptées au suivi des cellules. Alors que les paramètres physico-chimiques, tels que le pH, la température, la densité et l'adhésion des cellules, peuvent être suivi relativement simplement par des systèmes automatiques, de l'autre la mesure de la variation du métabolisme cellulaire reste un challenge à surmonter. En effet, la détection en temps réel de métabolites permettrait d'étendre notablement les connaissances de la biologie moléculaire à des fins thérapeutiques, ou encore dans le recherche de nombreux types de maladies. Les biocapteurs électrochimiques apparaissent comme les candidats idéaux pour le suivi de cellules, comme ils peuvent être intégrées au sein même de la partie électronique du système, ce qui conduit à des matrices haute densité de biocapteurs avec de meilleures performances en termes de rapport signal sur bruit, de vitesse de réponse et de la quantité d'échantillons. Cette recherche couvre la conception, la fabrication, la caractérisation et la validation d'un système à invasitivé minimale pour le contrôle en temps réel de différents métabolites dans une culture cellulaire. Le biocapteur électrochimique consiste en une matrice d'électrodes fonctionnelles d'or réalisées avec des procédés de micro-fabrication standard. Elles peuvent être successivement activées pour détecter jusqu' à cinq métabolites différents, tout en partageant le même compteur et la même électrode de référence. Le dépôt des nanotubes de carbone et leurs modifications sélectives par des enzymes sur des électrodes métalliques sont réalisés par un système modifié de distribution à très faible volume pour ADN et protéine. L'élément de mesure biologique assure une grande sélectivité pour la molécule cible à détecter, tandis que les nanomatériaux confèrent une performance accrue (par exemple en sensibilité) par rapport aux stratégies standards d'immobilisation. La détection en ligne de glucose, lactate et glutamate est faite par un système fluidique *ad hoc*. L'utilisation de sondes de micro-dialyse en contact direct avec la culture de cellule évite les problèmes de contamination, ainsi que les étapes de dilution pour les mesures de métabolites. Les biocapteurs à base de nanotubes de carbone, ainsi que le système de mesure en temps réel ont été validés avec deux lignes de cellules sous différentes conditions expérimentales. Le système électronique pour la mesure électrochimique est aussi conçu et réalisé à partir de composants discrets afin d'être interfacé avec la plateforme. La structure adoptée permet d'enregistrer de façon optimale la gamme des courants impliqués dans la cellule électrochimique, tandis que la communication sans fil entre le système électronique et la station à distance assure une invasivité minimale et une grande portabilité du composant. Les technologies et matériaux existants sont utilisés d'une manière originale, afin d'aboutir à un suivi en ligne des métabolites dans les cultures de types

cellules souches, ouvrant ainsi la voie vers le développements de composants hyper-sensibles, miniatures et bon marchés pour le contrôle continu de cellules.

Keywords : biocapteur ampérométrique, nanotubes de carbone, détection en temps réel, métabolisme cellulaire, oxydase, potentiostat.

Acknowledgements

When I joined EPFL for my Master project, and later for my PhD, I was attracted by a such world-class institute with a large spectrum of proposal in advanced research. However, passions and devotion alone cannot successfully drive towards a PhD degree. I can certainly affirm that the help and support of many different people and the stimulating atmosphere at EPFL definitely helped me to achieve this result.

My deepest gratitude goes to Prof. Giovanni De Micheli and Dr. Sandro Carrara. I have learnt a lot in these four years thanks to their constant and encouraging supervision. It has been an honor having the opportunity to work with such great scientists of world renown. However, they have not been just supervisors, but also two excellent persons able to create a friendly and very pleasant environment for both work and leisure time. Celebrating every success, planning hikes on the mountains, arranging ski tours are just few things that make the LSI a precious and unique environment for working.

Two excellent supervisors are crucial to do a good job. However, this research would not exist without founds. I would like to thank Prof. Laura Calzá and Prof. Christine Nardini to have been helpful partners in this project and offered me their knowledge and help. Financial supports were from the SiNo-Swiss Science and Technology Cooperation Program, with the project No. IZLCZ2123967, and from the NanoTera Project I-needle, evaluated by Swiss National Science Foundation.

The practical realization of the device was the result of the help from many people. Dr. Francesco Valgimigli and Dr. Fausto Lucarelli from Menarini Diagnostics helped me to get familiar with glucose biosensors and continuous monitoring. Giuseppe D. Albini have contributed to develop the model of electron emissions from carbon nanotubes and Monte Carlo simulations. SEM images were acquired with the aid of Dr. Marco Cantoni and the CIME staff. In particular, I would like to thank Ms. Fabienne Bobard for the innumerable hours spent to acquire the best images of carbon nanotubes and proteins, despite the complexity of the system. Microfabrication of the platform would not be possible without the expertise of all CMI staff. In particular, I would really like to thank Jean-Baptiste to have answered me to all kind of questions and doubts I have had during the different processes. I also wish to acknowledge Prof. Martin Gijs and Dr. Qasem Alramadan to have introduced me to microfluidics, for their precious suggestions, and for the time spent in their lab to practise with microchannels and

oxygen plasma. Measurements related to SN56 cell line were possible thanks to the precious help of Dr. Giovanna Del Vecchio. Together with Prof. Calzá, she conceived and performed all experiments related to SN56 cells. Thanks Giovanna for your patience in teaching me how to handle cells and for your friendship. Experiments with NG-108 cells would not have been possible without the aid of Prof. Horst Vogel, Dr. Joachin Piguet, and Mr. Luc Veya. Many thanks for the useful discussions and for the help to plan the experiments reported in the present work. Many thanks also to Dr. Solomzi Makohliso for his suggestions.

I should express my gratitude to Mrs. Marie Halm. She takes care of every single PhD student of Microsystems and Microelectronics Doctoral School, making us feeling as special members of a close group.

Unfortunately, four years at LSI have been passed too fast. Since I arrived there, I have had the feeling to belong to a big family. I wish to thank all of you guys for all the experiences, the numerous trips we did together, and the great time I have had there. I should express my gratitude to Christina, not only because she can really make our life easier whit bureaucracy and organization issues, but also for the friendship she offered me and the amazing hikes and ski-tours we did together, motivating each other till the top. Many thanks to Anil and Rodolphe for helping me whenever I needed. I wish to thank many other people from the lab: Jaume, Kyungsu, Alena, Giulia, Hassan, Elleni, Julien, Gözen, Francesca, Somayyeh, Davide, Wenqi, Hu, Dimitris for all lunches and coffee breaks we have done together; Sara, for the useful discussions on potentiostat architectures and electronic configurations; Fede and Michele, because arguing with them is priceless; Pierre-Emmanuel, for his help in this work; Ciprian, for all the hikes we did and for those we did not manage to accomplish; Vasilis, because he showed me how to behave when you are a serious Post-Doc; Shashi, for the astonishing entertainment he can offer at any time; Srini, because we did an amazing trip to India thanks to his wedding; my officemates Camilla and Irene, because they finally brought few womanliness in this lab; Andrea, that have had to stand all my moods during these four years; Antonio, because he is unique and we have had lots of fun thanks to him. A special thanks goes to Jack, for his unconditioned help in this work and in my life.

I found many friends at LSI, but also at EPFL, and more in general in Lausanne. I wish to thank Matteo and Ivan, because crazy things cannot be done alone; Anna, because sometimes you need someone that stops you when you are doing crazy things; Massimo, for all the breaks in Coupole; Marzia, for her help in biotechnological issues, but also for many invitations for partying; Mattia and Luigi, for all the parties where I was invited (by Marzia); Matteo, for our jogging time, and the dinners to recover from jogging; Seb, because he taught me the few French words I know and for the great time we had together; Luca, because it was a pleasure to share the apartment and a piece of my life with you; Livio and Marco, because it is still a pleasure to share my life (and some beers on the balcony!) with you. A special thanks goes to Ludo, for her unconditioned support, for all the good and bad things we shared together during these five years, and for her precious friendship.

I should express my gratitude to all friends I still have in Italy, who also supported me even if I was living abroad. Many thanks to Matteo and Gian, because although we meet every three-four months, we always re-start from where we left; to Fiammetta and Umberto, and their beautiful daughter Ariele, for all the dinners they offered me when I was back in Torino; my "godfather" Roberto with his wife and Gianluca, because they have kept me updated on all the events in the archery world, and the Arcieri Iuvenilia, because they have not forgotten me.

Finally, I wish to express my deep gratitude to my parents. I could start this adventure thanks to them. They have been always interested in my job, encouraging me whenever I met a problem, rejoicing at every success, and supporting me in every decision I took. Thanks mom and dad for your unconditioned love.

List of Abbreviations

BHF	Buffered Hydrofluoric acid
BSA	Bovine Serum Albumine
CE	Counter Electrode
CMOS	Complementary metal-oxyde-semiconductor
CNTs	Carbon Nanotubes
CVD	Chemical Vapor Deposition
DMEM	Dulbecco's Modified Eagle's Medium
DOS	Density of State
ELISA	Enzyme-Linked ImmunoSorbent Assay
ET	Electron Transfer
FAD	Flavin Adenine Dinucleotide
FIA	Flow-Injection Analysis
FMN	Flavin Mononucleotide
GC-MS	Gas Chromatography - Mass Spectrometry
GlOD	Glutamate Oxidase
GOD	Glucose Oxidase
H_2O_2	Hydrogen Peroxide
HPLC	High-Performance Liquid Chromatography
ICs	Integrated Circuits
ISFET	Ion-Sensitive Field-Effect Transistor
LDH	Lactate Dehydrogenase
LOD	Lactate Oxidase
LOR	Lift-Off Resist
LSB	Least Significant Bit
MEMS	Microelectromechanical System
MOSFET	Metal-Oxyde-Semiconductor Field-Effect Transistor
MWCNT	Multi-walled Carbon Nanotubes
NAD^+	Nicotinamide Adenine Dinucleotide
NPs	Nanoparticles
NWs	Nanowires
PCB	Printed Circuit Board
PDMS	Polydimethylsiloxane

PMMA	Polymethylmethacrylate
pO_2	oxygen partial pressure
PVD	Physical Vapor Deposition
RE	Reference Electrode
SAM	Self-Assembled Monolayer
SEM	Scanning Electron Microscopy
SHE	Standard Hydrogen Electrode
SiO_2	Silicon Oxyde
SPEs	Screen-printed Electrodes
SWCNT	Single-walled Carbon Nanotubes
WE	Working Electrode

Contents

1 Introduction

Cell analysis demands novel methods dedicated to the monitoring of metabolites involved in cell growth. Cell cultures can be used for many applications and a deep knowledge of their behavior is fundamental to optimize cultivation conditions. In particular, the variation of cell metabolism can reveal from one side the status of the cell culture, and from the other unknown mechanisms implied in cell growth and development, according to the type of monitored cells. Cells can be cultivated for several purposes, such as understanding and modeling some biological mechanisms, the development of new drugs and therapies, or in the field of regenerative medicine. All the aforementioned applications require a thorough knowledge of the biological system under study and advancements in technology can considerably help scientists to accomplish the objective.

1.1 Motivation

Current research is hampered by the lack of available technologies dedicated to cell monitoring. Pharmaceutical research, therapies development, diagnostics, regenerative medicine are some of the fields demanding smart, high-sensitive, and non-invasive platforms for cell monitoring. The development of a suitable device to accomplish the *on-line* detection of cell culture is the objective of the present work.
In the pharmaceutical field, antibiotics, vaccines, and therapeutic proteins are increasingly produced by microorganisms, such as bacteria, yeasts, and animal cell lines. In addition, drug efficiency is typically tested *in vitro*, prior to run clinical trials *in vivo*. The knowledge of the complex cascade of reactions involved in cell mechanisms can help to infer the potential efficacy of drugs, at least *in vitro*. These microorganisms require certain cultivation conditions and media composition differs from cell line to cell line, to ensure an optimal growth and yield rate. Pharmaceutical research demands also the development of recombinant organisms, so there is a need of specific strategies to model their metabolic pathways to address their genetic modification.
Within the diagnostic field, advancement in technology can noticeably extend the knowledge of the molecular biology for several types of diseases. As an example, mutations and altered

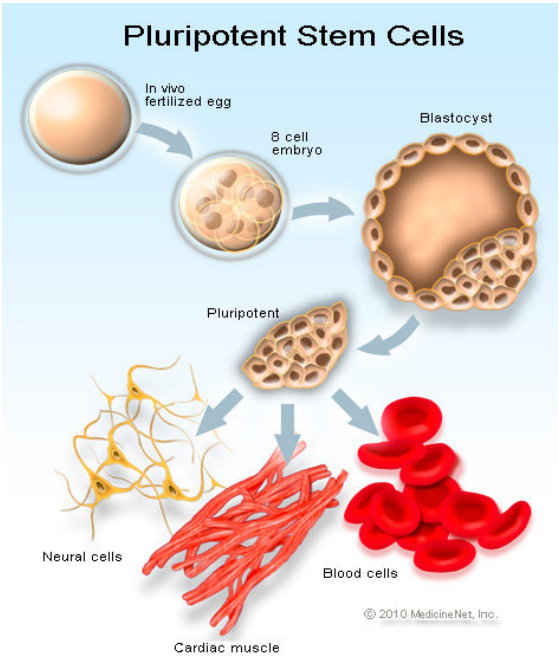

Figure 1.1: Pluripotent stem cell cycle. The embryonic stem cells can differentiate in several tissues. Reprinted from *www.medicinenet.com*.

gene expressions have all been detected in prostate cancer samples. However, it is also necessary to fully understand all the contributing factors and molecular mechanisms that are associated with this disease. Selak *et al.* [1], for example, showed that downregulation of the Krebs cycle enzyme, succinate dehydrogenase, led to the accumulation of succinate, which indirectly induces the expression of genes involved in tumor progression. Moreover, considerable evidences suggest that oxidative stress contributes to the aetiology and/or pathogenesis of prostate cancer, such as inflammatory processes [2]. Cells involved in inflammation produce and secrete oxidants, so biosensors can really help to monitor and quantify oxidants levels, such as hydrogen peroxide, and help in building an accurate model for prostate cancer, for example. As another example, modeling cholinergic neurons may help to better understand Alzheimer's disease, since their early loss is associated with a metabolic impairment in brain, whose extent is proportional to the severity of the cognitive deficits [3]. Pellerin *et al.* [4] developed the so-called astrocyte-neuron shuttle model in 1994, where they claim a net production of glutamate-derived lactate by astrocytes. Although glucose is traditionally considered as the preferential source of energy for neurons, they assumed that lactate might be transported within the different brain cell types (e.g. neurons and astrocytes), and consumed instead of glucose during neuronal activation. However, since the time of their hypothesis, no definitive data are available to support this theory, making this field of research very debated. To this purpose, the use of sensor arrays for sensing levels of such metabolites can definitely contribute to elucidate this point. Experiments to validate this hypothesis can involve simplified biological systems, e.g. neuronal cultures in dynamic metabolic conditions. Some measurements of

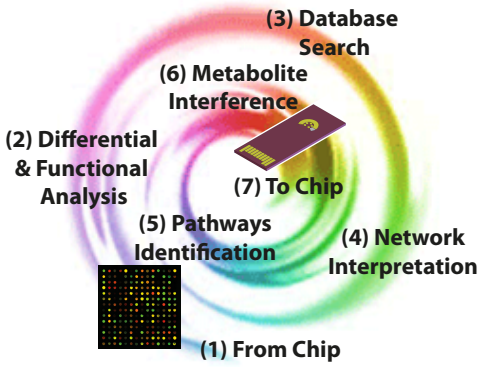

Figure 1.2: Schematic of an ideal path of biochip evolution, showing increasing precision and decreasing throughput. (1) Standard elaboration of high-throughput biochip; (2) Functional analysis of the obtained results; (3) Database search and comparison with obtained data; (4)-(5) Network interpretation and pathway identification; (6) Inference of metabolites involved in cell processes; (7) Real-time monitor by using the low-throughput biochip. Reprinted from [5].

metabolite levels in a neuronal line sensitive to stressors and metabolic alterations is reported in Chapter 5 and some of the results support the astrocyte-neuron shuttle model.

Cells can be also developed as therapeutic means, e.g. stem cells, dendritic cells, artificial tissues or organs based on the cultivation of hepatocytes for liver transplantation, keratinocytes for skin regeneration, etc. Newly/partially differentiated cells can be introduced *in vivo* and regenerate or repair part of organs, while *in vitro* they can generate entirely new tissues. Embryonic stem cells, also called pluripotent stem cells, are crucial to achieve these purposes, despite the difficulties arising from ethical concerns regarding embryos. Indeed, pluripotency is defined as the ability of differentiating into all types of tissues, as depicted in Fig. 1.1. Stem cells are extremely complex systems and an incredible number of variables is involved in cell fate. Therefore, it is of the utmost importance to offer technologies instrumental to the deciphering of such complexity. In particular, identifying the main processes involved in the differentiation and monitoring their evolution in real time constitute a crucial advancement in this area, since one pre-requisite for cell implant is the proper and precise knowledge of their state. The quest of such information can take the spirally formed shape of a path like the one illustrated in Fig. 1.2. The systemic view that microarrays offer can be used as a pre-condition to identify the main molecular variables involved in stem cell differentiation. The derived information is then processed with bioinformatics techniques (differential and network analysis) to identify the genes that show statistically significant variations in their expression, when comparing different states of the cells. Afterwards, the set of differentially expressed genes can be elaborated via integration with a variety of biological databases to generate a network of interactions from the list of genes. Finally, manual curation identifies the pathways that are more relevant, and from there infers the metabolites produced and the likely markers to be monitored: these metabolites, indeed, can ultimately serve as sensing variable in a low-throughput biochip [5].

In all aforementioned domains a correct and reliable analysis of the cell culture requires a ro-

bust experimental setup and measurements of the process. The so-called "low-level controls" based on temperature, pressure, pH, and pO_2 (oxygen partial pressure) are still the predominant strategies in routine production processes. Indeed, determination of nutrients, metabolic products, and secreted recombinant proteins is restricted to *off-line* analysis. More complex systems for handling sample purity and analysis time are required and only the integration of several building blocks obtained with various technologies can satisfy these demands.
This thesis presents a novel approach for the development of miniaturized electrochemical biosensors for the *on-line* monitoring of metabolites in stem cell-like cultures. The following chapters will describe the blocks composing the system. Some of the approaches used to develop particular blocks are well-established strategies used in an innovative way, to achieve the high-sensitivity detection of multiple metabolites in cell culture media.

1.2 Metabolic Monitoring in Cell Cultures: State-of-the-Art

Monitoring systems for the determination of glucose, and to a minor degree for lactate, glutamine, and methanol, are available on the market. Most of them are expensive and labor-intensive analytical methods, like *high-performance liquid chromatography* (HPLC) and *gas chromatography-mass spectrometry* (GC-MS). HPLC is a chromatographic technique used to identify, quantify and purify the individual components of a mixture, e.g. the sample. The sample is dissolved in a fluid (mobile phase), which carries it through a structure, typically porous silica or polymer particles (stationary phase). The sample moves through the two phases at different velocities, according to chemical affinity between the sample and the phases. The separation is based on differential partitioning between the mobile and the stationary phase. Then, the mixture typically flows through an optical detector. Retention time varies depending on the analyte. Stoll *et al.* [6] have presented, for example, an HPLC method for the simultaneous detection of glucose, lactate, glutamine, glutamate, pyrrolidone, carboxylic acid, and alanine in a mammalian cell culture. GC-MS working principles are quite similar to those of HPLC: the sample is again forced to pass through a column where there is a gas. The interaction between the sample and the gas gives different time retention, so a mass spectrometry can be performed at the outlet of the column to capture all the molecules separately. However, HPLC and GC-MS systems are quite bulky and expensive, they require the injection of the sample directly in the columns, and they are not suitable for *on-line* monitoring. Despite all reasons that restrict their application in cell monitoring, these two techniques are often used as reference to demonstrate the effectiveness of other methods.
Optical sensors are another common method for bioprocess monitoring, since they do not require much maintenance, they operate in a non-invasive way and they do not need sampling, as they can be placed outside from the bioreactor. Among the optical techniques, *near-infrared spectroscopy* (NIRS) and *mid-infrared spectroscopy* (MIRS) were successfully applied for the *in situ* analysis of glucose, lactate, glutamine, and ammonium in mammalian cell culture [7] [8]. However, these instruments suffer from the same drawbacks of liquid chromatography, even if they allow the *on-line* monitoring.

Electrochemical biosensors are the ideal candidates for the miniaturized and inexpensive monitoring of cell cultures. They have the ability to sense compounds in a selective manner by exploiting the intrinsic features of the biological recognition element. The most challenging issue in the development of biosensors is certainly the enzyme immobilization. Different immobilization strategies have been tested, especially for glucose sensors, and they will be discussed more in details in Chapter 5. In particular, electrochemical biosensors lend themselves to be integrated in miniaturized systems and that is why they have had such great success. The enzyme can be integrated, for example, in a *Flow-Injection Analysis* (FIA) system. By placing the sensor externally with respect to the cell culture, the enzyme can be stored at its optimal pH, without affecting the bioprocessor. FIA and electrochemical biosensors have been successfully coupled for determining glutamine in insect and murine hybridoma cell cultures by Male *et al.* [9], for example. The system was developed by using an anion exchange resin to remove the endogenous glutamate, which could interfere with glutamine measurement, and so performing glutamine detection in a single step. Renneberg *et al.* [10] also reported the use of a FIA device for the monitoring of glucose, lactate, and glutamine of mammalian cells over 10 days of cultivation. However, measurements performed by FIA systems require sample withdrawal, which can be feasible when dealing with high-volume bioreactors, but can be troublesome when working with smaller cell flasks. Coupling FIA systems with microdialysis probes can reduce sampling quantity, minimally affecting the volume of the process. Moreover, the sampling is based on passive diffusion, so the risk of membrane clogging and fouling is also minimized [11].

On-line metabolic monitoring can also be achieved by using microphysiometers, which consist of a microvolume flow chamber in which living cells are held, while a flow of culture medium provides nutrients and flushes away waste products. Instead of developing biosensors and fluidics aside from the Petri dish, integrating all the system afterwards, this approach foresees to build the chamber for cells and the other blocks in one step. Commercial microphysiometers are mostly dedicated to measure extracellular acidification rates and cell adhesion. The recent progresses in microfluidics and the adaptation of microfabrication techniques to biological applications have also permitted to conceive miniaturized single devices for the simultaneous monitoring of different metabolites in cells. Most of those devices are developed on silicon or glass substrates and they host the electrochemical biosensors next to the flow chamber, to measure the different metabolites downstream. The well for cell growth and the fluidics are typically made of polymer. Two examples of possible microphysiometer realizations are shown in Fig. 1.3 (a) and (b). The device depicted in Fig. 1.3 (a) is equipped with O_2 and pH sensors, concerning physicochemical parameters, and with glucose and lactate biosensors, concerning the metabolic monitoring. Also the device of Rodrigues *et al.* (Fig. 1.3 (b)) is fabricated on glass substrate and hosts an oxygen sensor and a glucose biosensor. Both the configurations work under flow conditions and do not integrate the electronics to perform electrochemical measurements.

On-line monitoring allows us to have a real-time statement of cell status. However, *off-line* sampling can also be successfully applied, even if it cannot give a continuous insight on the cell culture. For this purpose, Nayak *et al.* [14] proposed to monitor glucose consumption

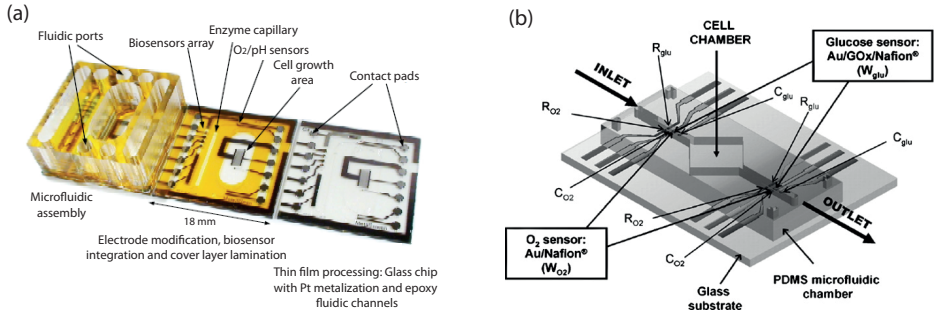

(a) The glass substrate hosts the electrochemical biosensors next to the flow chamber where cells live. Reprinted from [12].

(b) Polymeric chamber on glass substrate with oxygen sensor and glucose biosensor. Reprinted from [13].

Figure 1.3: Two example of microphysiometers for the detection of metabolites in cell cultures.

of hybridoma cells by using two different types of blood glucose self-monitoring devices designed for diabetes control. The *off-line* monitoring requires just the commercial glucometer, avoiding contamination issues thanks to the use of disposable electrodes. Glucometers need a mathematical correction factor obtained from calibration lines prior to be used in cell culture medium. Another successful approach to perform *off-line* measurements was proposed by Frey *et al.* by developing a disposable cartridge for the monitoring of glucose and lactate sampled by the cell culture [15].
Approaches without the use of the fluidic for the on-line monitoring have been also proposed. In these cases, the biosensor is integrated in the flask and immersed in the culture medium [16]. The commercial system CITSens Bio sensor (C-CIT, Switzerland) uses disposable electrodes for the detection of glucose, lactate, and glutamate (see Fig. 1.4). However, the system is bulky and does not allow the simultaneous measurements of the three metabolites in the same flask, since every electrode encapsulated on the cover can sense just one metabolite per time. Moreover, the disposable electrodes are screen-printed. Thus, any integrated solution is not possible with that approach.

1.3 Electrochemical monitoring of cell cultures

Electrochemical enzyme-based biosensors have been largely used, because among all their advantages, they show high versatility. Indeed, the immobilization strategy used for one type of protein can be also employed for several other enzymes. Electrodes have been structured with diverse strategies, using polymeric matrices [17], sol-gel [18], cross-linker [19], and mediators [20]. Also the choice of the electrode material is important. Most of the oxidase-based biosensors detect *hydrogen peroxide* (H_2O_2), whose concentration is proportional to the analyte sensed by the recognition element. The detection of H_2O_2 can be electrochemically performed on pure metal, such as gold or platinum, on metal alloys, or on carbon-based electrodes. Some authors claimed that the oxidation of hydrogen peroxide has to be performed on oxidized metals to obtain reproducible results [21]. Moreover, H_2O_2 is aggressive with metal surfaces, so

(a) Picture of the CITSens biosensor connected to the radio transmitter.

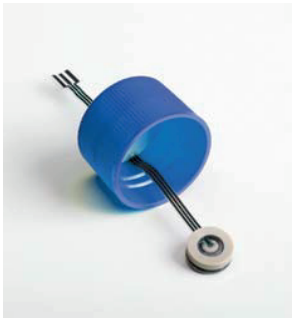

(b) Magnified image of the screen-printed electrode for *in situ* measurements.

Figure 1.4: CITSens Biosensor system for the on-line monitoring of metabolites. Reprinted from *www.c-cit.ch*.

carbon offers a valid alternative as electrode material. Carbon-based electrochemical sensors are commonly fabricated by the screen-printing of carbon inks, which is a suitable approach for mass production of disposable electrodes. Unfortunately, carbon screen-printing is not a microelectronic compatible technology, thus requiring separate processes and instrumentation with respect to the VLSI design. Consequently, it is not pursuable when developing integrated systems.

Recently, nanomaterials have been considered as alternative substrates to wire the enzyme and the electrode surface, enhancing the electron transfer and the sensitivity of the sensors. Among the different carbon materials, metallic *carbon nanotubes* (CNTs) have revealed great electrical [22] and electrochemical [23] properties, suitable to be applied on biosensors. Carbon nanotubes are an excellent material to immobilize biological recognition elements, since proteins easily adsorb on top of CNT sidewalls. Moreover, they can mediate electron transfer reactions with electroactive species in solution when used as the electrode material [24]. Purified carbon nanotubes have the appearance of a powder, which can be then dissolved in a solvent, depending on the application. However, CNTs are insoluble in almost all solvents and the challenge of solubilization has to be achieved by impairing their physical properties. Wang *et al.* [25] have shown that Nafion is an optimum solubilizing agent for CNTs when developing biosensors. Nafion is a perfluorinated sulfonated cation exchanger polymer with polar side chains, so carbon nanotubes dissolve homogenously in solution of Nafion in phosphate buffer or alcohol. Nafion/CNT solution does not impair the electrocatalytic properties of CNTs and facilitates their handling even in ultra-low volume, providing a valuable strategy for preparing CNT-modified amperometric biosensors. Therefore, it is possible to envisage a successive modification of the electrode surface by immobilizing carbon nanotubes and proteins on their surface, thanks to the liquid nature of both the solution. Miniaturization and integration of the biosensors, instead, can be achieved by microelectronic compatible technologies: the electronics to perform electrochemical measurements can be designed such as it is possible to develop an *integrated circuit* (IC), while electrodes and pads can be fabricated in the same step.

The combination of carbon nanotubes and biosensors has been widely presented. However, the development of amperometric biosensors based on carbon nanotubes for the particular purpose of bioprocess monitoring have never been exploited yet.

1.4 Research contribution

This research work covers the design, the fabrication, the characterization, and the validation of a self-contained and minimally invasive system to monitor different metabolites over the duration of a cell culture. The *on-line* detection is based on electrochemical measurements performed by amperometric biosensors modified with carbon nanotubes. The present study extends significantly the state-of-the-art of electrochemical biosensors for cell culture monitoring [26], [27]. The main contributions concern the following aspects:

- A novel approach to *on-line* monitoring of cell cultures, based on the development of self-contained platforms for the detection of multiple compounds. The results are related to the detection of glucose, lactate and glutamate. Thanks to the particular affinity between oxidases and carbon nanotubes, the system can be also further optimized for the detection of other compounds in a future work.
- Carbon nanotubes ensure a robust immobilization of the enzymes onto gold electrodes from one side, and high electron transfer between the protein and the electrode surface, thanks to their exceptional electrocatalytic properties. They have been extensively used for the development of electrochemical biosensors [28], [29]. This thesis presents for the first time CNTs that are used to structure electrochemical biosensors for the purpose of bioprocess monitoring.
- Electrode structuring with nanomaterials often requires complicated and expensive technologies. In the present research we show that it is possible to adapt technologies like ultra-low volume spotting, developed for DNA and protein drop cast, for the deposition of carbon nanotubes and enzymes onto metallic electrodes. It is the first time that non-contact piezo-electric spotting is reported as a suitable strategy for structuring amperometric biosensors.

1.5 Assumption and limitations

The self-contained system is successful in the *on-line* monitoring of cell cultures. However, some current limitations may be overcome by further research work. First the biosensors are optimized for the detection of glucose, lactate, and glutamate. As discussed later in Chapter 2, there are several other compounds that can be interesting to monitor, such as metabolites, nutrients and biomarkers. While the detection of some of these compounds is straightforward, since they can be detected by means of oxidases, some others may require new techniques. A second important limitation is the minimum size of the flask. Although microdialysis probes

are not invasive and do not require media sampling, the depletion of glucose, for example, during the continuous measurement can affect the cell culture. This is not a concern when measuring 25 ml or bigger flask, but it can influence the cell culture when media volumes are small. The typical 96-well plates, for example, cannot be measured by using this technique. Finally, since the oxidase family is characterized by the production of hydrogen peroxide, it is not possible to perform simultaneous measurements of different compounds without cross-talk among the electrodes. The detection has to be carried out with one working electrode at a time, while media flow ensures fresh solution at the electrode interface. It is also true that metabolite and nutrient concentrations in cell media do not change very quickly, so it is possible to acquire measurements every 5-10 minutes, without any information loss.

1.6 Organization of the Thesis

Following the Introduction, this thesis is organized as follows:

Chapter 2 gives an overview on biosensing strategies that have been developed in the last two decades, and in particular for bioprocess monitoring. Biosensors are classified according to the main building blocks and the sampling strategy. Nanomaterials used in biosensing are introduced, by elucidating the excellent properties that can convey to biosensors. Some examples of electrochemical biosensors based on nanomaterials are also reported for the purpose of metabolite monitoring.

Chapter 3 is focused on carbon nanotubes, which show really promising features suitable for biosensing applications. Their properties are discussed in general and the different strategies employed to develop amperometric biosensors by using carbon nanotubes are presented. Some results from simulations on CNT emission are reported, so that it is possible to define the best strategy for their immobilization. Finally, the mechanisms involved when proteins are immobilized on electrochemical biosensors are also discussed.

Chapter 4 describes the development of the self-contained platform. The system consists of three main building blocks, which are developed separately and integrated afterwards. The platform for the multiple detection of metabolites is accomplished by standard microfabrication processes. The selective modification of the electrode surface is performed by ultra-low volume dispensing. Finally, the sampling system is realized by rapid prototyping.

Chapter 5 shows the detection of three different metabolites by using the developed carbon nanotube-based biosensors. Preliminary experiments with commercial graphite electrodes are dedicated to optimize the enzyme immobilization and measure *off-line* some metabolites, like glucose and lactate, in a cell culture of cholinergic neurons in different experimental conditions. Afterwards, graphite electrodes are replaced with the microfabricated platform

and glucose, lactate, and glutamate detection are performed. The system is finally validated for the *on-line* monitoring of neuroblastoma cells during three days of cultivation.

Chapter 6 is focused on the design and realization of the device to perform electrochemical measurements with discrete components. System requirements are analyzed in detail for the particular application and the architectural solution is presented. The device is then interfaced with the microfabricated platform and tested for the detection of hydrogen peroxide.

Chapter 7 summarizes the contributions of this research for cell analysis and gives an outlook on the future of carbon nanotube-based biosensors for the metabolic monitoring of cell cultures.

2 Biosensing Strategies and Nanobiosensors

Detection of biological analytes is important in several domains, including medical diagnostics, genetic screening, discovery of unknown biological mechanisms, food and environmental monitoring. Biosensors integrate a biological recognition element to selectively detect and quantify the analyte of interest, using a transducer that can translate the detection in a measurable signal. Biosensor development necessarily requires the contribution from many discipline to be successful, including surface chemistry, electronics, mathematical modeling and analysis.

Most of the existing biosensors consist of a combination of different parts, such as the fluidic system, the detector, and the electronic circuit. Due to the heterogeneity of such technologies, the integration of the different blocks plays a fundamental role. There are many examples of integrated biosensors with different detection strategies that have been published in literature or even commercialized. Several works deal with integrated chips for label-free DNA detection by using capacitance measurements [30], or by means of redox couples [31]. Integration is also the key-point to develop implantable biosensors for long-term monitoring of different compounds [32], [33], [34], [35]. In the medical practise, existing FDA-approved sensors are not fully integrated. A notable example is the GlucoMen®Day, which can provide real-time measurements of subcutaneous glucose for up to 100 hours [36].

Electrochemical biosensors are a subgroup of the more general category of biosensors. According to IUPAC definition, "*An electrochemical biosensor is a self-contained integrated device, which is capable of providing specific quantitative or semi-quantitative analytical information using a biological recognition element (biochemical receptor) which is retained in direct spatial contact with an electrochemical transduction element.*" [37].

In the following chapter, strategies for the detection of biological analytes will be extensively discussed, with a particular focus on metabolic monitoring of stem cell cultures. Section 2.1 will propose an essential classification regarding biosensors based on the targets involved in cell proliferation and cell differentiation. Different sampling methods will be debated in Section 2.2, according to the way of cell cultivation. Section 2.3 will analyze nanotechnology-based sensors, focusing on peculiar properties of nanomaterials when applied in biosensing. Finally, Section 2.4 will present an overview on electrochemical biosensors, discussing the

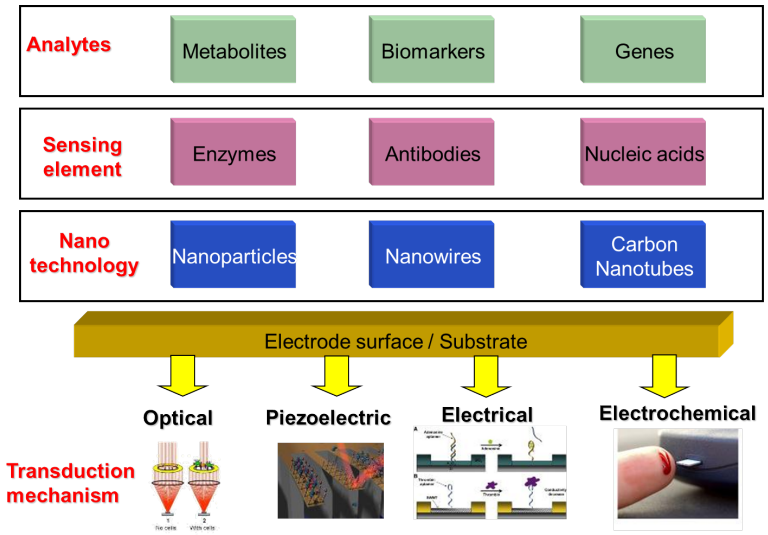

Figure 2.1: Resume of the main features characterizing biosensors for the monitoring of several analytes interesting in cell culture monitoring.

main electrochemical techniques used for detection and some examples will be reported.

2.1 Classification

Biosensors are a subgroup belonging to the wide family of chemical sensors. Biosensors may be classified in different ways. IUPAC recommends their classification according to the biological recognition mechanism or the transduction principle [37]. Hereunder, it is reported an essential classification of biosensors for cell culture monitoring that have been proposed in literature during the last decade. Fig. 2.1 resumes the following classification.

2.1.1 Analytes

When talking about analytes in cell culture, we generally refer to those compounds involved in cell proliferation, differentiation, and death. The optimization of nutrients, the monitoring of indicators of metabolic stress, the control of gene expression can lead to the optimal conditions for cell cultivation. **Nutrients** and **metabolites** are by far the most important parameters to keep under control. Limiting glucose levels, which is the most important carbon source for cells, leads to a more efficient metabolism and less accumulation of lactate, for example. Numerous off-line glucose biosensors have been developed, and some of them have been also commercialized, like the Yellow Springs electrochemical analyzer (Ohio, USA) in Fig. 2.2. Nayak *et al.* evaluated a blood glucose self-monitoring device for the purpose of monitoring glucose concentration in tissue culture media [14]. Real-time monitoring have been also proposed in FIA systems [10], in microflow systems [13], [38], and in quiescent conditions (CITSens Bio, Switzerland). Glutamine is another important energy and nitrogen source.

Figure 2.2: YSI 2300 STAT Plus - Yellow Springs Instruments for glucose and lactate monitoring in cell culture. Reprinted from *www.ysilifesciences.com*.

However, the catabolism of glutamine produces ammonia, which becomes toxic to the culture in high concentration, inhibiting its growth and glycolysation. Glutamine levels can be directly detected by ammonium ion-selective electrodes, according to the following reactions:

$$\text{L-glutamine} \xrightarrow{\text{glutaminase}} \text{L-glutamate} + NH_4^+.$$

Another approach for the indirect sensing of glutamine is the measurement of glutamate by using *glutamate oxidase* (GlOD):

$$\text{L-glutamate} + O_2 \xrightarrow{\text{GlOD}} \alpha\text{-ketoglutarate} + NH_4^+ + H_2O_2,$$

by measuring the H_2O_2 production [27] or the O_2 depletion [39]. Lactate is another common product of anaerobic metabolism and it is toxic for cells, as in the case of ammonia. Off-line detection of lactate is normally carried out by HPLC or enzymatic colorimetric methods. Electrochemical biosensors based on lactate oxidase can also be used and H_2O_2 production can be monitored. The functionalization of amperometric biosensors with oxidases specific for different compounds makes possible to develop platforms for multiple detection by using the same detection principles [40].
The pluripotential properties of stem cells can be evaluated by the expression of **biomarkers**. The two main features of pluripotent stem cells are the ability to unlimitedly proliferate, maintaining an undifferentiated state, whereas retaining the capability to differentiate into all cell type under chemical or mechanical stimuli. Embryonic stem cells, for example, can express biomarkers such as POU transcription factor octamer-4 (Oct-4), placental alkalin phosphatase (AP), several Stage-Specific Embryonic Antigene (SSEA), etc. [5]. Stem cell factor (SCF), FLT-3 cytokine receptor, interleukins, thrombopoietin growth and development factor belong to the family of cytokines, and they are other interesting biomarkers to monitor. Cytokines are involved in intracellular communication and they help cells toward proliferation

and differentiation into specific lineage. Such biomarkers can be detected by ELISA (Enzyme-Linked ImmunoSorbent Assay) test and immunoflorescence analysis. At last, supplied or released hormones, such as Insulin-like Growth Factor (IGF), are also interesting to monitor and they are typically bound to a fluorescent molecule to be detectable by simple microscopy.
Gene expression can be inferred by genome analysis, which requires DNA extraction in high concentrations. DNA strains are extracted by cells lysis and purified. DNA analysis can be determined by spectrophotometric methods at 254 or 256 nm, electrophoresis, or fluorescence methods [41]. However, microarray methods are by far the most common strategies for gene expression analysis [5].

2.1.2 Sensing element

The choice of the sensing element is closely related to the target of interest. Biological compounds are naturally selective and they can confer high specificity for the detection. Several biosensors are based on **enzymes**, characterized by a protein structure and an active site. When the active site binds the target molecule, the chemical reaction is catalyzed and transduced in a signal, typically electrical or luminescent, that can be measured and correlated to the analyte quantity. Enzymes need a cofactor to work, which is typically bound to the protein itself. The cofactor is the part of the enzyme specifically involved in the oxidation or reduction reaction. Denaturation and chemical stability are the two main concerns regarding enzymes. The immobilization of the protein onto solid support can improve the stability of the enzyme by decreasing movements of protein domains. Moreover, the addition of certain additives, like glutaraldehyde and *bovine serum albumin* (BSA), can have a beneficial effect on the stability of the enzyme. Oxidases are a large family of enzymes and they are frequently used for the development of electrochemical biosensors and in ELISA test. For the specific application of cell culture monitoring, examples of glucose oxidase [13], lactate oxidase [38], glutamate oxidase [27], amino acid oxidase [42] are largely reported in literature.
Antibodies are another common sensing element, able to specifically bind the corresponding antigen. Conversely to enzymes, antibodies do not promote or catalyze any chemical reaction, but they are typically coupled with a label molecule that can generate an electrical or fluorescent signal when the binding takes place [43]. The antigen can be a molecule or a cell, such as a bacteria. ELISA test is by far the most popular analytical assay based on the complex antibody-antigen. An example of the kit is illustrated in Fig. 2.3.
Nucleic acids are normally used for the monitoring of gene expression. Oligonucleotides (length <70 nucleotides) and immobilized *Polymerase Chain Reaction* (PCR) products (length around 400-1000 base-pair) are typically used in DNA array technology. The sensing mechanism, called hybridization, is based on the specific base-pairing of complementary nucleotides leading to double-stranded sequences of nucleic acids. Practically, the target gene is present in a solution and the specific strand sequence is instead immobilized as capture probe. The hybridization reaction is characterized by the affinity constant and by the kinetic constant of the association and dissociation reaction. Bonding of the guanine-cytosine (G-C) base pair is stronger than the one of adenine-thymine (A-T). Each base pair contributes to the strength

Figure 2.3: Example of an ELISA kit.

of the overall strain, so the affinity increases with the length of the matching nucleotides. Mismatches among nucleotides are possible, but they do not prevent the hybridization of the whole strand. However, signal intensity depends on the number of base pair binding and on the present mismatches. Nucleic acids are either immobilized by physical forces (electrostatic forces) or by chemical reaction (covalent bonding), typically on glass slides. Microarrays can be used to distinguish relevant modification in gene expression in different states of the stem cells. Bioinformatics can then interpolate such information to map the network of interactions among different distinguished genes. Manual curation can eventually help to identify the most relevant pathways to infer the metabolic behavior and the most relevant markers [5]. Electrochemical detection have been also used alternatively to optical techniques. Direct electrochemical oxidation of guanine, redox-active markers, and electron transfer properties of DNA have been also proposed [44], [45].

2.1.3 Transduction mechanism

Once the target molecule and the sensing element are defined, the next step is the definition of the transduction mechanism toward the development of the biosensor. **Optical methods** are by far the most common strategies, because of the numerous advantages. They allow *in situ* monitoring in the case of biomass monitoring and the use of disposable electrodes when integrated in flow-injection analysis systems or *ex situ* detection. Optical biosensors can be classified in four main categories: fiber-optic sensors, near-infrared sensors, fluorescence sensors, and Raman spectroscopy-based sensors. *Fiber-optic sensors* are also known as optodes and they are based on the change in the optical properties of a particular indicator, such as a dye. Biosensors are developed by immobilizing the indicator at the tip of an optical fiber, where the light can be guided in. pH and CO_2 levels can be measured with this technique. Moreover, biological compounds such as oxidases can be coupled to the optode for the detection of targets like glucose and hydrogen peroxide [46]. *Near-infrared spectroscopy* can quantify the concentration of certain organic species by the analysis of the adsorption bands in the spectrum. In fact, each chemical species occupies a specific position in the

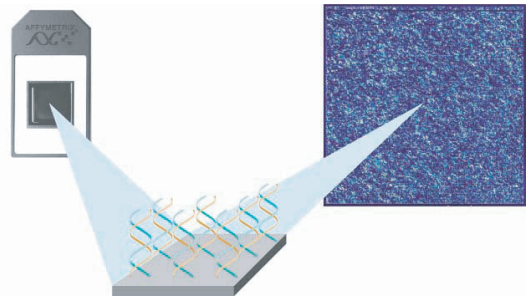

Figure 2.4: GeneChip® Microarrays - They are used for DNA detection by exploiting fluorophores and chemiluminescent compounds bound to the probe. Reprinted from *www.affymetrix.com*.

spectrum and shape and size can be correlated with its concentration. Advanced data-analysis algorithms can automate the process to extract analytical information in a reliable manner [47]. *Fluorescence sensors* are based on the response of particular molecules which emit light after an excitation at particular wavelength. For example, the reduced form of *Nicotinamide Adenine Dinucleotide Phosphate* (NADPH) gives a fluorescence signal when excited at 260 nm. Moreover, several intra- and extracellular fluorophores can be detected optically, leading to two-dimensional fluorescence spectroscopy. DNA microarray, in particular, are often developed by exploiting fluorophores and chemiluminescent compounds bound to the probe or to the target. The sample solution is pre-treated to have the fragments coupled permanently with marker molecules. When those fragments are captured by a complementary strand, an optical signal is generated, which intensity depends on the strength of the hybridization. By knowing the map of the probes in the glass slide, it is possible to go back to the targets that bound the probes (see Fig. 2.4).

Impedimetric and **capacitive methods** are often used for biomass and viability measurements, and they will be discussed in Section 2.1.4. **Nuclear Magnetic Resonance (NMR)** is another established method giving information about the enzymatic reactions happening in the bioreactor [48]. It is a completely non-invasive technique, since the bioreactor can be placed within the magnetic chamber, and it allows to follow cell metabolism. Main drawbacks are that NMR needs high cell density and synchronization of cell population from the metabolic and the physiological point-of-view to obtain precise measurements. Moreover, NMR spectrum needs time to be recorded and the equipment is quite costly.

Electrochemical biosensors are the easiest and cheapest solution for bioprocess monitoring and they are the most widely described [38], [14], [10]. They allow *in situ* and *on-line* measurements, since they need to be in contact with the cell medium. However, they suffer from some drawbacks, such as thermal stability of the immobilized enzyme during sterilization process, electrode fouling due to the continuous contact with the solution, consume of the analyte and bioprocess interference. Different strategies have been proposed to overcome those disad-

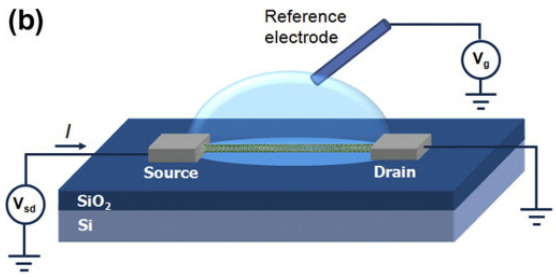

Figure 2.5: Carbon nanotube field-effect transistor with liquid-gate configuration. Reprinted from [51].

vantages. The biological element can be contained in a separate reservoir, separated from the bulk by a sterilized membrane. Therefore, the analyte can diffuse through the membrane and interact with the enzyme, although the measurement is no more *in situ*. Electrochemical biosensors will be discusses more in details in Section 2.4.

2.1.4 Monitoring physicochemical parameters

Small changes in medium composition, pH, temperature, and dissolved gases pressure can alter cell metabolism, especially in the case of stem cells. On the contrary, an accurate control of such parameters in the culture environment can lead to optimal conditions for growth and differentiation mechanisms. Moreover, strategies for monitoring cell density and quantify viable cells have been also proposed. The strategy of sensing strictly depends on the physicochemical parameters. Temperature, pH, gases, and cell density needs just sensors for their detection.

Temperature and cell growth rate are strictly connected and should be kept constant over the cell culture. Sensors based on platinum *Resistance Temperature Detector* (RTD) can be easily developed by thin film technology or purchased from the market [49]. The measure is based on the change of the electrical properties of RTD, where the Pt wire resistance varies according to the temperature. Temperature can also be measured by using a diode-based *proportional-to-absolute temperature* (PTAT) thermometer, which generates an output voltage proportional to the temperature [50].

pH is by far the most widely and controlled parameter in cell culture, even if pH sensors are difficult to integrate. Ammonia is the primary nitrogen source and its uptake causes acidification of the medium due to the release of NH_4^+. The measurement is often performed by standard potentiometric ion selective glass electrode. A gel layer with mobile hydrogen ions is dept in an aqueous solution. Ions produced by the pH modification diffuse through the gel layer and generate a voltage drop between the working and the reference (typically Ag/AgCl) electrodes. Spoiling of the reference electrode is quite common in such sensors for cell culture applications [26]. *Ion-Selective Field-Effect Transistors* (ISFET) can be also used to monitor small pH variations. The gate voltage is applied to the reference electrode directly in contact with the solution (refer to Fig. 2.5). Other configurations foresee to deposit a layer of

Si_3N_4 as the gate, which plays the role of the chemical sensing layer. Typical sensitivities for such devices can be around 56 mV/pH and they can be microfabricated with *Complementary Metal Nitride Oxide Semiconductor* (CMNOS) technology [52].
Partial pressure of dissolved gases like $\mathbf{O}_2$ and $\mathbf{CO}_2$ are other important parameters to control. Oxygen is hardly soluble in aqueous solutions and cells can suffer from oxygen limitation. Clark amperometric electrodes [53] are by far the most common strategy to measure dissolved oxygen, according to the following electrochemical reaction:

$$O_2 + 4e^- + 2H_2O \rightarrow 4OH^-, \tag{2.1}$$

when a potential around +600-750 mV is applied. The current generated by the depletion of electrons from the electrode (4 e^-) is proportional to the dissolved oxygen concentration. The drawback of this method concerns the consumption of the dissolved oxygen, that can become a problem when handling low volume bioreactors. An alternative method to detect oxygen can be achieved by exploiting the same reaction. OH^- ions locally produce a pH-changing in the immediate proximity of the ISFET gate [54]. Carbon dioxide can also affect growth of animal cells, which often require its supplementation. Severinghaus electrodes consist of a glass electrode separated from a bicarbonate solution by a CO_2 permeable membrane. Partial pressure of CO_2 can be measured by pH variation of the bicarbonate solution. As in the case of dissolved O_2, carbon dioxide can also be sensed by ISFET.
Cell density, **cell viability**, and **adhesion** can also be quantified by optical, electrical, and calorimetric-based methods. As mentioned previously in Section 2.1.3, transmitted, reflected or scattered light can be used *in situ* to determine the number of cells present in the bioreactor. Optical methods are typically non-invasive and non-destructive, highly desirable when dealing with cell cultures, and they do not interfere with the culture environment, reducing contamination risks. Major problems concern turbidity of the medium, which can change over the cell culture, gas bubbles formation along the light path, light dispersion on cell debris, and noisy measurements. Optical density has been proposed for measuring cell growth and biomass concentration and commercial *on-line* and *in situ* biosensors are typically based on light absorption (Optek-Danulat, Germany) or scattering (Cerex MAX ™, USA). However, distinction between viable and dead cells is not possible with this method. Near-infrared focused light should be preferred, because the wavelength is closer to cell dimensions [40]. *In situ* microscopy is another well-establish technique and it can be coupled with image analysis to automate the monitoring [55]. Optical methods to measure cell density can encounter problems due to change in morphology, cell aggregation, and turbidity of the medium [46].
Impedimetric and capacitive methods, instead, can be used to sense biomass, cell viability and adhesion. Undamaged cell membrane exhibits dielectric properties, so cell viability and adhesion can be detected by measuring the effective electrode impedance at low frequencies [56]. Capacitance spectroscopy over a wide range of electric field can be also used to determine the average cell size and the number of cells [57]. Finally, heat generated during growth have been also presented in the past to measure the amount of active cells in the bioreactor [58].

Figure 2.6: Cell culture flask with equipped with *in situ* sensor for the detection of nitric oxide. Reprinted from [16].

2.2 Sampling methods

Sampling has the purpose to obtain a representative specimen from where it is possible to extract information on the overall state of the process. Sampling should be invasive as less as possible not to compromise microbiological purity of the process. Sampling methods are typically divided in two main categories: *ex situ* sampling (indirect sampling), where a small volume of the medium is withdrawn from the bulk and transported to the external biosensor, and *in situ* sampling (direct sampling), where the monitoring is performed directly in the bulk without sample removal. The choice between *in situ* and *ex situ* methods depends on the sensing element and the transduction mechanism.

***In situ* measurements** gives a direct insight to the bioreactor conditions and response time is reduced due to the proximity of the biosensor. Few devices are available on the market for *in situ* measurements of bioreactors [40]. *In situ* sensors should be able to function for long periods of time (at least for the time of the culture). Common problems are related to sensor fouling and baseline drift due to precipitation of cells and proteins on the surface of the detector. *In situ* sensors should endure to sterilization process and they should not require continuous calibration. Sensors that do not involve a biological recognition element and for physicochemical parameters are the most common used for *in situ* monitoring (an example is reported in Fig. 2.6).

***Ex situ* sampling** requires sample removal from the bioreactor. When the detector interface is in direct contact with the process, then the analysis is defined as *in-line*. Biosensors integrated in the bioreactor with membranes as interface between the process and the detector belong to that category [12]. *On-line* analysis implies the use of a recirculation loop or by-pass, where the sample is automatically removed from the process and brought in contact with the detector. If the analysis is performed in a remote location, instead, we talk about *off-line* measurements. Disposable electrodes are very often *off-line* measurements. Nayak et al. [14], for example, proposed the use of two types of blood glucose self-monitoring devices, used in diabetes disease, for the evaluation of glucose concentration in common culture media. The authors

proposed a comparison between an enzyme-based biosensor, which detects glucose by means of an amperometric measurement, and a reflectance meter, based on the change of the optical properties of the medium, according to different levels of glucose. Thereby, samples of the culture media were withdrawn and analyzed *off-line* on a disposable electrode. Finally, if the detector is located in close proximity to the bioreactor, the analysis is defined *at-line* or *quasi on-line*.

2.2.1 Flow-Injection Analysis (FIA)

FIA systems are the most common example of *on-line* sampling for the automatic monitoring of culture media. The basic components of a FIA system are a transport system, typically consisting of a pump, tubes, valves, and a carrier stream. A small volume of the sample is injected into a continuous flow of the carrier solution. The two fluids are mixed through radial and convection diffusion along the fluidic path, before reaching the analysis site. A chemical reaction usually occurs during the flow and the products are measured by the sensing element. Peristaltic pumps are typically used to stream the liquid through the detector. Physical sample treatment can also be implemented, such as separation, extraction, and diffusion. The schematic of a typical FIA system is depicted in Fig. 2.7. The flow-rate is typically in the range of 0.2 - 1.0 ml/min. FIA systems allow low reagent consumption and high automation.
Metabolite concentrations can be detected by using optical or electrochemical-based biosensors, depending on the sensing element. Regarding optical biosensors, Dremel *et al.* [59] described for example a fibre optic oxygen sensor as transducer for the detection of glucose and lactate in an animal cell culture. They combined the use of oxidases to specifically detect glucose or lactate with an optical readout to sense the oxygen consumption during the enzymatic reaction in a FIA system. Another example of optical transduction in FIA foresees to enzymatically oxidize glucose and lactate and the hydrogen peroxide formed by the reaction can be then detected by chemiluminescence. In fact, hydrogen peroxide can react with chemiluminescent reagents and detected by using a photodiode, for example [60], [61].
As aforementioned before, electrochemical biosensors can be also coupled with FIA system by using membranes, and the analyte can pass through the membrane either by a pressure gradient (filtration) or a concentration gradient (diffusion). In the case of filtration, the bioreactor sample can be directly injected into the carrier stream. The cells can afterwards be separated from the culture medium via a microfilter. The retentate can be returned to the bioreactor, while the filtrate is drawn through the microfilter by a peristaltic pump and sent to the injection valve [62]. In this way it is possible to avoid contamination problems and sterilization issues, since the biosensor is not in direct contact with the cell culture. On the other hand, clogging and fouling of the microfilter are quite common, due to cell precipitation. Yellow Springs Instruments, already discussed in Section , is a commercial available example of FIA system to perform real-time analysis. Typical used membranes are made of polycarbonate with 0.2 μm pore size. Bilitewski *et al.* showed the detection of glucose, lactate, and glutamate by using electrodes functionalized with different enzymes and coupled with a FIA system [63]. Wentz *et al.*, instead, proposed the *on-line* monitoring of glucose, lactate, and ammonia by

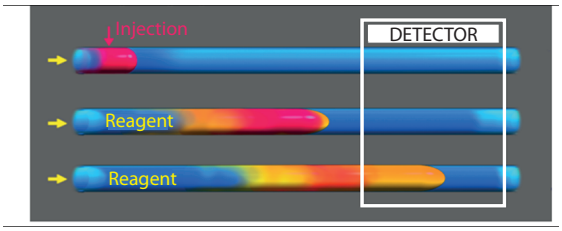

Figure 2.7: Schematic of the path for a FIA system. The sample is depicted in red, while the product of the reaction between the sample and the reagent is in yellow. Reprinted from *www.flowinjection.com*.

using a tubular filter consisting of hydrophilized polypropylene microfiltration membrane for the *in situ* sampling of the culture medium.

2.2.2 Microdialysis probe

The use of microdialysis for the sampling of biological fluids was originally set for intracerebral applications. They were often coupled with microelectrodes for the simultaneous electrical stimulation/recording and the measurements of chemical in the tissue. However, its application in the area of biotechnology has gained popularity, because of its capability not to perturb the kinetics of the reactions under study. The sample has to be reflective of the bioprocess, without any depletion of the compounds involved in the bioprocess, i.e. excessive consumption of the interesting analytes can affect the reaction kinetics. Moreover, samples should be representative of the bulk concentration, so usually dialysis is restricted to small volumes. Dialysis technique is based on diffusion: the bulk enriched with the analyte and the perfusate are separated by a selective membrane; the difference in analyte concentration will determine the diffusion rate.The transport across the membrane is caused by a concentration gradient, so membrane fouling is hardly likely respect to microfiltration techniques.
There are two possible mode of dialysis sampling: continuous-flow and stopped-flow. The choice of the mode highly depends on sampling intervals and bioprocess volume. Continuous-flow technique is more suitable when the bioprocess volume is bigger and the analyte concentration is high. In fact, the degree of analyte depletion during on-line continuous-flow sampling can be quite high, affecting the composition of the bioreactor, especially if the measurement has to be carried out for several hours [64]. In stopped-flow the perfusion is carried out only during sampling. The advantage is that the amount of analyte taken from the bioreactor can be minimized and the sampling can be also performed to intervals when a sample is required for analysis.

Microdialysis can be quantified by determining the dialysate *extraction factor* (EF):

$$EF = \frac{(C_d^{out} - C^{in})}{(C_b - C^{in})} \tag{2.2}$$

where C_d^{out} is the analyte concentration in the dialysate, C^{in} is the analyte concentration in the perfusion liquid, and C_b is the analyte concentration in the bulk. Eq. 2.2 can be reformulated as follows:

$$EF = 1 - exp\left[-\frac{1}{Q_d(R_d + R_m + R_{ext})}\right] \tag{2.3}$$

where Q_d is the perfusion rate, whereas R_d, R_m, and R_{ext} are resistances to diffusion due to the dialysate, the membrane, and the bioreactor solution, respectively. The extraction factor does not reflect the concentration of the total available analyte, since precipitation and adsorption processes may trap analytes. From Eq. 2.3 we note that EF depends on the membrane resistance to diffusion, which can be defined as follows:

$$R_m = \frac{ln\left(\frac{r_o}{r_i}\right)}{2\pi L_{edl} D_{eff} \phi_m} \tag{2.4}$$

where r_o and r_i are the outer and inner radii of the membrane, respectively, L_{edl} is the effective dialysis length, D_{eff} is the diffusion coefficient in the aqueous phase of the membrane, and ϕ_m is the aqueous phase volume fraction of the membrane. Thereby, by playing with r_o, r_i, and L_{edl} it is possible to tune the membrane resistance so that the EF can be changed.
Microdialysis probe should be flexible, sterilizable, an with an optimal extraction factor according to the interested analyte. Many designs have emerged in literature and in the market and they mainly fall in three categories. The *hollow-fiber probes* are conceived with an exposed central region of the dialysis probe, while both ends of the probe are glued to an interfacing tube. The *planar probes* consists of a flow channel, which is covered by a planar microdialysis membrane. The *concentric probe* incorporates two coaxial channels glued at one end. A schematic is depicted in Fig. 2.8. The outer wall is a membrane, whose pore size is chosen according to analyte size. The perfusate is flown through the inner channel and pushed to pass outside at the end of the probe. The solution leaving the probe is enriched by molecules, which can diffuse through the outer membrane from the medium. Several concentric probes are currently available able for repeated use and sterilization prior to each experiment [64].
Membranes are typically made of polymers, such as *polysulphone* (PS), *polyethersulphone* (PES), *polyamide* (PA), *polycarbonate* (PC), *cuprophan* (CU). Membrane has to be chosen according to its application, ensuring that the exposure to complex bioreactor conditions does not result in modification affecting its performance. Membrane material composition and the zeta potential, i.e. the electrical potential in the interfacial double layer, are typically sufficient criteria to establish the proper membrane to choose. These two criteria ensure that the membrane does not affect the bioreactor conditions. Moreover, membrane-protein interaction is highly undesirable, since it can lead to membrane fouling, and extraction factor

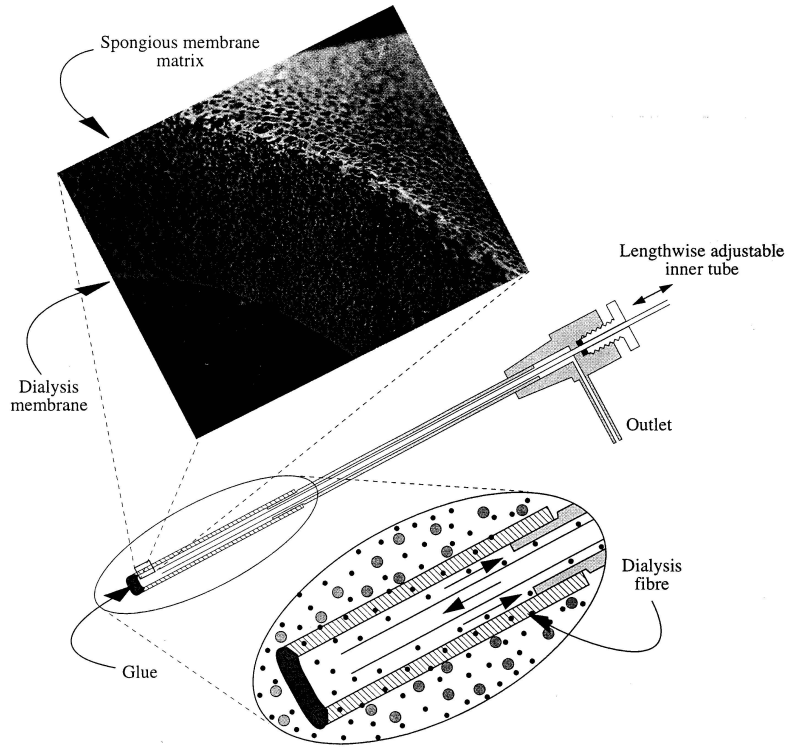

Figure 2.8: Schematic representation of a microdialysis probe, showing the spongious membrane matrix of the inner membrane. Reprinted from [65].

can also depend on the interaction of membrane material with the analyte. However, for small-scale bioprocesses the concentration of protein is not so significantly high. Thereby, membrane fouling by protein adsorption is rarely envisaged. Another important criteria for choosing the proper membrane is the nominal molecular weight cut-off, so that it is also possible to minimize interference molecules at the sensor site. Proper membranes for bioprocess monitoring should be hydrophilic enough to allow unassisted wetting and they should be reusable after being air-dried. For bioprocess monitoring, the optimum membrane cut-off range is between 5 and 30 kDa.
Microdialysis sampling units have been often coupled on line to HPLC systems [66], mass spectroscopy [67], and FIA systems [68]. Microdialysis technique is intrinsically a dilution technique and it can be used as an advantage when sample concentration is very high. Microdialysis probes can be also used together with electrochemical biosensors to avoid fouling of the electrode surface. Thanks to the probe, it is possible to reject detection interferences, such as ascorbic acid and 4-acetaminophen, by choosing the appropriate membrane cut-off [69].

2.3 Nanotechnology-based biosensors

According to many researches [70], [71], nanomaterials are the new frontier of biosensing. They exhibit many interesting properties from the biosensing point-of-view, including com-

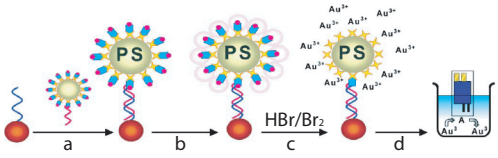

Figure 2.9: DNA detection by using polymeric beads carrying multiple gold nanoparticle tracers. Reprinted from [75].

parable dimension with biological recognition elements, high electron transfer rate [72], considerable electronic emission [73], and high surface area [74], due to their 3-dimensional structure. Nanomaterial-based biosensors have been widely presented in literature and their application have been mainly focused on diagnostic and therapeutical purposes. Up-to-date, the use of nanomaterials has not been yet exploited to enhance the sensitivity of detectors developed for bioprocess monitoring.

Nanoparticles (NPs) are typically metallic, exhibiting interesting electrical and magnetic properties for biosensing applications. NPs are often made of gold, because of the numerous way to modify Au and obtain high affinity surfaces with biomolecules and bioprobes (see Fig. 2.9). They show proper optical properties to be used in biosensing, but also interesting electrical features, as high sensitivity and improved limit of detection in voltammetry [76]. Quantum dots are semiconductor crystals whose size is within 10 nm. Quantum confinement confers different properties to quantum dots with respect to larger particles. Thereby, they have remarkable optical properties, suitable to be used as labels for sensing elements [77]. Core shell are a subfamily of NPs, with a metallic core and an organic or inorganic shell, to improve biocompatibility and reduce particle aggregation [74].

With the improvement of micro- and nanofabrication techniques, **nanowires (NWs)** have been receiving more interest in biomedical applications, since they can interact with biomolecules at the nanoscale. They can be metallic or semiconductive, according to their atomic arrangement, and can provide different transduction mechanisms. NWs can be functionalized with proteins, enzymes or antibodies (as in the case of Fig. 2.10) in conductive measurements or in field-effect transistors [78].

Carbon nanotubes (CNTs) exhibit interesting electrochemical properties and their use in electrochemistry will be largely debated in Chapter 3. The electron current through the nanotube is based on ballistic conductivity, so the measured mean-free path results to be two orders of magnitude higher then the best macroscale conductor [80]. Electron transfer depends on atomic arrangement, so emission properties are different for tips and walls of CNTs [81], [82]. Moreover, they have been largely reported for their ability to adsorb proteins onto

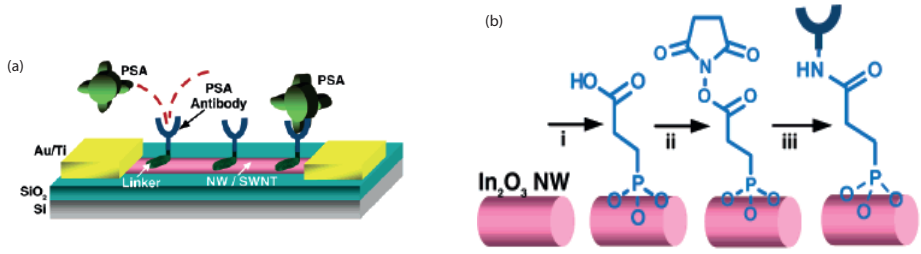

(a) PSA-antibodies are anchored to the NW surface and they can recognize PSA antigene.

(b) Reaction sequence for the NW functionalization.

Figure 2.10: Schematic diagram of the NW-based biosensor. Reprinted from [79].

their walls, resulting in an excellent immobilization method [5]. Surface modification by using carbon nanotubes can be accomplished in different manner and for several purposes. Directly growing of aligned carbon nanotubes have been proposed on different substrates[71]. Self-assembling is another way to obtain aligned CNTs by modifying surfaces with thiols or other functional groups [28]. Carbon nanotubes can be also randomly dispersed on the electrode surface and many efforts have been addressed to obtain well-dispersed CNT solutions. Carbon nanotubes can be used as a forest of nanomaterials, patterned arrays or as single-sensors. NWs and CNTs can be used to replace the channel in field-effect transistors for biosensing purposes. As in the case of electrochemical biosensors, the biological recognition element can be adsorbed either on NWs or CNTs surface and modify the conductivity of the channel [83].

2.4 Electrochemical biosensors

If we dip a metal into an aqueous solution plenty of ions of the same metal, we can observe an exchange of ions between the surface of the metal and the solution. Some ions migrate from the metal to the solution, leaving an excess of electrons onto the metal surface, while other ions go from the solution to the electrode, absorbing electrons. A layer of charges develops onto the interface of the two phases. If we add a second electrode to the cell, we can measure a drop potential between these two electrodes, due to the exchange of ions between the metal and the solution. The second electrode is standard for convention, and it can be made of a platinum leaf covered by spongy platinum and lapped by burbling hydrogen immersed in a strong acid, in order to maintain unitary the activity of the protons. This electrode is called *reference electrode* (RE), while the metal dipped into the solution is called *working electrode* (WE). The measurement of the potential difference between these two electrodes has to be carried out with a voltammeter with infinite input impedance in order to avoid current flowing through the two electrodes. The potential is expressed by the following equation:

$$E = V_{WE} - V_{RE} = [E^{\Theta}_{O/R}]_{SHE} + \frac{RT}{nF} ln\left(\frac{a_O}{a_R}\right), \tag{2.5}$$

where $[E^{\Theta}_{O/R}]_{SHE}$ is defined as standard redox potential with respect to the *standard hydrogen electrode* (SHE), R is the gas constant, T is the absolute temperature, n is the number of the electrons involved in the redox reaction, F is the Faraday constant, a_O and a_R are the activity of the oxidized and reduced species, respectively. The standard redox potential is defined as the potential measured at standard state, i.e. solutes have an effective concentration of 1 mol/l and gases have a pressure of 1 atm. This potential E represents the drop potential between the two electrode, and not the drop potential between the WE and the solution. The above equation is called Nernst's equation and it is written from a thermodynamics point-of-view, because it can be directly derived from Gibb's law. In fact, the potential is a function of the activity. In an ideal solution, the molecules do not interact with each other and the concentration of the species is equal to its activity. In a real solution, there is a certain interaction among the molecules and it results in a diminished activity of the molecules, due to the fact that the solution behaves like it would contain a concentration of the dissolved species lower than it actually contains. The activity can be related to the species concentrations by means of the activity coefficient γ_i and the Nernst's equation can be expressed in function of the concentration as follows:

$$E = V_{WE} - V_{RE} = [E^{\Theta}_{O/R}]_{SHE} + \frac{RT}{nF} ln\left(\frac{C_O}{C_R}\right), \tag{2.6}$$

where $[E^{\Theta}_{O/R}]_{SHE}$ is the formal redox potential with respect to the standard hydrogen electrode, C_O and C_R are the oxidized and reduced concentrations of the species, respectively. This formulation of the Nernst's equation is from an electrochemical point-of-view, because it is expressed in function of the specie concentrations.
We can measure the standard redox potential for different redox reactions and build a table with those values. For convention, the standard redox potential of hydrogen peroxide is equal to 0 V. For species with higher standard potentials the oxidation will result more difficult, if the standard potential is much higher from 0 V: on the other hand, the reduced species will be more stable. For species with lower standard potentials the reduction will result more difficult, if the standard potential is much lower than 0 V, but the oxidized species will be more stable. Since the hydrogen electrode is quite complicated and not easy to reproduce in daily experiments, it is replaced by other RE, as the Ag/AgCl electrode, for example. If we apply the Nernst's equation, we can measure the standard redox potential of the Ag/AgCl with respect to the SHE, which is 0.222 V. If we add 0.222 V to the standard potential referred to the SHE for any kind of redox reaction, we obtain the standard potential referred to a Ag/AgCl reference electrode.
Once we know the equilibrium potential (E_{eq}) of a redox couple, i.e. the potential where the concentration of oxidized species is equal to the concentration of reduced species, we can decide to drive the reaction to an extra-production of oxidized or reduced species by only applying an overpotential much higher or much lower than the equilibrium potential. This is because the applied potential depends on the predominance of the numerator or the denominator in the Nernst's equation.

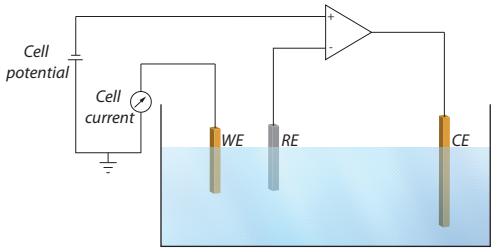

Figure 2.11: Schematic of an electrochemical cell with three electrodes.

2.4.1 Electrochemical techniques

Under electrode polarization, i.e. when a potential is applied between the WE and the RE, the ions move from the electrode surface to the solution, or viceversa. We can measure the ion flux that is generated by introducing a third electrode in the cell, which is called *counter electrode* (CE). A schematic of an electrochemical cell is illustrated in Fig. 2.11. Thus, the current flowing between the WE and the CE is proportional to the oxidized or reduced species, according to the polarization. If we apply an overpotential much higher than the formal redox potential, we will have a preponderance of oxidized species and we will record an anodic current, which is positive according to the IUPAC convention. On the contrary, if we apply an overpotential much lower than the formal redox potential, we will have a preponderance of reduced species and we will record a cathodic current, which is negative according to the IUPAC convention. The total current recorded in the electrochemical cell will be the sum of the anodic and the cathodic current. Many techniques can be used to apply an overpotential to the solution and they can be grouped into two main families: potentiodynamic methods and potentiostatic methods. Cyclic voltammetry belongs to the first category, while chronoamperometry belongs to the second category.

Cyclic voltammetry

Cyclic voltammetry consists of applying a potential variable in time and in recording the current flowing between the WE and the CE. The current is typically plotted in function of the potential. The current generated in the cell is the sum of the anodic and the cathodic current, expressed as follows:

$$I_a = nFAk_aC_R(0), \qquad I_c = -nFAk_cC_O(0), \tag{2.7}$$

where k_a and k_c are the kinetic constants for the oxidation and the reduction processes and A is the surface of the WE. We can now express the net current in function of the applied

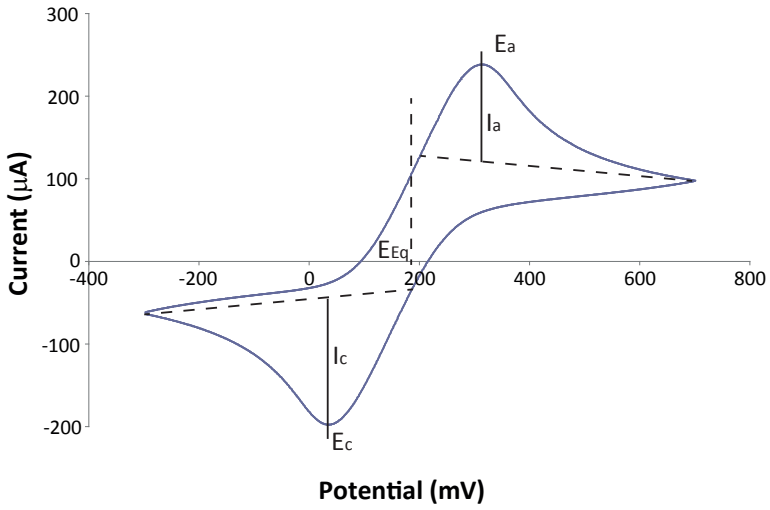

Figure 2.12: Plot of a typical cyclic voltammetry.

potential with the equation:

$$I = I_{Ox} + I_{Red} = I_0(e^{\alpha nF\eta/RT} - e^{-(1-\alpha)\alpha nF\eta/RT}), \tag{2.8}$$

where I_0 represents the exchange current density, α is the symmetric coefficient of the reaction, η is the overpotential with respect to the equilibrium potential (E-E_{eq}). This equation is called Buttler-Volmer equation.
Cyclic voltammetry applies a linear-sweep potential between the working and the reference electrode, forward and backward within a potential window. The applied potential varies linearly and the variation velocity is called scan rate, which is expressed in mV/s and is fixed by the user. Typical values are from 10 to 500 mV/s. The plot from a cyclic voltammetry is reported in Fig. 2.12. The scan begins at a positive potential far from the formal redox potential. At that time, no current flows through the cell. When the electrode potential becomes close to the formal redox potential, the reduction begins and current starts to flow. As the potential continues to grow more negative, the surface concentration of the species drops; hence, the flux to the surface (and the current) increases. As the potential passes the cathodic potential peak (E_c), surface concentration drops nearly to zero, mass transfer reaches a maximum rate at the surface, and then it declines as the depletion effect sets in. This is the case where the current is limited by the diffusion of the reagents to the electrode surface. When the potential is swept in the opposite direction, symmetric mechanisms take place and the whole oxidized species is reduced again at the anodic potential peak (E_p).
The hysteresis plot gives qualitative and quantitative information about the detected target. In particular, the peak hight is proportional to the analyte concentration, whereas the position with respect to the potential gives qualitative information, since compounds has different oxidation and reduction potentials.

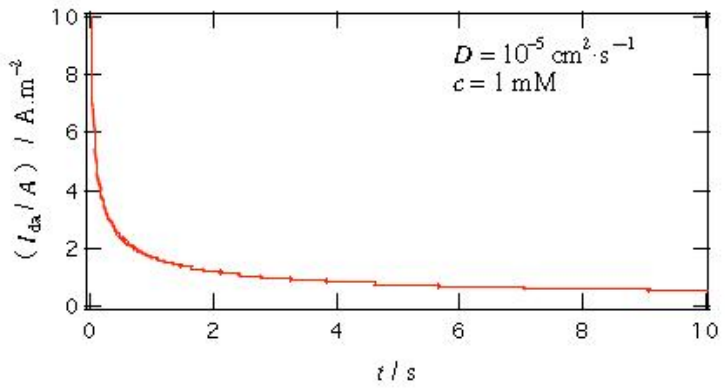

Figure 2.13: Plot of current vs. time in a chronoamperometry.

Chronoamperometry

Chronoamperometry belongs to the potentiostatic techniques and it consists of applying a fixed potential and recording the current in function of the time. The applied constant potential typically corresponds to the oxidation or the reduction potential of the analyte. The net current flowing through the cell is described by Cottrell's equation as follows:

$$I(t) = nFAC_R\sqrt{\frac{D_R}{\pi t}}, \tag{2.9}$$

where D_R is the diffusion coefficient of the species. Current generally decays over the time and it reaches an approximative steady-state after a certain time, which intensity is proportional to the analyte concentration. An example of the current trend in chronoamperometry is shown in Fig. 2.13.

Hydrogen peroxide can be easily detected in chronoamperometry by applying a constant potential of +650 mV. Under the application of such potential, the following reaction takes place:

$$2H_2O_2 \rightarrow 2H_2O + O_2^+ + 4e^-, \tag{2.10}$$

where the four e^- released to the electrode are then detected by the potentiostat. It is possible to exploit the electrochemical properties of H_2O_2 for the indirect detection of many compounds by using oxidases, as it will be described in the next section.

2.4.2 Examples

In the following section, we will present some examples related to amperometric biosensors for the detection of glucose, lactate, and glutamate. Both bare and CNT-based biosensors will be considered.

Glucose biosensors

Glucose biosensors have been extensively investigated. Examples regarding diverse surface modification and functionalization are largely reported in literature [84], [85], [86], [87], [88]. Glucose detection can be performed by means of *glucose oxidase* (GOD). The enzyme typically reacts with glucose according to the following reaction:

$$\text{Glucose} + O_2 \xrightarrow{\text{GOD}} \text{gluconolactone} + H_2O_2.$$

Then, H_2O_2 can be electrochemically detected according to the principles already discussed in 2.4.1. The main drawbacks of the proposed solutions are related to detection performed at high potential, low sensitivity of the biosensor, and poor long-term stability. Structuring the electrode with polymers is the most straightforward solution adopted for enzyme immobilization. Many types of polymers, especially conducting types, and techniques of immobilization have been tested. The most widely used conducting polymers for enzyme immobilization are polyaniline, polypirrole, and polythiophene, because they offer a stable and porous matrix for the immobilization. As an example, Kausaite *et al.* [89] developed a glucose biosensor based on GOD encapsulated within polyaniline matrix. The developed biosensor displays a wider linear detection range (up to 356 mM) and a long-term stability of 90 days with a retained activity of 60%. Another widely used approach for the development of glucose biosensors involves the use of mediators. Typical mediators are based on ferrocene derivatives, such as ferrycianide, organic salts, quinone compounds, etc. Prussian blue (or ferric ferricyanide) has been extensively used for the development of amperometric biosensors based on oxidases. It is an inorganic compound with the ability to catalyse the reduction of H_2O_2 around 0 V vs Ag/AgCl reference electrode. Wang *et al.*, for example, developed a glucose biosensors based on the electrodeposition of Prussina blue and chitosan directly on gold electrodes. The sensor works in a linear range within 2 and 400 μM and a sensitivity of 0.31 μA/mM cm^{-2}. However, Prussian blue shows poor operational stability, within range of hours, and high dependence on pH.

Nanotechnologies have led to many new technical developments and applications, including the use of nanomaterials in the biosensing area. The effective electrical wiring of redox enzymes on the electrode can be envisaged thanks to similar dimensions of nanomaterials and redox proteins. Various nanomaterials, including nanocrystals, nanoparticles, and carbon nanotubes, have been used to develop diverse biosensors, not only for glucose detection. *Cadmium sulfide* (CdS) nanocrystals, for example, can be incorporated with glucose oxidase for realizing a direct electron transfer between the nanocrystals and the redox center. Huang *et al.* showed a sensitivity of 74 μA/mM cm^{-2} in a linear range within 50 μM and 33 mM and a detection limit of 50 μM. Gold nanoparticles have arisen great success as well. Gold nanoparticles can be first self-assembled on gold electrodes and functionalized with amino groups. The prepared substrate is particularly suitable for a covalent bonding of GOD onto these nanoparticles. The developed biosensor shows a sensitivity of 8.8 μA/mM cm^{-2} in a linear range between 20 μ and 5.7 mM.

Literature on carbon nanotubes applied to electrochemical biosensors is by far the most numerous. Many reviews summarize the main works related to the development of CNT-based electrodes. Carbon nanotubes offer favorable surface orientation and act as electrical connectors between the redox center of the protein and the electrode surface. The physical and electrocatalytic properties and some examples of CNT-based biosensors will be discussed more in details in Section 3.3. Regarding specifically CNT-based glucose biosensors, there are some remarkable works. Wang *et al.* [25], for example, evaporated a thin Au film onto grown CNTs and they drop cast GOD on top of the nanotubes, showing a sensitivity of 14.2 μA mM^{-1} cm^{-2}. Another approach can be to mix CNTs and GOD in the same solution, with the addition of Nafion to increase the solubility of nanotubes. Tsai *et al.* proposed this approach in [70], where they drop cast the mixed solution on glassy carbon electrodes. In a linear range from 0.025 to 2 mM, they got a sensitivity of 4.7 μA mM^{-1} cm^{-2}. Regarding sensitivity, quite similar results were shown by Ryu *et al.*: CNTs forme a network on the electrode (called mat) and GOD is covalently bound to the nanotubes [90]. The highest result in terms of sensitivity was presented in [91], showing a value of 23.5 μA mM^{-1} cm^{-2} for CNT-based sensor with *butyric acid* (BA) functionalization and GOD immobilization.

Lactate biosensors

While glucose detection is mainly performed by using glucose oxidase, many works regarding lactate monitoring present comparable results by detecting lactate either with *lactate oxidase* (LOD) or *lactate dehydrogenase* (LDH). LOD mechanism is the most straightforward, since it operates according to the following reaction:

$$\text{L-Lactic acid} + O_2 \xrightarrow{\text{LOD}} \text{Pyruvate} + H_2O_2.$$

The generated current can be measured as we already described in 2.4.1. As in the case of glucose biosensors, different immobilization strategies and sensitivity improvements have been explored in literature. CNTs can be incorporated with mineral oil to form a paste and used as electrodes [92]. The resulting sensitivity is quite low, resulting in a value of 0.204 μA mM^{-1} cm^{-2}, but the linear range is extended up to 7 mM. CNTs have been also incorporated into sol-gel film to form a further matrix for the immobilization of the enzyme. Huang *et al.* [93] deposited the obtained matrix onto glassy carbon electrode, showing a sensitivity ten times higher that in the previous case. By the successive drop casting of N-doped CNTs, LOD, and modified-Nafion onto glassy carbon electrode, it is possible to further increase the sensitivity of the biosensor by a factor of 10, as in the case of Goran *et al.* [94]. However, the linear range is very narrow (from 0.014 to 0.325 mM), which cannot fit with physiological lactate concentrations.
Another approach for the detection of lactate foresees to use lactate dehydrogenase. LDH is an enzyme specific for lactate that works in the presence of a coenzyme, the *Nicotinamide Adenine Dinucleotide* (NAD^+), according to the following reaction:

$$\text{Lactate} + \text{NAD}^+ \xrightarrow{\text{LDH}} \text{Pyruvate} + \text{NADH} + \text{H}^+.$$

Thus, NAD^+ is called oxidizing agent, since it is an electron acceptor, while NADH is the reducing agent, so the electron donor. LDH-based biosensors are less developed in literature, since they need to immobilize both the enzyme and the coenzyme. Tsai *et al.* [95], for example, mixed the LDH and its coenzyme with CNTs and chitosan and they casted the mixture on a glassy carbon electrode. Due to the presence of the NAD^+, it is also necessary to optimize the quantity of the coenzyme, which influences the final sensitivity of the electrode. Teymourian *et al.* [96] developed a CNT-based biosensor by loading the carbon nanotubes with Fe_3O_4 nanoparticles, which play the role of the mediator. The LDH and the NAD^+ are instead linked to the sidewalls of the carbon nanotubes and the biosensor shows a sensitivity similar to what reported by Goran [94] at a potential of 0.0 V, thanks to the mediator.

Glutamate biosensors

Glutamate is a neurotransmitter and its monitoring can be crucial for neurochemical experiments. Moreover, as already discussed in Section 2.2.1, glutamine can be indirectly detected by means of glutamate. Thus, its detection is crucial for many applications. Lots of microsensors have been proposed to be implanted in the brain and most of them are not based on carbon nanotubes. Pan *et al.*, for example, covered a Pt electrode with Nafion matrix to entrap glutamate oxidase. The detection was carried out in a really narrow range within 1 and 13 μM, obtaining a sensitivity of 16.1 μA mM^{-1} cm^{-2} [97]. Alternatively to Nafion immobilization, Zhang *et al.* [98] described the entrapment of GlOD in chitosan, with a sensitivity of 85 μA mM^{-1} cm^{-2} within 0 and 200 μM. Similar linear range was also explored by Ammam *et al.* [99]. Differently, they used CNTs and polyurethane onto Pt electrodes to increase the sensitivity (384 μA mM^{-1} cm^{-2}) and GlOD was dispersed in polypirrole. All aforementioned examples have a narrow linear range (up to 200 μM), while commercial culture media contains up to 4 mM of glutamine (and glutamate). Consequently, it is necessary to develop a biosensor in a wider concentration range.

2.5 Chapter contribution and summary

In this chapter an essential classification on biosensors for cell culture monitoring is presented. Biosensors can be clustered according to the target analyte, to the sensing element, and to the transduction mechanism. We presented many strategies for the development of such biosensors showed both in literature and in the market. We have also included in the classification those sensors that do not require a biological recognition element, such as for monitoring physicochemical parameters. Biosensors can be also divided according to where they are placed with respect to the sample. *Ex situ* sampling is the less invasive sampling technique, where the sensor does not enter in direct contact with the solution to measure. This approach shows many advantages, like avoiding contamination, no sample removal, etc., but it does

not allow, or partially allow, a continuous and real-time monitoring. On the other side, *in situ* methods suffer from biosensor fouling and poor long-term stability.
The chapter is also focused on the combination of nanotechnologies for biosensing purposes. Nanomaterials have been extensively combined with biological recognition elements to develop high-sensitive biosensors. In particular, carbon nanotubes show such promising properties, from the point-of-view of electron transfer rate, surface area and nanoscale structure, to be the right candidates for biosensor structuring.
The chapter concludes with a briefly overview on electrochemical biosensors. The principles and the detection mechanism are explained and some examples about glucose, lactate, and glutamate detection are reported.

3 Carbon Nanotubes and their Role in Electrochemistry

From their discovery, CNTs has increasingly attracted interest for several applications, due to their peculiar electrical, mechanical and chemical properties. For the first time in 1991, Iijima [100] observed and described in detail the atomic arrangement of such new type of carbon structures. Grown by a technique used for fullerene synthesis, he produced needle-like tubes at the cathode of an arc-discharge evaporator. From that time, carbon nanotubes have been described for several applications and represent one of the most typical building blocks used in nanotechnology. Their peculiarities include unique properties of field emission and electronic transport, higher mechanical strength with respect to other materials, and interesting chemical features.

Carbon nanotubes have been used in diverse applications. Thanks to their optimal properties of electron field emission, they have been used as electron source in electron beam devices. Typical electron sources consist of hot tungsten wires, heated materials, or sharp tips. However, such tools require ultra-high-vacuum conditions, the application of high voltages, while heated materials suffer of low work functions. A film of aligned carbon nanotubes, instead, has showed high field-emission current densities respect to typical approaches used to develop electron guns [101]. Such example opens new opportunities for the realization of flat panel displays and new tools for electron microscopy.

Carbon nanotubes are objects at the nanometer scale, so it is possible to exploit such feature to achieve sub-nanometer resolution in *scanning force microscopy* (SFM), for example. To that purpose, a single nanotube was attached to the side of a silicon cantilever tip for *atomic force microscopy* (AFM). Thanks to CNTs flexibility, they are resistant to tip damage, while their diameter allows to achieve sub-Ångström recesses in surface topography [102]. Moreover, due to their high electrical conductivity, they can be also used for *scanning tunnelling microscopy* (STM), making them suitable as high-resolution scanning probes.

As already aforementioned, another interesting property of carbon nanotubes is their capability to sustain large elastic deformation without damaging. Therefore, their promising mechanical properties make them suitable as reinforcement filler for polymeric materials. Once dispersed and distributed in the polymeric matrix, they have shown higher tensile strength and tensile modulus with respect to typical polymer composite [103].

Carbon nanotubes applied to electronics are by far the most common application for such nanomaterials. The miniaturization towards nanometer scale of basic components like *field-effect transistors* (FET) have been driving research in that field since 1970s. Numerous studies have proposed single CNT [104], [105] or bundle of CNTs [106] acting as the FET channel, thanks to semiconductor properties of carbon nanotubes.
The following chapter aims to give a brief introduction about carbon nanotubes and their use in combination with proteins for biosensing purposes. Section 3.1 will introduce such nanomaterials and will describe the main strategies for their production. Then, physical, chemical, and electrical properties will be discussed in Section 3.2. Section 3.3 will be dedicated to give an overview about the main strategies for the development of CNT-based electrochemical biosensors. Electrical properties and electron transfer are debated more in detail in Section 3.4 and some simulation are presented. Section 3.5 will focus on the combination of CNTs and proteins and the principles of electron transfer between those elements will be explained. Finally, in Section 3.6 we will resume the numerous advantages and the potential applications of carbon nanotubes in biosensing, with a particular emphasis on enhanced performance in the case of electrochemical biosensors with immobilized proteins onto carbon nanotubes.

3.1 Introduction to Carbon Nanotubes

Carbon is a very interesting element, since it can assume several stable molecular structures. Any molecule entirely composed by carbon is called fullerene. It can assume the form of hollow spheres, needles or ellipsoid [107]. Graphene is an allotrope of carbon, where atoms are arranged in sp^2 bonding state, with hexagonal honeycomb lattices arranged in a seamless structure. Graphene sheets can be stacked one on the top of the other and form graphite, the most popular form of carbon structure. Single or multiple graphene sheets can also be rolled along a lattice vector of the sheet and form a carbon nanotube. Depending on the number of rolled sheets, it is possible to identify two categories of such nanotubes: *single-walled carbon nanotubes* (SWCNTs) and *multi-walled carbon nanotubes* (MWCNTs). The different chemical structure confers different properties to those types of carbon nanotubes.
Single-walled carbon nanotubes consist of a single cylinder with a diameter of 0.4-2 nm. SWCNTs can be metallic, semi-conductors or small band gap semi-conductors, depending on their chirality and diameter. The chirality refers to the alignment of the π-orbitals when the graphene sheet rolls up [71]. Fig. 3.1 depicts three possible configurations of chirality, which confers different conducting properties. Typically, two-thirds of the SWCNTs are semi-conductors and one-third are metallic. Recently, several researches have proposed methods to separate SWCNTs with different conducting properties. Krupke *et al.* achieved to separate semi-conducting from metallic SWCNTs by using alternating current dielectrophoresis [108]. An alternative method proposed by Chattopadhyay *et al.* [109] foresees to functionalize SWCNTs with amines. Amine groups have much more affinity with semiconducting than with metallic SWCNTs, promoting the precipitation of SWCNTs on polar ethers.
Coaxial multilayer graphene sheets, instead, form multi-walled carbon nanotubes. The diame-

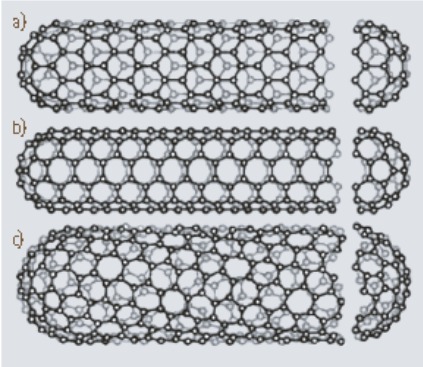

Figure 3.1: Three possible configurations of SWCNTs with different chirality: a) zig-zag type nanotube, b) an armchair tube, and c) a helical nanotube. Reprinted from [111].

ter ranges from 1.4 to 100 nm, depending on the number of rolled layers and hollow diameter, while the interlayer space is of 0.34 nm [110]. Fig. 3.2 shows a TEM image of an individual multi-walled carbon nanotube: graphite layers are regular and concentric rolling is evident. MWCNTs own metallic properties, which makes them suitable as electrodes.
Purification steps are often used for both types of carbon nanotubes. Nitric acid and sulfuric acid are often used to remove nanotube caps and leave open-ended tubes. Such treatments eliminate metallic impurities and create dangling bonds on the tubes, which allow their further functionalization with oxygenated groups, like quinones and carboxylic groups. The tips and the walls have different electrical and physical properties. The walls are highly hydrophobic, that is why the tubes have the tendency to coagulate in aqueous solution. The ends, instead, often terminate with oxygenated species, which confer quite hydrophilic properties. Due to that behavior, carbon nanotubes are often dispersed in non-polar organic solvents, surfactants or polymer solutions. Wang *et al.* [25] have shown that Nafion, a perfluorinated polymer, is an optimal solubilizing agent for both single and multi-walled carbon nanotubes. Moreover, they demonstrated that Nafion does not affect electrocatalytic properties of carbon nanotubes.

3.1.1 Synthesis

CNT synthesis essentially requires the pyrolysis or thermal decomposition of a carbon source, such as hydrocarbons or carbon monoxide. Metal nanoparticles serve both as nucleation sites for the vapor molecules and as catalyst to reduce the activation energy needed for the decomposition of the hydrocarbon vapor [112]. Arc-discharge evaporation was the first method used by Iijima to produce carbon nanotubes in 1991 [100]. Laser ablation and *chemical vapor deposition* (CVD) are the other two common techniques for carbon nanotube synthesis. Arc-discharge evaporation and laser ablation use solid-state carbon as precursor for nanotube. Growing temperature is typically high, around thousands of degrees Celsius. CVD, instead, takes place at lower temperature, generally 500-1000 °C, using metal catalyst particles as growing starters and hydrocarbon gases as carbon suppliers. The first two methods are able

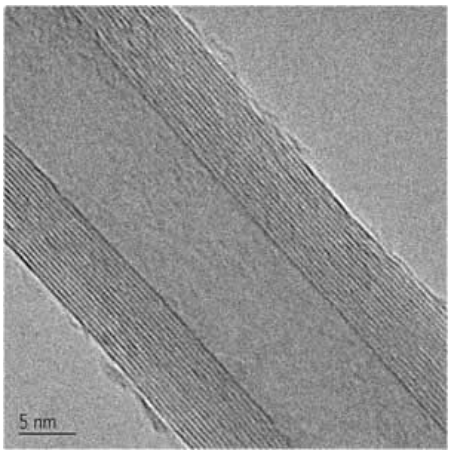

Figure 3.2: TEM image of an individual MWCNTs. Reprinted from *www.nanotech-innovations.com*.

to produce high-quality carbon nanotubes with quite perfect structure, since they are well-established techniques. However, none of the described methods allows to produce SWCNTs with controlled chirality and homogeneous diameters [113].

Arc-discharge evaporation

Arc-discharge produces carbon nanotubes through arc-vaporization of two carbon electrodes enclosed in a chamber, usually filled with inert gas (Argon, Helium, etc.) at low pressure. The graphite electrodes are separated by a gap of the order of millimeters and a voltage around 20 V is applied between the two electrodes; thus, a current of about 100 A is generated inside the chamber. The combination of low-pressure inert gas (typically 600 mbar) and the formation of an electrical discharge (reaching temperature up to 6000 ° C) sublime carbon atoms contained in the graphite anode (solid graphite is directly transformed in gas). At that step, pressure arises and carbon atoms are ejected on the chamber environment, forming a plasma. Then, they accumulate on the cathode as soon as they reach colder zone of the chamber. Nanotube growing crucially depends on the type of metal catalysts at the cathode bulk [114], [115]. If transition metals such as Fe, Co, Ni, and Y are present in the bulk, then SWCNTs are favorable grown at the cathode. In particular, if graphite anode is enriched with pure powdered cobalt, it is possible to produce carbon nanotubes with single-layer walls and quite uniform diameter of 1.2 nm [116]. Otherwise, in the absence of metal catalysts, MWCNTs are the predominant produced species.

Laser ablation

Laser ablation takes place in a quartz tube, filled with low pressure Argon, mounted in a high-temperature furnace (maximum temperature of 1200 °C). A scanning laser beam is focused to a metal-graphite target with 6-7 mm diameter spot. Targets are a mixture of high-

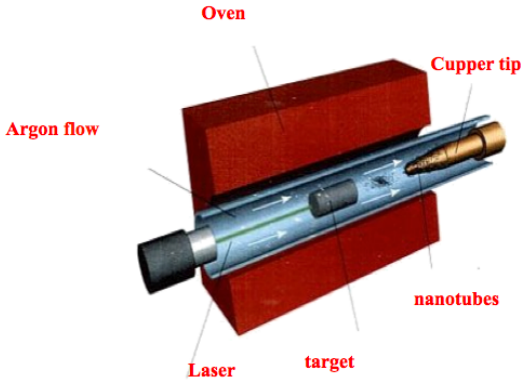

Figure 3.3: Schematic of a general laser ablation apparatus.

purity metal with graphite powder. The laser scans target surface uniformly, to maintain smooth target surface. The soot produced by the laser evaporation is carried from the high-temperature zone to a water-cooled copper collector outside the furnace. A schematic of the laser ablation apparatus is depicted in Fig. 3.3. Direct vaporization allows great control over growth conditions and massive production of carbon nanotubes with respect to arc-discharge technique. The laser ablation method produces mostly SWCNTs with a relatively narrow diameter. They are often arranged in tight bundles over the cold collector, held together by van der Waals inter-nanotubes forces.

Chemical vapor deposition

The CVD synthesis of CNTs occurs in a sealed high-temperature furnace (~ 500 - 1000 °C). A mixture of hydrocarbon (methane, ethylene, carbon monoxide, etc.) and organometallic compounds are used as precursor of carbon nanotubes. The liquid mixture is preheated to a temperature close to 200 °C before entering into the main chamber. As soon as the liquid exits in the furnace, it is immediately volatilized and carried into the reaction zone by Argon flow. The carbon carrier gas nucleates on the surface of the metal particles, which catalyze the dissociation of the carbon gas and the freed carbon atoms arrange in a cylindrical manner to form a nanotube. The furnace is then cooled down to lower temperature (< 300°C), before exposing CNTs to air to prevent oxidation. Purity, chemical structure, and yield can be controlled by playing with furnace temperature, hydrocarbon and organometallic ratio, flow rate, etc. CNTs diameter distribution is often related to particle size distribution, whereas CNT length is dependent of the duration of growth.
Carbon nanotubes are formed on the wall of the furnace and on substrates placed in the chamber [117]. The CVD process can be optimized to produce randomly oriented CNTs as well as horizontally and vertically aligned nanotubes. Plasma-enhanced CVD (PECVD) can facilitate the growth of nanotube forest perpendicular to the substrate, due to the vertical electric field applied in the chamber. Moreover, the plasma allows to decrease the growth temperature, possibly down to room temperature .

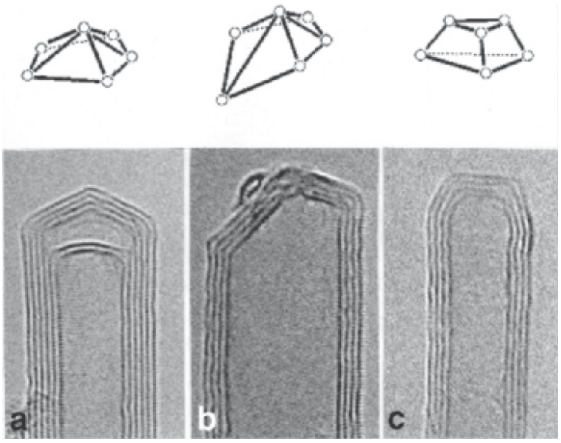

Figure 3.4: TEM images of MWCNTs tip morphologies due to different spatial distribution of pentagons. Reprinted from [115].

3.2 Carbon nanotube properties

In 1991 Iijima described in detail lattice structure of carbon nanotubes by high-resolution electron micrographs [100]. He observed the graphite structure of several carbon nanotubes produced by arc-discharge evaporation. He found that the thinnest tube had an inner diameter of 2.2 nm, corresponding roughly to a ring of 30 carbon hexagons. Therefore, planar bonds of the hexagons on the ring resulted to have smaller angles respect to those of fullerene C_{60} (6° instead of 42°). Iijima also investigated the rotation of individual graphite sheets with respect to the tube axis by electron diffraction patterns of individual carbon nanotubes. Consequently, carbon nanotube properties depends on symmetry of graphene. Since the first description in 1991, CNT properties have been largely examined and described.

3.2.1 Surface properties

High-temperature growing processes are less affected by defects. In fact, graphene crystallinity of the layers strongly depends on synthesis techniques and post-synthesis treatments. High-temperature methods, for example, lead to almost perfect periodic honeycomb structures, while low-temperature synthesis enriches nanotube walls of defects. Carbon rings can present pentagons or heptagons instead of hexagons lattice, which can change the local curvature of the nanotube surface. Tips can also be affected by those defects, leading to hemispheric or conical ends if pentagons are present instead of hexagons. Some examples of the tips are depicted in Fig. 3.4. Defects can also take place along the tube wall and depending on their positions, they can modify tube geometry. For example, pentagons or heptagons located on the same side of the wall can confer localized diameter modifications, whereas if located on the opposite side, they can origin elbow configurations and tube deformations.
Carbon atoms located in the defects are much more reactive than those in hexagonal conformation. Therefore, they can chemically adsorb other molecules and form surface groups or

complex, which can confer different properties to the surface with respect to regular configurations. Surface modification can be induced by intrinsical surface properties, such as defects already present in the lattice, or it can be also caused by chemical or thermal treatments, which artificially add defects in the structure.
Oxygen is by far the most common element present on carbon surfaces and can create different types of functional groups on the surface. Those groups are stable at 25°, whereas they decompose at higher temperature. There are two families of oxygen-based groups that bind with carbon: acid groups and basic groups. Among all the possible functional groups, carboxyl groups (COOH-based) exhibit favorable properties for electrochemical purposes. In fact, Chou *et al.* [118] showed that CNT electrochemistry and rate of the electron transfer are dominated by oxygen-based species at the tips rather than pure carbon structure. Surface groups can be added for further nanotube functionalization or to confer different properties to CNTs. Chen *et al.* [119] described chemical modification of SWCNTs containing COOH groups with *octadecylamine* (ODA) to dissolve them in organic solvent, such as chloroform, benzene, toluene, carbon disulfide, etc.

3.2.2 Surface structure of CNTs

Carbon structure reactivity is primarily dictated by the pyramidalization angles of the carbon atoms. According to the number of atoms surrounding one carbon atom, it is possible to distinguish different configuration. In the case of graphene and its possible arrangements, two configurations are possible: sp^2-hybridized (trigonal) structure and sp^3-hybridized (tetrahedral) structure. The first configuration is planar (graphene) and it does not require pyramidalization angles, whereas the second implies angle of 19.5°. Among those two stable configurations, more pyramidalization angles exist, like the case of C_{60} with pyramidalization angles of 11.6°. SWCNTs are 1-D cylindrical aromatic macromolecules. Pyramidalization angles and misalignment of the π-orbitals induce curvature of the surface and a local strain. That is the reason why carbon nanotubes are expected to be more reactive than a flat graphene sheet.
Carbon fullerene and the side-walls of the carbon nanotubes are both curved, but there are several structural differences which reflect also in their chemistry. First of all, fullerene is curved in 2-D, whereas the nanotubes are curved in 1-D. Thus, carbon binds in fullerene are more distorted than those belonging to nanotubes. Pyramidalization angles for carbon atoms of a nanotube can be of about 3.0°, while the angle of a fullerene with equivalent radius is 9.7°. The strain energy of pyramidalization is almost proportional to θ_P^2 (which is the pyramidalization angle), so fullerene should absorb about 10 folds more the strain energy of pyramidalization per carbon atom than an equivalent carbon nanotube of the same diameter. Carbon nanotubes can be break down into end caps and side-walls. End caps resemble a hemispherical fullerene and their curvature is higher than sidewall curvature. Since it is not possible to reduce pyramidalization angles of any fullerene below 9.7°, it is ensured that end caps will always be more reactive than the sidewalls, regardless of the nanotube diameter.
Despite all the carbon atoms are equivalent, there are two types of bonds: those that run

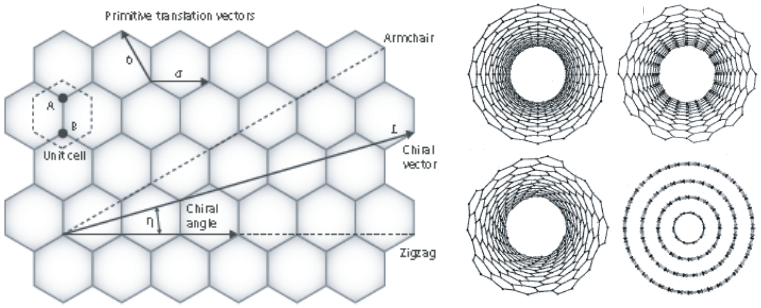

Figure 3.5: On the left: the honeycomb lattice of graphene. The chiral vector is given by $\boldsymbol{L}$, whereas the chiral angle is given by η. Reprinted from [121]. On the right: models of different wrapped sheet of graphene, depending on η. Reprinted from [122].

parallel to the circumference and those at an angle to the circumference with π-orbital misalignment angles. π-orbital alignment is almost perfect in fullere, whereas this is not the case for carbon nanotubes. π-orbital misalignment angles are the main source of strain in the carbon nanotubes and they represent a clear contrast with fullerene chemistry. Pyramidalization angles and π-orbital misalignment angles of SWCNTs scale inversely with the diameter of the nanotube, so a differentiation of CNT reactivity is expected for CNTs with different diameter [120].

3.2.3 Electronic properties

As already discussed in Section 3.1, SWCNTs can behave as metals, semiconductors, or small band-gap semiconductors, depending on their chirality, diameter, and the quantity and type of impurities present in the tubes. Single-walled carbon nanotube is a seamless rolled sheet of graphene wrapped either along one of the symmetry axis (depicted in Fig. 3.5(a) and (b) on the right) or in a way that each unit cell is aligned on a spiral (illustrated in Fig. 3.5 (c) on the right). Zooming on the honeylattice structure of the graphene, it is possible to introduce the vector $\boldsymbol{L}$, which is the chiral vector, whereas η is called chiral angle. A schematic of those vector and angle is illustrated in Fig. 3.5 on the left. The chiral vector can be described by its primitive translation vectors:

$$L = n\mathbf{a} + m\mathbf{b}. \tag{3.1}$$

Therefore, the structure of the nanotube can be described by the set of integers **a** and **b**. As an example, zigzag nanotubes (shown in Fig. 3.5 (a)) have η=0, while armchair tubes have η=π/6.

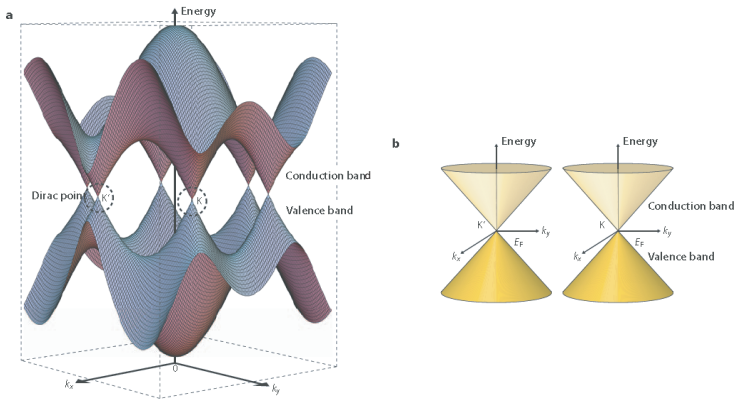

Figure 3.6: Energy bands near the Fermi level in graphene. Reprinted from [121].

Tubes with different η angles are called generally chiral tubes. The (n, m) indices univocally define the chirality and the diameter of the SWCNTs, so then also the electronic properties. If $n - m = 3q$, where q is an integer, then the SWCNT is metallic. Otherwise, if $n - m \neq 3q$, then it is semiconducting. About two-third of all the SWCNTs are semiconductive. [123] [121] The electronic structure of a single-walled carbon nanotube can be simply derived by that of graphite. Energy bands near the Fermi level for graphene structure are depicted in Fig. 3.6. The conduction and the valence bands intersect in 6 corners of the Brillouin zone, called Dirac point (K points). It can be demonstrated that the energy bands of SWCNTs are a set of 1-D cross-sections of those for two-dimensional graphite. N pairs of 1-D energy dispersion relations are obtained, where N is the number of hexagons per unit cell. N can be obtained as a function of n and m as:

$$N = \frac{\boldsymbol{L} \times \boldsymbol{T}}{a \times b} = \frac{2(m^2 + n^2 + nm)}{d_R} = \frac{2l^2}{a^2 d_R}, \tag{3.2}$$

where $\boldsymbol{T}$ is the translation vector, which is parallel to the nanotube axis and normal to $\boldsymbol{L}$, l is the circumferential length of the nanotube, and d_R is the greatest common divisor of (2m + n) and (2n + m). As already mentioned, the N pair of energy dispersion curves correspond to the cross-sections of two-dimensional energy dispersion surface, where cuts are made at a fixed distance depending on the lattice vectors in the reciprocal space. So, if for a given (n, m) nanotube, the cutting line passes through one of the K points depicted in Fig. 3.6, then the one-dimensional energy bands have a zero energy gap. Moreover, the *density of states* (DOS) at the Fermi level has a finite value, meaning that such carbon nanotubes are metallic. On the other side, if the cutting line does not pass through a K point, then the carbon nanotube behaves as a semiconductor, with a finite energy gap between the valence and the conduction band [124].

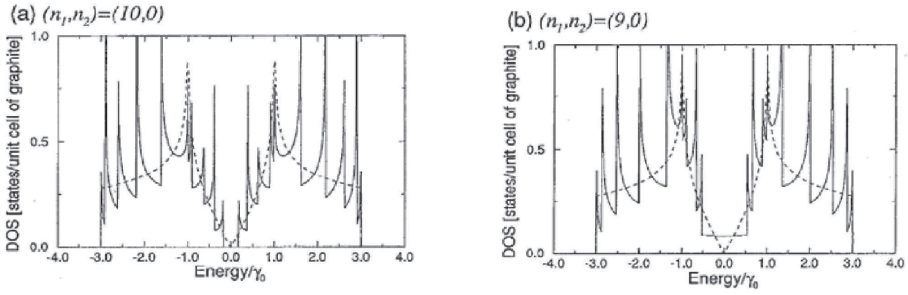

Figure 3.7: Density of states per unit cell for carbon nanotubes with metallic (a) and semiconducting (b) behaviors. The dotted-line refers to the DOS of graphene. Reprinted from [124].

Fig. 3.7 compares the density of states for metallic (9, 0) and semiconducting (10, 0) nanotubes. It is interesting to notice that near the Fermi level, located at E=0, semiconducting nanotubes show a null value, whereas metallic nanotubes have non-zero value. In particular, the energy gap (E_g) of semiconductive nanotubes is inversely proportional to the nanotube diameter (d_t):

$$E_g = \frac{|t| a_{C-C}}{d_t}, \tag{3.3}$$

where $|t|$ is the nearest neighbor C-C tight binding overlap energy and a_{C-C} is the nearest neighbor C-C distance on a graphene sheet. Moreover, carbon nanotube DOS shows several discontinuities, called singularities, that are absent in graphene DOS [124].

3.2.4 Transport properties

As we mentioned in the previous section, the electronic structure of SWCNTs depends both on the orientation of the honeycomb lattice with respect to the tube axis and on the radius of curvature of the graphene sheet. In the case of MWCNTs, the electronic conduction takes place essentially through the external tube, even if the interaction among internal sheets may make vary the electronic properties. Energy dispersion curves can also vary due to the application of a stress to the tube. That is particularly important for carbon nanotube-based composites, when both mechanical and electronic properties have to be take into account.
The conduction of charge carriers in metallic SWCNTs is thought to be ballistic independently from the nanotube length. The electric conductance is predicted as twice the fundamental conductance, due to the existence of two propagating modes. Because of the reduced scattering, current densities up to 10^9 A/cm^2 can be transported without damages. Such values are three orders of magnitude higher than in copper. In case of defects, electrons often localize and charge transport is dominated by tunneling effects.

3.2.5 Electrochemical properties

Ideally, carbon nanotubes should be electrochemically inherent and should not exhibit any voltammetric response in the potential window normally used. In general, CNTs own two kinds of carbon atoms: the tips behave like the edge plan of highly oriented pyrolytic graphite, while the sidewalls resemble the basal plane of highly oriented pyrolytic graphite. The electron transfer of sidewalls and tips will be discussed later in Section 3.4.1. However, CNT fabrication inevitably introduces some impurities, such as metal atoms as defects in the graphite structure, amorphous carbon, and structural defects. Chemical and thermal treatments can increase functional oxygenated groups at the nanotube tips and defects along the sidewall. As a consequence, the electrochemical properties of other compounds, such as ferricyanide, can be enhanced by the presence of these defects. Electrochemical properties can be correlated with the length of the nanotubes and the presence of oxygenated groups at the tips. Li *et al.* [125] observed that in cyclic voltammetry of ferricyanide, the peak current was proportional to the length of the tubes. Moreover, a faster rate of electron transfer could be attributed to the oxygenated ends, apparently allowing a more efficient electron transfer than in edge planes of pyrolytic graphite. Hence, it is valid the hypothesis that electron transfer occurs predominantly at sites where oxygenated species exist.
The conductivity of nanotubes can be increased by doping. In addition to creating functional groups, the acid treatment can result in ion penetration in the centers of the tubes and the alteration of their electronic properties by injecting electrons or holes into the valence or conduction bands of the tubes. Therefore, the electrochemical properties of nanotube are sensitive to the method of tube pre-treatment and purification.
Many studies have reported high electrode capacitances, clearly remarkable from the large separation of the baselines between the anodic and the cathodic scans in cyclic voltammetry. Azamian *et al.* showed that the capacitance at SWCNTs paper electrodes is from three to four orders of magnitude higher than on other carbon electrodes [126]. They divided the capacitive effect in a fast process and in a slow process. The fast process is responsible of the charge of the electrical double layer, whereas the slow process appears to be a pseudocapacitance related to surface Faradaic reactions of redox active oxides. Surface oxides produce distinct redox peaks, which contribute to the apparent capacitance.
Electrodes based on carbon nanotubes show peak-shaped voltammograms like macroscopic electrodes, despite the potential for each nanotube to act as a nanoelectrode. In most cases CNT density is sufficiently high for significant overlap of the diffusion layers to each nanotube, such that the overall diffusion layer approximates to linear diffusion. However, Taurino *et al.* pointed out that horizontal CNTs show a cyclic voltammogram more sigmoidal in shape, similarly to a nano-electrode ensemble [127].

3.3 Strategies for the development of CNT-based electrochemical biosensors

The application of electrodes modified with carbon nanotubes leads to a novel type of electrochemistry, where the favorable electrochemical properties of CNTs can be exploited to enhance sensor performance in terms of sensitivity and detection limit. Such interesting properties can be also combined with the nanoscale dimension of CNTs, which makes them ideal for interacting with biomolecules and proteins.
One of the main problems when handling CNTs is their tendency to aggregate together in almost all kinds of aqueous and organic solutions, due to the intrinsic hydrophobicity of the sidewalls and the van der Waals forces between the tubes. Therefore, it is quite difficult to obtain homogeneous CNT solutions or composites. On the other hand, due to their interesting electrochemical properties, several strategies have been proposed for the immobilization of CNTs on electrodes. Covalent and noncovalent functionalizations are by far the most common strategies for solubilizing and manipulate CNTs. Then, it is also necessary to ensure a stable bonding between such nanostructures and the electrode surface to develop durable biosensors. The following section gives an overview about the main strategies for the preparation of CNT-based electrodes.

3.3.1 Drop casting of random distributed CNTs

The most straightforward strategy to modify electrodes with carbon nanotubes is by drop casting. A drop of the CNT dispersion can be cast onto the surface and let dry before electrode use. So, the main issues to achieve an homogeneous modification are CNT solubility, to have well-dispersed solution, solvent volatility, to avoid residuals after drying step, and solvent chemical inactivity, not to interfere with the electrochemical measurement. Different types of solutions have been proposed typically for glassy carbon and gold electrodes.
Some researches reported the dispersion of MWCNTs in acids. In particular, Wang et al. developed modified glassy carbon electrodes by dispersing MWCNTs in a solution of concentrated sulfuric acid in one case [128] and concentrated nitric acid in another case [129]. The electrodes were let dry at 200° C for 3 h and at room temperature for 30 min, respectively. Surfactants were also proposed as dispersing agent for MWCNTs, like dihexadecylhydrogenphosphate (DHP) [130] and sodium dodecyl sulfate (SDS) [131].
The dispersion of organic solvents have driven by far the research in most of the literature. CNT powder was dispersed in polar solvents such as acetonitrile [132], which can dry in air at room temperature, and dimethylformamide [133], which can be dried under infrared lamp. Non-polar solvents, like bromoform, have been also proposed for the detection of dopamine, for example [24]. Chloroform is another type of non-polar solvent and is often used to disperse MWCNTs. We performed the detection of glucose and lactate in PBS by modification of graphite *screen printed electrodes* (SPEs) with MWCNTs. The powder of MWCNTs is diluted in chloroform to a concentration of 1 mg/ml and the mixture is then sonicated for 30 min to obtain an homogeneous solution [134]. MWCNTs-chloroform solution is stored at 4° C to

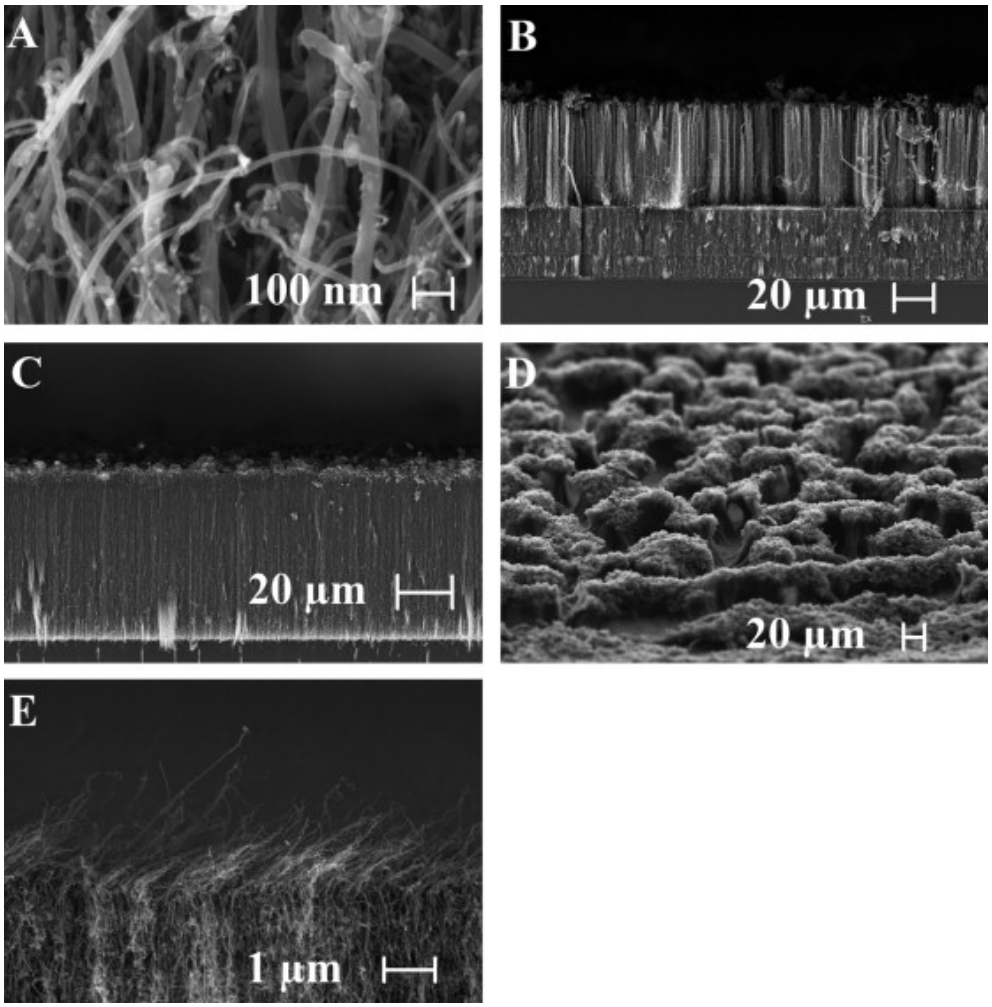

Figure 3.8: FE-SEM image of vertically aligned MWCNTs. Reprinted from [127].

reduce chloroform evaporation. For the preparation of the electrodes, 40 μl of the MWCNT-chloroform solution are deposited by drop casting (5 μl each time) onto the working electrode. Electrode drying is performed at room temperature [134].

3.3.2 Aligned CNTs

As mentioned previously in Section 3.1.1, chemical vapor deposition allows the growth of aligned CNTs [127]. An example of vertically aligned MWCNTs is depicted in Fig. 3.8. The growth can be performed directly onto a silicon wafer, so CNTs are used as pure electrodes, coupled with conductive paints or pastes to guarantee the connections. Otherwise, they can be transferred to a metallic substrate after the growth process [87]. Alternatively, nanotube functionalization with thiol groups permits to align CNTs on a gold surface by self-assembly [135]. Most of the literature on CNTs used for biosensing is based on the assumption that tips are responsible for their electrochemical activity. Gooding *et al.* investigated the electron-

transfer properties of redox enzymes attached to the end of aligned SWCNTs [72]. They found that the rate constant for electron transfer for the redox enzyme on top of the aligned carbon nanotubes was similar to that for redox enzymes directly attached to a modified gold electrode. Tips of SWCNTs do not add any significant electrical resistance.

3.3.3 CNT-paste electrodes

CNT-paste electrodes are typically manufactured by hand-mixing CNT powder with mineral oil to obtain an homogenous paste. Then, the paste can be packed into a micro-cavity connected with an electrical conductor and used as working electrode [136]. The development of CNT-paste electrodes opens the opportunity to new strategies for the fabrication of electrodes. CNT-paste can be also used as an ink to prepare screen-printed electrodes, for example. Wang et al. showed that the developed ink deposited on alumina ceramic plates has a microporous structure of flake-shaped particles non-uniformly distributed [137].

3.3.4 CNT-polymer nanocomposite electrodes

Conductive polymers such as polypyrrole (PPy) and polyaniline (PAn) has been used in the preparation of CNT-polymer nanocomposites. Gao et al. [138] grew aligned carbon nanotube array on a quartz substrate by CVD. Separately, pyrrole monomers were electrochemically oxidized in buffer solution containing GOD and the resulting mixture was used to uniformly coating the aligned CNTs. The developed biosensor was used to detect glucose concentration up to 8 mM. PAn was also used as CNT-based composite for the immobilization of cholesterol oxidase by the electrophoretic technique. The colloidal suspension of PAn-MWCNTs was electrophoretically deposited to form a uniform film on a ITO-coated glass plate, and cholesterol oxidase was then covalently immobilized on the composite film via amide bond formation [139].
A different approach was proposed by Wang et al. [25], where Nafion was used as solvent for well-dispersed CNTs solutions. Nafion is a perfluorinated ionomer widely used to confine electrocatalysts and biomolecules on electrode surface. The difference between PPy or PAn and Nafion is that the latter is an insulating polymer instead of conductive. However, Wang demonstrated that it has an excellent capability to solubilize the CNTs in solution and confine them onto the electrode surface. Insulating polymers can be superior compared to conductive polymers when employing cyclic voltammetry, because the faradaic response for the redox species is more discernable than the charging current. Furthermore, CNTs are highly conductive and their long length makes them more similar to nanowires, which form a uniform matrix across the insulating polymer [110]. An example of MWCNTs dispersed in a Nafion matrix together with GOD is reported by Tsai *et al.* [70]. The working electrode was structured as depicted in Fig. 3.9.
Chitosan (poly(1, 4),-β-d-glucopyranosamine) is a natural biopolymer with excellent properties like biocompatibility, film forming ability, nontoxicity, affinity with proteins, and good adhesion to the chemically modified fabrication. CNTs can be well-dispersed in chitosan and

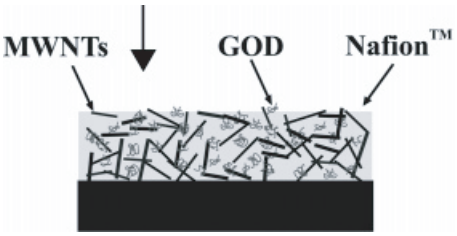

Figure 3.9: Schematic sketch of the MWCNT-Nafion-GOD biocomposite film to modify glassy carbon electrodes. Reprinted from [70].

easily form a uniform film on glassy carbon electrodes. Therefore, chitosan was extensively used for CNT entrapment [140].

3.3.5 Layer-by-layer assembly of CNTs

Layer-by-layer method is based on the alternate adsorption of oppositely charged species from their solution. In the case of CNTs, negatively charged oxygenated groups can be exploited pairing them with positively charged layers to assembly a CNT-based composite. This procedure allows to achieve uniform and homogenous CNT multi-layer films with highly controlled physical and mechanical properties. Several layers can be immobilized by simply repeating the procedure and the number of layers can be optimized to obtain the best performance of the biosensor. Deng et al. [141] described the immobilization of CNTs by alternatively assembling cationic *poly(ethylenimine)* (PEI) layers and glucose oxidase layers. As another example, Wang et al. [142] used *poly(diallyldimethylammonium chloride)* (PDDA) as highly positively charged polymer to disperse SWCNTs. GOD was then adsorbed on PDDA to form a multilayer film on Pt electrodes. They performed an optimization of the biosensor sensitivity according to the number of deposited layers, finding out that seven layers were optimal for this particular example.

3.4 Theory of Carbon Nanotube Emission

As already discussed in Section 3.2.3, carbon nanotubes have considerable field emission properties. Some previous works have shown results on properties of the nanotube tips, for example. Mayer *et al.* [143] proposed a three-dimensional simulation of field emission from hydrogen-saturated open and capped carbon nanotubes. They found that currents extracted from an ideally open carbon nanotube are on average 20 times larger than those obtained from close structures. Moreover, hydrogen saturation of the open structure multiplies the extraction currents by an additional factor of 200. Those results were also confirmed from

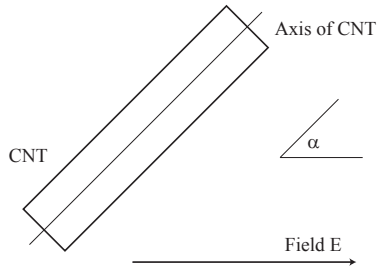

Figure 3.10: Model for a linear segment of CNT. Reprinted from [134].

another group [144]. They also investigated the dependence of the emission on the tube radius, by simulating field emission for single and multiwall carbon nanotubes. The current extracted from singlewall nanotubes was observed to decrease with the radius of the structure. In addition, MWCNTs show better performance as emitters than SWCNTs [73].
The role of the sidewall is presently under investigation. Electrochemical activation of carbon nanotubes results in an introduction of defects into the walls of the nanotubes. These defects lead to a higher density of electroactive sites and, consequently, to increased values of electron transfer rate constant [145]. Taurino *et al.* [127] proposed a comparison among different carbon nanotube orientation in order to investigate the reactivity of tips and sidewalls. They grew three differently oriented CNTs: horizontally MWCNTs randomly oriented, densely packed vertical MWCNTs, and vertically aligned MWCNTs with oriented tilted tips. They found out that horizontally MWCNTs randomly oriented had the lowest current density, due to the poorest exposition of the tips, and the lowest density of the active sites. The introduction of wall defects by acid treatment was more effective on vertically aligned MWCNTs with oriented tilted tips. Moreover, those CNTs showed also the best electrocatalytic activity for ferricyanide and hydrogen peroxide detection.

3.4.1 Emission of randomly dispersed individual CNTs

In the present section, electron emission from both sidewalls and tips is presented [134]. The purpose of this model is to mathematically describe sidewall and tip contribution, prior to perform experiments with randomly distributed CNTs. The developed model needs to consider the arbitrarily oriented carbon nanotubes with respect to the field, where the CNT axis is parallel to the substrate and, therefore, perpendicular to the field E. The developed model is based on the following three assumptions:

1. the electron emission occurs through the CNT-half surface facing the anode;
2. the field E is uniform both in direction and intensity in the neighborhood of the substrate

and of the CNT;

3. the current emitted across the surface σ obeys the Fowler-Nordheim equation considering the projection of E on the normal to σ. In other words, assuming σ as a flat surface, the Fowler-Nordheim equation is

$$I = K_1 \sigma E_\perp^2 \exp\left(-\frac{K_2}{E_\perp}\right), \tag{3.4}$$

where I is the current emitted across σ, $E_\perp$ is the projection of E on the normal to σ, and K_1 and K_2 are suitable constants. Then, if it is considered an infinitesimal portion of the CNT surface, $d\sigma$, the current will be expressed as follows:

$$di = K_1 d\sigma E_\perp^2 \exp\left(-\frac{K_2}{E_\perp}\right). \tag{3.5}$$

Assuming cylindrical coordinates with the axis of CNT as z-axis, whose origin is at one end of CNT, and the direction of E as origin of coordinate ϑ, $d\sigma$ and $E_\perp$ can be expressed as:

$$d\sigma = \rho d\vartheta dz, \qquad E_\perp = E\cos\vartheta, \tag{3.6}$$

where ρ is the radius of the carbon nanotube. By substituting Eq. 3.6 into Eq. 3.5, we obtain:

$$di_S(E) = K_1 \rho d\vartheta dz (E\cos\vartheta)^2 \exp\left(-\frac{K_2}{E\cos\vartheta}\right). \tag{3.7}$$

The total current emitted across the side surface of the CNT is obtained by integrating on the portion of surface of CNT facing the anode:

$$\begin{aligned} i_S(E) &= K_1 \rho E^2 \int_0^L dz \int_{-\frac{\pi}{2}}^{\frac{\pi}{2}} \cos^2\vartheta \exp\left(-\frac{K_2}{E\cos\vartheta}\right) d\vartheta \\ &= K_1 \rho E^2 L \int_{-\frac{\pi}{2}}^{\frac{\pi}{2}} \cos^2\vartheta \exp\left(-\frac{K_2}{E\cos\vartheta}\right) d\vartheta. \end{aligned} \tag{3.8}$$

If the axis of CNT is not perpendicular to the field, but form an angle α (as depicted in Fig. 3.10), Eq. 3.8 changes as follows:

$$i_S(E,\alpha) = K_1 \rho E^2 L \int_{-\frac{\pi}{2}}^{\frac{\pi}{2}} (\cos\vartheta\sin\alpha)^2 \exp\left(-\frac{K_2}{E\cos\vartheta\sin\alpha}\right) d\vartheta. \tag{3.9}$$

Therefore, Eq. 3.9 permits to compute the current at the sidewall of the nanotubes.
In the case of the tips, we will consider the case where the CNT tip faces the anode. The current from the tip obeys the Fowler-Nordhein equation, which can be expressed as:

$$i_T(E,\alpha) = K_1^{'} A (E\cos\alpha)^2 \exp\left(-\frac{K_2^{'}}{E\cos\alpha}\right). \tag{3.10}$$

The entire current emitted by an oriented CNT forming an angle α with respect to the field is

$$i(E,\alpha) = i_S(E,\alpha) + i_T(E,\alpha). \tag{3.11}$$

The above equation can be used to investigate the role of randomly dispersed carbon nanotubes on metallic electrodes. In the experimental activity on biosensors, possible parameter values may be ρ = 10 nm and L = 100 nm, where L is the linear shape of CNTs. The applied field E may range from 100 to 1000 V and the emitted current from 0 μA to about hundred of μA. Therefore, suitable values for the constants that appear in Fowler-Nordheim equations where considered $K_1 = 10^{12}$, $K_2 = 35$, $K_1^{'} = (5/2)*10^{12}$, and $K_2^{'} = 20$, by comparison with experiments performed in vacuum [146]. In case of a wet environment, such as the usual one when dealing with biosensors, the emitted current is further enhanced by the presence of water molecules close to nanotube surface [147].

3.4.2 Monte Carlo simulations

Numerical simulations are performed to obtain the final distribution of carbon nanotubes drop cast on gold electrodes. The simulations are implemented considering Eq. 3.11 and according to the model illustrated in Fig. 3.11. In the case of protein cast on carbon nanotubes,

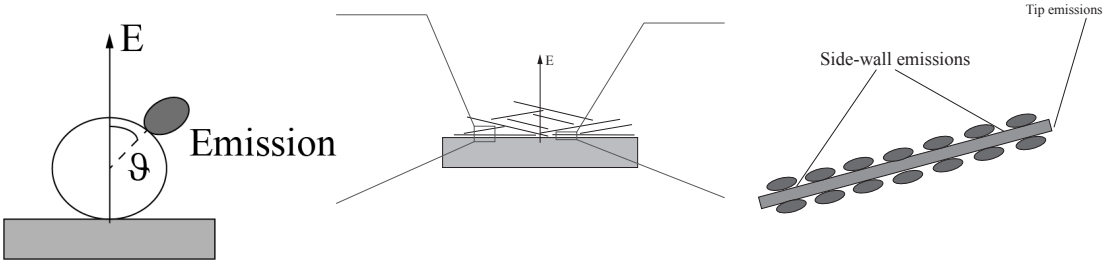

Figure 3.11: Carbon nanotubes randomly organized onto the electrode surface and covered with proteins. Reprinted from [134].

ideally active redox species are in contact with all the available surface of the nanotube. Electron emission toward redox species would happen both from the sidewall and the tip. The electric field is typically normal to the baseline of the electrode. However, metallic and graphite electrodes have a mean corrugation in the 10 nm scale. Thus, the single carbon nanotube is positioned forming a certain angle with respect to the electrode baseline, depending on the region where it was landing. Therefore, Monte Carlo simulations are performed to simulate the landing of each single carbon nanotube onto the electrode surface. The final situation reached by each simulation is similar to the drawing in Fig. 3.11. The figure depicts some carbon nanotubes differently organized onto the electrode surface, each of those presenting a differen angle with respect to the electric field, which is orthogonal to the electrode.

3.4.3 Electron emission from carbon nanotubes

Initial results obtained from Monte Carlo simulations include the angle distribution of CNTs longitudinal axis with respect to the electrode surface. Fig. 3.12a illustrates such a distribution for one of the simulations. The large majority of carbon nanotubes is distributed to lower angles and the number of nanotubes with angles larger than 10° decays very rapidly. Consequently, the sidewall emission decreases with the increasing angle of the nanotubes. Fig. 3.12b shows that decay in the sidewall current is almost linear in a logarithmic scale, confirming first-order approximation of the sinus in Eq. 3.9, while the tip current follows a quadratic shape coherent with first approximation of the cosinus in Eq. 3.10. It is interesting to note that sidewall contribution to the total current is larger than tip contribution by orders of magnitude, even if current density is higher from the tip. Simulations shown in Fig. 3.12b allow to conclude that the tip emissions in drop cast CNTs are not negligible although the large majority of carbon nanotubes presents angles below 10° with respect to the substrate [134].

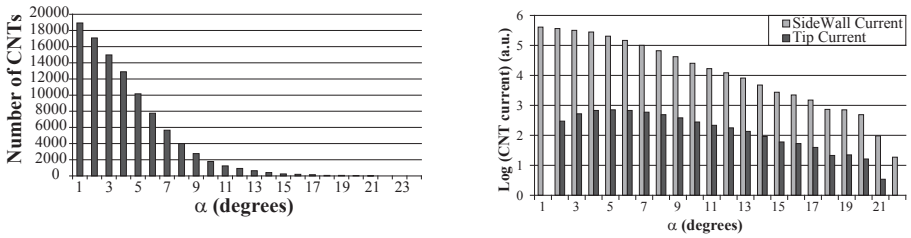

(a) Results from Monte Carlo simulation for the distribution of carbon nanotubes into a flat-surface.

(b) Results from simulation regarding emission current from carbon nanotubes comparing the sidewall and the tip components.

Figure 3.12: Distribution of drop cast carbon nanotubes and emission current. Reprinted from [134].

3.5 Protein Electron Transfer on Carbon Nanotubes

As already discussed in Section 2.1.2, enzymes and co-factors can be used as probes to detect both endogenous and exogenous molecules. In particular, the family of oxidases covers a quite wide range of metabolites, like glucose, lactate, glutamate, cholesterol, etc.
Many redox-enzymes host the co-factor *flavine adenine dinucleotide* (FAD) in their active site, that is why they are also called flavoproteins. The molecule consists of a riboflavin complex plus an *Adenosine Diphosphate* (ADP) molecule, as depicted in Fig. 3.13a. When FAD is bound to a protein, it can exist in three states. The quinone form is fully oxidized (Fig. 3.13b), semiquinone form accepts one electron and one proton, and the hydroquinone form accepts two electrons and two protons. However, only the first and the last configurations exist in aqueous solutions. Flavine adenine dinucleotide is a complex present in glucose and

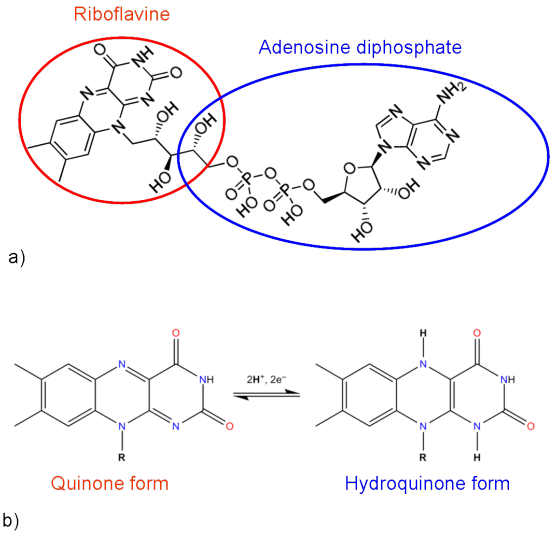

Figure 3.13: Molecule structure of flavine adenine dinucleotide.

glutamate oxidases, as illustrated in Fig. 3.14a and 3.14c. From the picture it can be notices that flavin groups are deeply buried in the protein shell, so the active site is not so accessible. Lactate oxidase, instead, has a slightly different prosthetic group called *flavine mononucleotide*

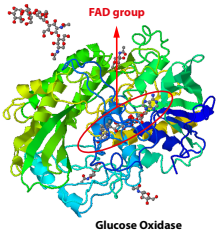

(a) Protein structure of glucose oxidase.

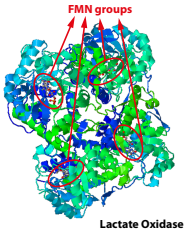

(b) Protein structure of lactate oxidase.

(c) Protein structure of glutamate oxidase.

Figure 3.14: Protein structure of oxidoreductase and prosthetic group locations. Images reprinted from *www.rcsb.org*.

(FMN) (refer to Fig. 3.14b), that takes part in both one or two electron transfer, as well.

3.5.1 Mediated electron transfer

The straightforward scheme to model protein electron transfer foresees just to have the enzyme laying on the electrode surface and a direct electron donation/reception. Naturally, the prosthetic group of many enzymes needs to be “recycled” once the oxidation/reduction

reaction takes place. The prosthetic group regeneration is usually performed by a co-substrate, like molecular oxygen or NAD^+. Those complexes play the role of **electron transfer shuttles** between the protein and the transducer.
Detection can be achieved either by measuring co-factor depletion (for example Clark-oxygen electrodes [53]) or by sensing current change after substrate addition under a proper working potential. Biosensors based on these principles are mentioned as first-generation biosensors. In this case, the main issue is enzyme immobilization on the transducer surface in order to preserve long-time stability of the sensor. A variety of diverse approaches have been proposed in literature, including fixation in membranes [148], entrapment into polymers [149] and sol-gel [150], mixing into a carbon paste [151], cross-linking with glutaraldehyde [152]. The drawback is that enzyme "recycling" is limited by co-factor availability. In the case of co-factor depletion measurements, instead, the key-condition to achieve accurate measurements is the dependence of sensor response to O_2 concentration in the environment surrounding the biosensor itself. Due to all these complications, research has moved to second-generation biosensors.
Natural co-factors are replaced with artificial redox mediators, that allow in some cases to decrease the working potential and chemical interferants. Suitable redox mediators should have fast electron transfer kinetics to compete with O_2 reduction in the enzyme regeneration. In the simplest configuration, artificial redox mediators, such as ferrocene derivatives and quinones, can be added freely in the solution and act like electron transfer-shuttles. Redox catalysts can also work together with co-factors: the mediator can be covalently bound to the enzyme (for example, dehydrogenase), while co-substrate NAD^+ is free to diffuse in the sensor environment. The diffusion of the redox mediator is a key condition for an optimal electron transfer. Two alternative mechanisms can be distinguished when dealing with redox mediators and free-cofactors, besides the electron transfer-shuttle mechanism:

- **electron-hopping**: the overall electron transfer processes can be divided into a sequence of electron exchanges between adjacent redox mediators, which can be covalently bound to a matrix (refer to Fig. 3.15).

- **seaweed and whip mechanism**: the redox mediator can be covalently attached either to the electrode surface (seaweed mechanism) or to the outer surface of the enzyme itself (whip mechanism).

Mediator and enzymes can be also integrated in the electrode paste, especially in the case of carbon-based biosensors. Carbon paste can be mixed with the mediator, but also with the enzyme, even if it is preferable to have the enzyme on top of the electrode. The disadvantage is the long-term stability of such biosensors, due to a leakage of the mediator from the paste. Another strategy presented in literature concerns the so-called electro-enzymes, where the co-factor is directly bound to the protein itself. Such structure is supposed to shorten the electron transfer distance between the active site of the enzyme and the mediator, allowing an electron-hopping mechanism via the binding that can work fast if the complex is close to the

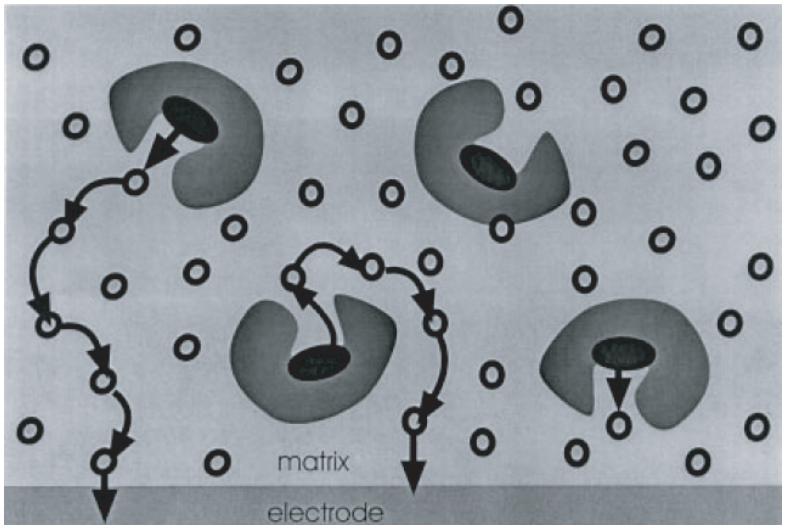

Figure 3.15: Electron-hopping mechanism in a mediator-modified immobilization matrix. Reprinted from [153].

electrode surface.
Last example foresees to "engineer" polymers to bind the redox complex to the polymeric matrix, and afterwards immobilize the enzyme into the matrix. Redox polymers and hydro-gels have been extensively described in literature [154] [155] [156].

3.5.2 Direct electron transfer

Direct electron donation/reception is highly desirable, but we have already seen that protein shell plays the role of a barrier and direct electron transfer via tunneling mechanism is rarely encountered. However, some strategies have been developed in the last 20 years to achieve direct electron transfer. Some main conditions should be taken into account when designing third-generation biosensors:

- the electron transfer-distance between the redox protein and the electrode surface has to be as short as possible, or at least, the electrode architecture should have predefined electron transfer-pathways interconnecting the redox site within the enzyme and the electrode surface;
- the protein should be directly adsorbed on electrode surface and working, avoiding denaturation phenomena of the enzymes;
- direct electron transfer is only possible with the first monolayer of adsorbed proteins, since they limit the electron transfer-pathway for further protein layers laying on top;
- the orientation of the protein and the prosthetic group facing the electrode may drastically increase the rate of direct electron transfer. The isotropic adsorption of the enzyme

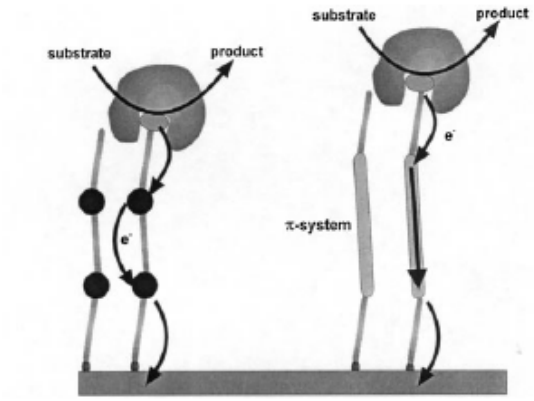

Figure 3.16: Possible design for "molecular cables"-based biosensors through SAM. Reprinted from [153].

molecules in the first monolayer leads to a partial contribution to the sensor signal;

- direct electron transfer should occur at the redox potential of the prosthetic group itself.

According to the aforementioned constrains, several solutions have been proposed. *Self-assembled monolayers* (SAMs) can be used to prevent protein denaturation while adsorbing on the electrode surface, but they can also help for an oriented immobilization of the enzymes. In an optimal configuration, high molecule concentration at the first monolayer can dramatically contribute to the current signal. SAM-modified surfaces can be used for the formation of enzyme monolayers, but also for new sensor architectures based on electron transfer cascades. When protein adsorption is not possible, conductive relays and oligomers can be used as "molecular cables". The overall electron transfer distance is then subdivided in short segments through SAM immobilization (see Fig. 3.16). Direct electron transfer can be also optimized through the entrapment of enzymes in conducting materials. Such immobilization matrices actually increase the electrode surface, allowing enzyme molecule entrapment also far away respect to the electrode surface, without preventing their contribution to the final electron transfer reaction. This strategy is much more important in the case of miniaturized electrodes, since shrinking the transducer surface leads to dramatically decrease the number of immobilized enzymes. The entrapment of enzymes into various conducting materials like sol-gel composite and polymers has been extensively exploited. Random distributed carbon nanotubes can be definitely considered as a conductive matrix with optimal properties for protein immobilization.

3.6 Chapter contribution and summary

In this chapter carbon nanotubes are introduced with a particular emphasis on their role in the development of electrochemical biosensors. CNTs are graphene sheets rolled along a lattice

vector of the sheet. Thanks to their extraordinary electrical, chemical, and physical properties, they have been used in diverse application, like the development of new materials or used to design new electrical devices. Especially metallic carbon nanotubes exhibit attractive properties suitable to develop electrochemical biosensors. Indeed, they are electrochemically inherent and chemical and thermal treatments can increase the number of functional groups, which enhance their electrochemical properties. In addition, the conduction of charge carriers in metallic CNTs is thought to be ballistic. The combination of functional groups and conducting properties impart really interesting electron transfer properties to CNTs.
The modification of electrodes with carbon nanotubes and their combination with proteins lead to novel types of electrochemical biosensors. In this chapter a novel model of the electron emission of sidewalls and tips is presented. The emitted currents from both CNT zones are computed and a general equation of the emitted current for randomly dispersed carbon nanotubes is formulated. Afterwards, the emitted current is calculated in the case of random dispersed CNTs according to Monte Carlo simulation, to model the realistic case where carbon nanotubes are drop cast onto the electrode surface. The chapter concludes with an overview on the mechanisms of electron transfer between carbon nanotubes and proteins and the presentation of some possible scenarios of enzyme immobilization.

4 Fabrication of the Multi-Sensor Platform

The *on-line* and real-time detection of metabolites in cell culture requires many heterogeneous building blocks: the electrochemical cell, typically with three electrodes; the biological recognition element, to ensure detection selectivity; the electronics, for carrying out measurements; the fluidics, because such biosensors cannot be kept in direct contact with cells. Different technologies are required to fabricate and assemble all these components together, and sometimes conventional techniques are not suitable for this purpose, especially in the case of miniaturized systems.
Disposable electrodes are by far one of the most popular strategy, coupled with electronics, to develop point-of-care devices and, more in general, electrochemical biosensors. Although disposable electrodes offer several advantages when dealing with end-point measurements, monitoring of biological processes requires a higher degree of integration for the development of *on-line* systems, that can perform less invasive measurements for longer time. Thus, system miniaturization becomes highly important and conventional approaches, like disposable electrodes, are a bottleneck for decreasing the size of the system. A potent approach to address this limitation is the integration of all the components described before with the electronic portion of the system. A benefit of integration is better performance with respect to signal-to-noise ratio, especially favorable when dealing with biological signals, that are typically weak and noisy. High-density arrays of biosensors and multiple detection can be achieved by reducing the sensor area with microfabrication technologies for *Microelectromechanical Systems* (MEMS). System miniaturization decreases also the response time and requires smaller samples. Thus, system integration and scaling strategies are key issues for self-contained biosensors.
In the following chapter, we will discuss system integration for a self-contained device with multiple working electrodes for the real-time detection of metabolites. Section 4.1 will introduce in general the principles and the equipment of the *Complementary Metal-Oxide Semiconductor* (CMOS) processing steps related to our microfabrication. Then, in Section 4.2 we will describe the process outline for our microfabrication and the parameters used in every step. Lithographic techniques are used to transfer the pattern of the electrodes and the pads onto silicon wafers. Thin film technologies for metal deposition is employed to realize the five working and the counter electrodes in gold, while the reference electrode is in platinum.

The oxide layer is used to insulate electrical connections and obtain controlled electrode area. We will also present solutions to overcome some problems encountered during our microfabrication. Surface electrode modification by using carbon nanotubes and enzymes is discussed in Section 4.3. Ultra-low volume dispensing is originally developed for DNA and protein drop cast. We will adapt this existing technologies for the deposition of carbon nanotubes and enzymes onto our working electrodes. Finally, Section 4.4 will describe our strategy to measure pure cell culture medium *on-line* with a sampling method as less invasive as possible. We will mold a *polydimethylsiloxane* (PDMS) chamber on top of the silicon chip, connected to a microdialysis probe and to a peristaltic pump, to ensure the continuous *on-line* sampling of culture medium.

4.1 Microfabrication processes

Research on MEMS has remarkably progressed in the past three decades, thanks also to the manufacturing advancements in the IC industry. MEMS developments often tracks technological advances in the IC industry and CMOS technology. Many microfabrication processes are available for the development of MEMS. Lithography (E-beam or light-based), thin film deposition, etching processes are the main steps used for MEMS development. Some of those facilities are also available at the *Center for Micro- and Nanotechnologies* (CMI) at EPFL. CMI is mostly dedicated to the fabrication of MEMS and microelectronic devices and structures. CMI offers several working areas in a class-100 environment, but also some zones in class-1'000 and 10'000, for less restricted processes. Those environments offer optimal conditions for microelectronic applications, avoiding possible sources of contamination. Moreover, some of the equipments are uniquely dedicated to microelectronic-compatible technologies. MEMS processing can require the deposition of some metallic films in early stages of the process flow, like in our case, and metallic thin films may contaminate high-temperature furnaces. Thus, microelectronic-compatible equipments dedicated to poly-Si deposition and oxide growth are kept separated to avoid any metallic or organic contamination.
Typically, MEMS fabrication is the result of a sequence of microfabrication steps. The general procedure when dealing with microfabrication, and also in the case of processes at CMI, foresees to define a **process flow**, which describes all the required processing steps for the microfabrication. The process flow helps the user to define the best strategy for the microfabrication by checking the feasibility of the processing steps together with a staff of experts and the equipment compatibility, according to the substrate to process. Process flow details also the dimensions of the structures and the thickness of the layers. It is typically a graphic presentation of a section of the wafer with detailed deposited, grown or etched layers, according to the different processing steps. The specific process flow for our microfabrication is reported and described in Section 4.2. When the process flow is defined and accepted, the user can also compile the **run card**, which refers to the process flow and has to be followed through all the processing steps. In the run card there are all the detailed parameters used for each step, such as working temperature, pressure, exposure time, etc.

The following section aims to give a general overview about processes used for the microfabrication of our self-contained platform, while in Section 4.2 we present the process flow and the run card specifically designed for our microfabrication. During this research work we have developed three designs, trying to address some encountered problems. The first design we developed was based on squared electrodes. In Section 4.2.6 we will then discuss all issues related with this design. The second version was instead conceived with round electrodes. A Cr stick layer was used to enhance the adhesion of metal film with SiO_2. However chromium needs more processing steps to be etched, so we moved to the final solution, which is the one described in Section 4.2.

4.1.1 Photolithography

Photolithography employs a light source, an optical projection system, and a mask. Both masks and wafers can be covered by a photoresist film, prior to be lithographically processed. The photoresist typically consists of a mixture of organic polymers, combined with photosensitive additives. Photolithography belongs to the more general family of lithographic techniques, which are classified according to the source light used for the exposition. E-beam lithography, for example, is based on a focused beam of electrons, deflected by an electromagnetic system, that scans across the substrate surface. The beam is only deflected to the areas where it needs to pattern the resit. E-beam lithography allows us to reach resolution as low as 20 nm and the pattern to transfer is defined through software mask.
Photoresist is designed to change solubility due to UV light exposure. Two types of photoresist are available, depending on the required application: *positive photoresist* increases its solubility when exposed to UV light, so the exposed areas can be removed afterwards, while *negative photoresist* decreases its solubility when light irradiates the exposed area. The chemistry of such materials allows an extremely high contrast, exhibiting sharply-defined features down to 800 nm, depending on the light source (laser or UV light). Photolithographic methods include direct-write lithography, used for mask fabrication, and soft-contact lithography, used to transfer a pattern designed on a mask onto wafers. Depending on feature dimensions to transfer, the direct-write can be accomplished by a laser source (low resolution) or by electron beam (high resolution). For our microfabrication process we use laser lithography, so the next paragraph will describe the direct-write by means of a laser beam.

Direct-write laser lithography

Masks are typically produced by direct-write lithography. Masks consists of a support plate, usually made of glass or quartz, a thin film layer of chromium, and a photoresist spin coated on top. The mask can be processed with an optical pattern generator, based on fast laser scanner. The laser directly writes on the photoresist film, transferring the pattern to reproduce through the software. The laser can be generated by solid state diodes for a resolution above 1 μm, or by kripton gas, when it is necessary to achieve resolution below the μm. At the end of the scanning, the photoresist on top of the Cr film is developed and the areas exposed to

the laser are removed. Then, wet etching of chromium is performed in correspondence of the zones where the photoresist is removed. Cr etching can be performed with a mixture of perchloric acid and ceric ammonium nitrate. Thus, the mask results in an alternation of transparent and opaque regions, forming the desired pattern. Chromium has the advantage to be opaque to UV light, so masks can be then used for soft-contact lithography.

Soft-contact lithography

Masks are used to transfer the desired pattern onto the surface of the photoresist layer. Soft-contact lithography permits to produce a 1:1 image by using an optical projection system. Photoresist is spin coated onto wafer surface with a thickness that depends on the used photoresist, the desired resolution, and the successive steps. Once the photoresist is deposited, the wafer is placed in a contact aligner, consisting of a UV light source for exposure, a microscope, a wafer holder, and a mask holder. Masks and wafers can be aligned through alignment markers, usually designed also in the mask pattern. The alignment is accomplished by rotating and displacing the wafer relatively to the mask. Once aligned, wafer and mask are placed in closer proximity or full contact for the exposition. The image is then transferred from the mask to the photoresist layer. Light intensity, power, and exposure time strictly depends on the photoresist and feature dimensions to transfer on the wafer.

4.1.2 Thin film technologies

Thin film technologies involve the deposition of thin layers of some materials, such as metals and insulators, onto the wafer surface. CMI offers three main strategies to deposit metals and insulators: evaporation, sputtering, and electroplating. The first two methods will be used to fabricate our chip and they will be explained in detail. In particular, physical vapor deposition is one among several other techniques belonging to the evaporation technologies. Electroplating is part of the more general family of electrochemical techniques. Electrochemical deposition involves the reduction of metal ions from aqueous, organic, or fused-salt electrolytes. An external power supply provides the electrons for ion reduction. The general setup of an electrochemical deposition cell foresees two electrodes immersed into an electrolyte. An electric current is applied between the electrodes and the reduction takes place at the cathode, while oxidation occurs at the anode. A thin film of the metal results to be deposited onto the cathode. Thick film of some μm can be deposited by using this technique.

Physical vapor deposition

Physical vapor deposition (PVD) relies on the physical transfer of metal atoms from a metal source to a wafer substrate. Evaporative deposition belongs to physical methods for the deposition of thin metal film. The metal is heated sufficiently to create a vapor, which diffuses and recondenses in solid form on other surfaces. The evaporation chamber is usually under

vacuum conditions (10^{-5} mbar) to create a high-purity process environment. Moreover, due to vacuum conditions, the metal vapor tends to follow a straight path, leading to very directional deposition. Despite the heating of the metal, the wafer substrate is typically at room temperature. Wafer are usually mounted upside-down on a hemispherical chamber ceiling and they are rotated during the deposition process to improve uniformity. The solid metal to be deposited is hosted in a ceramic crucible. A *Quartz Crystal Microbalance* (QCM) is usually mounted inside the chamber to monitor the deposition rate. Thickness from 10s to 100s of nanometer can be achieved by PVD.

RF sputtering

Sputtering is a physical process where accelerated ions interact with atoms of a solid target in a potential gradient environment. During the bombardment, the energized atoms are extremely volatile and spread out as a vapor to land all around and on the sample substrate. The sputtering process requires a vacuum environment with pressure around $5*10^{-7}$ mbar. The bombardment gas, usually Ar, is introduced to the chamber and ionized into Ar^+ by applying bias voltage between the anode and the cathode. Sputtering can be performed by using a *direct current* (DC) or an *radio frequency* (RF) power source. To uniform the film deposition, mechanical movement can be applied during sputtering process, such as rotation of the substrate holder. Ar^+ ions knock out atoms from a solid target, which spread out as a vapor and land all around, including on the sample substrate. RF sputtering systems also require a DC bias voltage to generate Ar^+ ions. However, the major driving force acting on the Ar is exerted by the alternating current source (typically at 13.56 MHz). Because alternating current can flow across dielectric materials, RF sputtering systems can deposit not only on electrically conducting materials, such as metals, but also dielectric materials, such as SiO_2 without charging effects.

4.1.3 Etching technologies

Etching process consists of the systematic removal of material by using a liquid etchant or via physicochemical methods. In the first case we talk about *wet etching*, while in the second case we refer to *dry etching*. Etching may involve chemical reduction-oxidation reactions. The main parameter in etching process is the etching rate, which can be enhanced by increasing the concentration of the reactants or the temperature, or by mixing the bath. Etching can be isotropic or anisotropic, depending on the used method. In the following section we detail wet etching and *Deep Reactive Ion Etching* (DRIE) for SiO_2 thick film as examples of wet and dry etching, respectively.

Wet etching

Etching process is generally carried out in wet benches, where tanks of liquid etchant can host one or more wafers in vertical orientation. They can be also equipped with heater, thermocouple, refilling system, and agitator. The tank is typically installed under chemical hood to avoid the dispersion of toxic vapors. Close to the etch tanks there are also rinsing tanks filled with deionized water to clean the wafers after etching procedure. Wafers are generally transferred manually from the etch bath to the rinse bath. Silicon dioxide etches well at room temperature with hydrofluoric acid (HF) mixed with water or with a buffering agent (BHF), such as ammonium fluoride, to regulate the ionic concentration of HF_2^- in the etchant and provide uniform etch rates over long period of use. Oxide etch rates vary significantly with etchant concentration. Deionized water is used for rinsing the etchant from the wafer surfaces. The pH and the resistivity of the water can be monitored to ensure a perfect cleaning.

Dry etching

Dry etching processes include reactive ion etching, plasma etching, chemically assisted ion beam etching, ion milling, and gas phase chemical etching. We describe plasma etching as an example. It consists of an *Inductive Coupled Plasma* (ICP) source, a diffusion chamber, a substrate holder, and an *End Point Detection* (EDP) system. The ICP source is made of an antenna connected to the RF power supply and wrapped around an alumina cylinder. The RF current induces an electromagnetic field in the alumina cylinder and the inelastic collisions between hot and neutral electrons give plasma. The plasma moves then in the diffusion chamber, which is surrounded by permanent magnets to limit wasting of charged particles on the wall and keeping a better plasma density. The substrate holder is placed in the diffusion chamber, so while the ICP source is powered, the substrate holder is grounded. Accelerated ions from plasma are directed towards the substrate at the desired energy, which is controlled by the supply power of the substrate electrode. Reactive plasma consists of two kinds of species: ions and radicals. Radicals are electrically uncharged species that reach the substrate, bond to the surface, and react readily with the material to etch. If the reaction takes place instantaneously and the volatility of the products is high enough, the interaction results in an isotropic etching. Instead, charged ions contained in the plasma are entirely responsible for the anisotropic etching. Finally, etching process can be monitored by an EDP system. EDP is based on laser interferometry that can measure transparent films etch rate, such as SiO_2 and Si_3N_4, during etching process [157].

4.2 Process flow

As already discussed in Section 4.1, for every microfabrication process it is necessary to define the process flow. Our purpose is to develop an integrated electrochemical cell with multiple working electrodes. Silicon wafers are chosen as substrate for metal and oxide deposition, not to preclude the possibility of manufacturing the integrated electronics and the electrodes

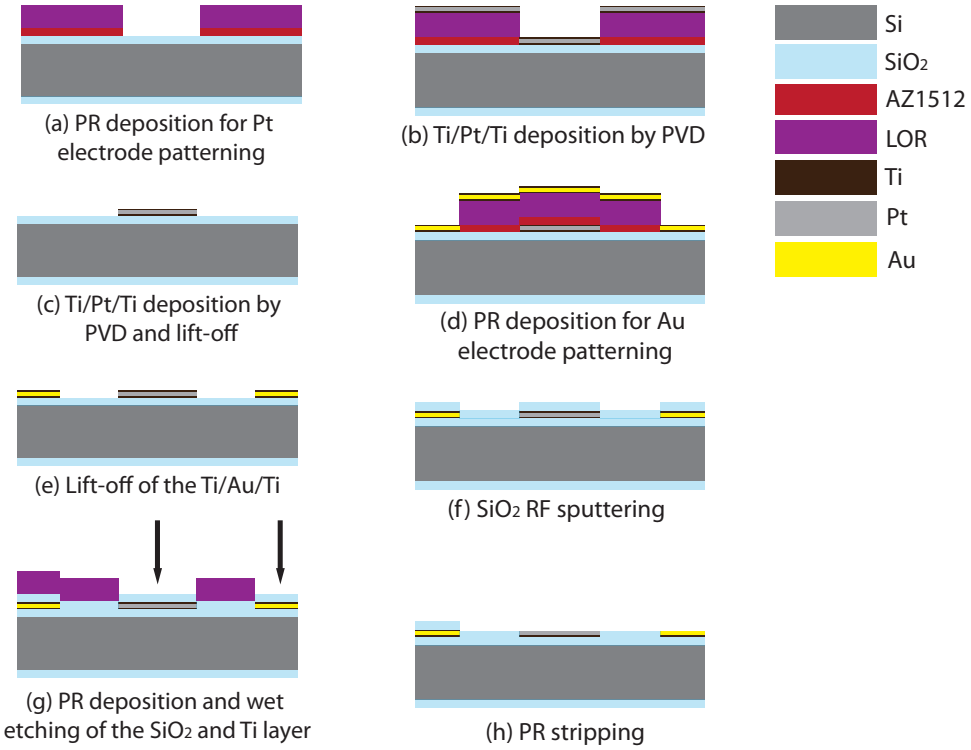

Figure 4.1: Process flow for the microfabrication steps of the electrochemical cell with multiple WEs.

with the same microfabrication process. A thin film of 500 nm is grown on top to uniform the Si surface and to have a good insulation layer to deposit our metals on top. This section goes through all the steps required for the microfabrication of our platform, following the process flow illustrated in Fig. 4.1. The detailed process parameters, the used equipment, the thickness of every layer are instead described in the run card. However, mask fabrication is not reported neither in the process flow or in the runcard. Our microfabrication process requires three masks: the first is used for the Pt electrode structuring, the second for the Au electrode patterning, and the last one is used to open the passivation layer next to the electrodes and pads, while keeping the SiO_2 over the electric connections. The process flow reported in Fig. 4.1 is related to the last version of the chip. In the course of this project, we have tested couple of strategies for the realization of the integrated platform. In the first run we designed squared gold working electrodes. We noticed that border effects arise from sharped angles and reduce the active area of the electrode, so we chose to design round electrodes. Another issue we encountered regards the adhesion between the passivation layer and the gold connections. We have tested both Cr and Ti as adhesion layers for the SiO_2. The first and second designs of the chip and the solved issues are briefly discussed in Section 4.2.6. The microfabricated electrochemical cell is conceived with five working electrodes. For the present research we have characterized the detection of three metabolites, like glucose, lactate, and glutamate. As future work we can think to use the remaining two electrodes for glutamine and hydrogen

peroxide, as well. Glutamine detection is straightforward, since it can be indirectly sensed by glutamate oxidase, as already discussed in Section 2.2.1. Hydrogen peroxide, instead, can be detected on CNT-based sensors or by peroxidase, another enzyme quite similar to oxidases, and its evaluation can be fundamental to measure oxidative stressors, as mentioned in Section 1.1.

4.2.1 Mask design

The masks available at CMI are glass substrates with Cr plus photoresist films on top (5"x5" Cr-blanks). Mask fabrication is performed with direct-write laser lithography by using the *Heidelberg DWL200*. The input file required by the lithographic system is a CIF or a GDSII file, which maps the layout designed with any layout editor, like *Virtuoso* by *Cadence* or *L-Edit* by *Tanner EDA*. We chose the latter editor to draw the mask layout, because it offers a user-friendly interface and easy functionalities. *L-Edit*, as also the majority of layout editors, is centered on cells, which are the fundamental building blocks at all levels of hierarchy. The final design is a collection of cells, that can be also individually replicated or form further cells when grouped. We need three mask layouts, so alignment markers has to take into account the chronological order of use. CMI staff offers templates for the correct design of the masks. Alignment markers are included in the template on the two sides of the mask layout. Cross markers are also available for the dicing and their thickness already take into account the thickness of the saw blade. Another template is also available to add text for mask labeling. A picture of the three developed masks is illustrated in Fig. 4.2. Fig. 4.2a reports the mask used for the Pt electrodes. All the dark parts will be transferred on the wafers, corresponding to the areas where the photoresist will be not removed after the development, while the white parts correspond to the zones where the Pt will be deposited. Fig. 4.2b illustrates the layout related to Au electrode patterning. This mask needs to be aligned with the previous structures on the wafer before exposition. Proper alignment markers are designed on the two sides of the masks and they need to be superimposed to the markers reported on the wafer during alignment procedure. Finally, Fig. 4.2c is related to the SiO_2 opening next to the electrodes, while connections between electrodes and pads remain covered by the passivation layer.
The laser lithographic system has both Kr laser source and solid state laser diode. Since the smallest feature of our final design is above 100 μm, we chose the latter as laser source with 10 mm head. After writing step, photoresist on top of Cr film has to be developed by using the *Süss DV 10*. The chromium is subsequently etched in wet bench by dipping masks in a mixture of perchloric acid and ceric ammonium nitrate, and photoresist is eventually stripped by using the *Remover 1165* by *Shipley Microposit*. Masks are carefully rinsed with deionized water and let dry overnight under chemical hood. Afterwards, they are ready to be used for soft-contact lithographic processes.

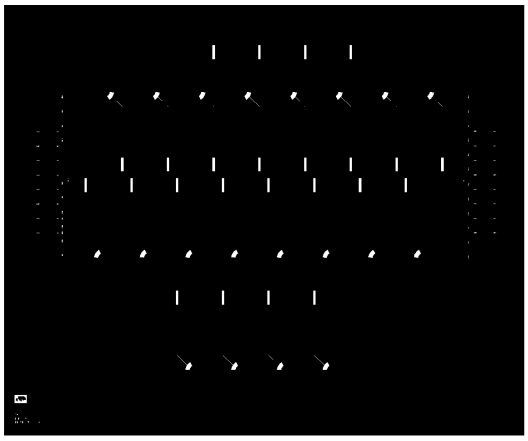

(a) First mask for the Pt reference electrode structuring.

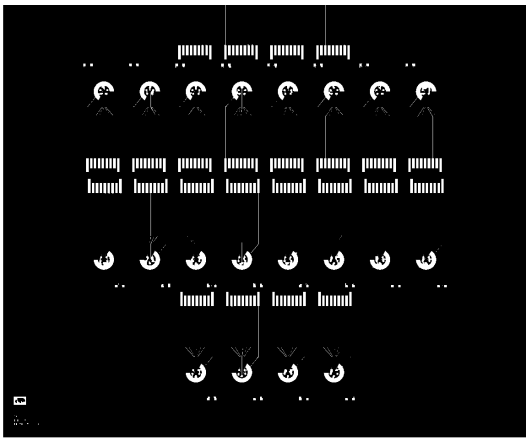

(b) Second mask for the Au working electrode patterning.

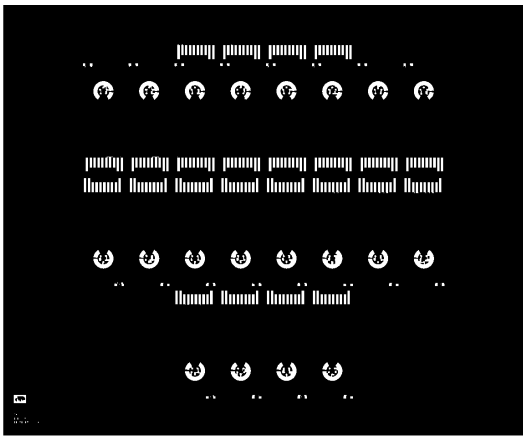

(c) Third mask for the SiO_2 opening.

Figure 4.2: The three mask layouts for our self-contained platform.

4.2.2 Pt electrode structuring

Electrode structuring with platinum is performed in three steps: soft-contact photolithography, metal evaporation, and lift-off. In the first version of our chip we fabricated the reference

electrode in silver instead of platinum. However, since silver tends to oxidize over the time, we decided to choose platinum as an alternative material, due to its chemical stability and also because from the electrochemical point-of-view H_2O_2 detection can be performed at the same potential.

Photolithography

We used a stack of two resists, *Lift-Off Resist* (LOR) and AZ1512 by *MicroChemicals*, for lift-off step. LOR is a polymer, based on polydimethylglutarimide, which dissolves in an alkaline solution. It is used as a sacrificial layer, because it can be etched with standard developers by extending the development time of the top resist (the AZ1512 in our case). Both the sacrificial layer and the photoresist are successively spin coated with the *EVG150* by EVG. Before the coating, wafers need a dehydration step in the oven at 180 °C for minimum 15 mins. *EVG150* has already a pre-saved list of recipes suitable for any type of resist or layer that can be spin coated. LOR is deposited with a thickness of 400 nm on bare Si wafers. Afterwards, AZ1512 photoresist is spin coated with a thickness of 1.1 μm on top of the LOR layer. Coated wafers are then exposed in *Süss MA6/BA* by using the first mask. Manual alignment is not required for the first mask. The exposure time is chosen equal to 2.8 s, according to the type and thickness of photoresist. Successively, wafers can be developed by using the appropriate recipe again in the *EVG150*.

Metal evaporation

Metals are evaporated with *LAB 600H* by Leybold Optics. This equipment allows the PVD of several metals, including titanium and platinum for our application. Ti is used as stick layer for SiO_2 and is deposited on top and under the metal layer to improve the adhesion of platinum and gold onto SiO_2 surfaces. A stack of Ti/Pt/Ti (20/200/20 nm) layers is deposited on top of silicon wafers. *LAB 600H* permits to simultaneously evaporate up to 8 wafers with the same recipe. As for the case of *EVA150*, also *LAB 600H* has a pre-saved list of recipes with different combination of metal layers that can be evaporated.

Lift-off

Lift-off step is performed by dipping the evaporated wafers into the *Remover 1165* until the resist dissolves. The metal film is chemically peeled-off from wafer surface. A lift-off step typically takes couple of days to remove all the excess of metal film. The required time depends on the thickness of metal layers, but also from the age of the bath. Ultrasounds can help to peel-off quickly all the metallic excess. Wafer are eventually rinsed with deionized water and dry in the spin rinser dryer.

4.2.3 Au electrode structuring

The five working and counter electrodes are fabricated with thin layer of gold. Every working electrode has a diameter of 282 μm, so that the electrode area is equal to 0.2 mm^2. The working electrodes are arranged along a semi-circle and they are surrounded by a gold counter electrode. Counter electrode area is designed as big as possible, in order to collect the maximum current generated on the WEs. Electrical connections between the electrodes and the pads are ensured by gold traces (except the case of reference electrode, where the connection is in platinum), which width is of 100 μm. Pad footprint is designed according to the footprint given in the datasheet of the connector. Au deposition follows the same steps as for platinum, going through photolithography, metal evaporation, and lift-off. Photolithography is performed with the second mask. In this case an alignment step is necessary by using the *Süss MA6/BA* mask aligner. During the previous deposition, Pt alignment markers were deposited at the opposite sides of the wafer along one diameter, to accurately adjust also possible misalignment in rotation. Thus, markers designed on the second mask can be overlapped next to those on the wafer. As the previous case, we deposit a stack of Ti/Au/Ti (20/200/20 nm) by *Lab 600H*.

4.2.4 SiO_2 passivation

SiO_2 can be deposited onto metallic layers by RF sputtering. CMI offers several equipment for non-microelectronic compatible technologies and we use the *Spider 600* by Pfeiffer for silicon oxide passivation. A SiO_2 layer of 500 nm is grown onto wafers to cover all the exposed metals. Then, the third mask is necessary to open the passivation layer next to the electrodes and the pads. Since we just need to deposit a normal positive photoresist, we do not need the sacrificial layer anymore. We deposit just one layer of AZ1512 with a thickness of 1.1 μm. Prior photoresist deposition, we process the wafers with *YES III HMDS* primer oven at 150 °. During this process, *hexamethyldisilazane* (HMDS) is deposited on the wafer in order to enhance the adhesion of the photoresist to the silicon dioxide film. Exposition and development of AZ1512 are performed as in the previous steps by using the last available mask. Once the photoresist is developed, we proceed with oxide and titanium wet etching. SiO_2 and Ti can be etched by buffered hydrofluoric acid in the same immersion in wet bench. The isotropic etching results where the photoresist is developed, while etchant cannot act where the wafer is protected by the resist. *Remover 1165* is used again for resist stripping. Then, wafers are rinsed with deionized water and eventually dried in the spin rinser to ultimate the wafers.

4.2.5 Chip dicing

In each wafer there are hosted 24 chips, so chip dicing is required. The automatic saw offered by CMI can cut glass or pyrex wafers, as well as silicon wafers. A nickel blade is used for cutting our wafers. Crosses deposited during the first metal deposition are used as references for dicing. Final chips result to have 9.5 x 23.3 mm (w x h) size.

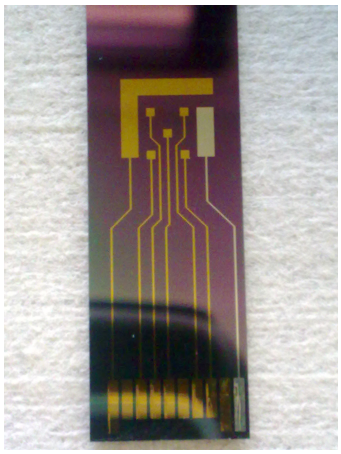

Figure 4.3: Optical image of the first version of the chip with five gold working electrodes, a gold counter electrode, and a silver reference electrode.

4.2.6 Encountered problems and proposed solutions

We developed in total three versions for the integrated electrochemical cell. The first version of the chip was realized with squared gold working electrodes (electrode area of 0.25 mm^2), squared counter electrode, and silver reference electrode. A picture of the fist integrated electrochemical cell that we developed is showed in Fig. 4.3. The first problem we encountered was the spontaneous oxidation of the reference electrode after some months from the microfabrication process. Initially, silver was used because the screen-printed electrodes tested so far were based on silver reference, and we wanted also to compare results obtained with screen-printed electrodes with those obtained with microfabricated ones. Due to the described oxidative problems, we decided to move toward pseudo-reference electrodes in platinum. From experiments, we noticed that the oxidation potential for hydrogen peroxide is practically the same for silver and platinum reference electrodes. Platinum is a much more stable metal and it does not show oxidative phenomena on its surface also after several months of storage in environmental conditions. Moreover, square electrodes can arise border effects, due to acute angles, and the active surface area can be smaller than the geometrical one. For this reason we designed a second version of the chip with a round geometry for electrodes.
Another important problem was due to delamination phenomena for the passivation layer. Fig. 4.4 illustrates some details of the reference electrode just after the wet etching step for the opening of the electrodes and pads. The SiO_2 layer tends to crack and delaminate after the etching step. This is due to bad adhesion of this layer with the underlying metal layers. When all oxide is removed next to the electrodes and etchant comes across the metal layer, it penetrates along the border anisotropically and delaminates the oxide layer deposited for sputtering. To avoid delamination effects, we tested two strategies, both of them based on the use of a stick layer. We deposited a thin film of chromium in the second version and titanium in the third version on top of the metal layers. In the case of chromium, we have a couple of issues to take into account. First, chromium can diffuse in the gold layer at temperatures

Figure 4.4: Magnified optical image of pads and connection after wet etching of SiO_2.

higher than 100 °C (which are usually required for photoresist baking), so the deposition of gold and platinum has to be swapped. Then, BHF can just etch SiO_2, so Cr layer has to be etched in a second step with a mixture of perchloric acid and ceric ammonium nitrate. Delamination phenomena were avoided by following this approach, but local anisotropic etching was observed in the case of Cr layer. When titanium was used as stick layer in the third version of the chip, we both tried dry and wet etching to remove the oxide. The dry isotropic etching gave sharper borders along the electrodes, but the disadvantage is that it can etch the oxide, but not the titanium layer on top of the metal, so another wet etching step is required. Instead, wet etching with BHF can remove both oxide and titanium from the metallic layers. Therefore, we used the latter approach for the last version of our process flow.

4.3 Electrode modification by spotting technique

Both carbon nanotubes and the enzymes need to be precisely placed onto the different working electrodes. Multiple analyte detection can be achieved by a selective functionalization of the five working electrodes. The dispensing of carbon nanotubes and enzymes has to be precise enough to spot both of them onto a surface of around 0.2 mm^2 with an accuracy higher than 50 μm. We exploit a spotting system developed for the automatic dispensing of biological samples, typically DNA, biomarkers, oligonucleotides, peptides, proteins, antibodies, and cell printing. The novelty of this work lies in the fact that a technology, such as the ultra-low volume spotting, developed for DNA and protein printing can be adapted for the deposition of carbon nanotubes and enzymes. In the next section we will give an overview on the instrument itself, with some information about its working principles and features. Then, we will explain how we can modify the standard spotting procedure to accomplish carbon nanotube placement. Finally, we will present some results about the spotting of CNTs and proteins onto our integrated electrochemical cell.

Figure 4.5: Image of the sciFLEXARRAYER DW.

4.3.1 Equipment

We used the sciFLAXARRAYER DW spotter by Scienion (Germany) in a novel and unique way. It is a piezo-dispenser non-contact liquid handling and spotting system, which dispenses volumes as low as 100 pl for each drop with an accuracy as low as 50 μm. The liquid handling station uses a glass dispense module mounted to an automatic lever. The relative movement between the lever and the substrate is given by the rotation of a disk, where the substrate can be hosted. An image of the whole system is depicted in Fig. 4.5. The apparatus hosts 16 seats for 200 μl vials and 16 seats for 40 μl vials. There is also a wash-station for cleaning and ultrasonication of the nozzle after each spotting, and a dispense control station to capture the trajectory of the drop and evaluating the drop volume. The system is completely automated, but it allows the user to choose the vial from where withdrawing the sample and to customize the geometry and the drop volumes of the spots. The four main building blocks of the system are the liquid handling station, the movement system, the dispense control station, and the software.

Liquid handling station

Fig. 4.6 depicts a schematic of the system liquid flow. The piezo-dispense capillary is conveyed to a liquid system composed by a syringe pump, a valve, and a system liquid reservoir. The flow of the system liquid is controlled through the valve. During the aspiration, the valve is in

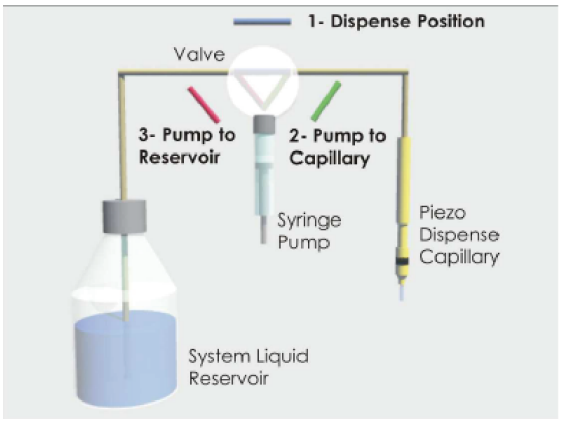

Figure 4.6: A schematic of system liquid flow. Reprinted from *www.scienion.de*.

position 2, while the syringe pump moves down, and the sample is aspirated into the capillary. The uptake is stopped by changing the valve to position 1, so that the piezo-dispenser is connected to the system liquid reservoir. The holding pressure in the tube is determined by the height difference between the system liquid and the nozzle (they underlie the law of equilibrium tubes). The nozzle consists of a glassy capillary with an integrated piezo-ceramic element cemented onto the capillary. By applying a rectangular voltage pulse, the piezo-ceramic contracts, initiating a pressure wave. This forces the solution out of the nozzle and a drop being ejected from the tip of the nozzle to the substrate. Since the voltage is pulsed, there will be as many drops as the number of pulses. Thus, the drop can be acquired with a camera taking frames with the same frequency of the pulses and its volume and shape can be controlled through the dispense control station. As soon as the sample dispensing is finished, the tubes are flushed with system liquid. Thus, the valve switches to position 3 first and the syringe fills up with the system liquid. Eventually, the valve switches to position 2 and the syringe pumps the liquid out to flush the dispense capillary.

Movement system

The movement system consists of the robotic lever, where the nozzle is hosted, and the target holder, that is a rotating disk with an adhesive film for fixing the individual targets. The robotic lever moves the nozzle in the different positions: in the wash station, into the vials to uptake the sample, and on the target. Movements are controlled by software according to system coordinates. Linear coordinates result from the angular movement of the lever combined with the rotating movement of the target holder. The calibration of the movements and coordinate references can be performed by using the head camera. The camera is mounted next to the nozzle head and can be used for the calibration of the nozzle tip prior spotting procedures. Calibration is carried out by moving the camera to specific reference coordinates, which correspond to an hole on the target holder. Then, the center of the camera, pointed with a cross, is moved until it matches with the center of the hole, by adjusting the rotation angle of

Figure 4.7: Drop image acquired by the dispense control station. Reprinted from *www.scienion.de*.

the lever and the target holder. The movements can be done through an iterative procedure embedded in the software, that analyzes the image and finds the right coordinates for the reference point. The head camera can be also used to find structures on the target, so that the absolute position of the drop deposition can be defined, and to acquire the results of the spotting.

Dispense control station

The dispense control station includes a stroboscopic LED for image illumination and a video camera. The camera is situated close to the dispense capillary for visual inspection of the drop formation performance. The nozzle dispenses drops with a fixed frequency. The LED for image illumination is triggered by the piezo-ceramic frequency, but it flashes at a user-definable delay. Using this approach, the drop image can be captured at any point of the trajectory, simply by changing the LED delay time. Thus, it is possible to acquire a stable image of the drop, so that it is possible to optimize the drop size, the drop velocity, and the drop trajectory. Fig. 4.7 illustrates the image of a drop acquired by the camera of the dispense control station. The diameter of the droplet is usually greater than the orifice diameter. Drop characteristics are mainly influenced by the width and the amplitude of the electrical pulse. The amplitude and the pulse width of the voltage affect the speed and the volume of the drop. Typical voltage parameters are in the range of 60 - 130 V. Higher pulse width will result in a larger drop volume. Typical pulse widths range from 30 to 60 μs. These two parameters are inter-dependant. When increasing the voltage, the pulse width should generally be reduced and vice-versa. Parameter optimization can be performed by looking at the drop image acquired by the dispense control station. The frequency of the pulses is another important parameter. Values around 500 Hz are typical for spotting procedures.

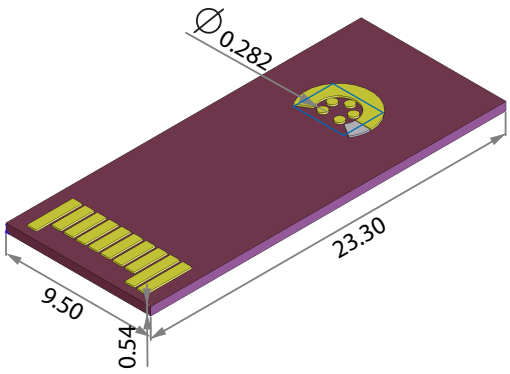

Figure 4.8: A schematic of the microfabricated chip reporting its dimension, used to program the spotting area.

Software

The software controls all the functions of the spotter. The drop control and the spotting process are under full software control. User can entirely customize the geometry of the target, create routines for the spotting procedures, and regulate the sample volume to spot on the target. The instrument has already pre-defined routines, including standard wash procedure, which drives the nozzle toward the cleaning station and activates the ultrasounds as long as the tip is dept in the cleaning tank. Individual tasks are the building blocks of a procedures. Tasks regard a low-level programming of the instrument, while user can work at a higher level by combining pre-defined tasks to build his own procedure. In the single procedure tasks can be repeated many times by means of loop function, such as the *Begin Loop* and the *End Loop*. As already mentioned in the previous section, the drop can be controlled by the camera in the dispense control station. The software allows us to estimate the volume of the drop by image processing of the drop.

4.3.2 Printing pattern

The dispenser is originally developed for the spotting of biological samples onto glass slides. We customize the spotting pattern with the characteristics of our biochip. The main parameters are resumed in Table 4.8. All the following description are referred to the last version of the microfabricated chip.

Target setup

The dimensions of the microfabricated chip are reported in Fig. 4.8. According to this geometry, we customize the target with the size of our chip. Dimension X, Y, and Z refer to the overall dimensions of the target substrate. In our case they are the dimensions of the biochip. Inside the target substrate, it is necessary to specify a rectangular spot area, highlighted in blue in

Table 4.1: Example of the parameters to define for the creation of a customized target. All the values are reported in μm.

Parameter	Value
Dimension X	9500
Dimension Y	23300
Dimension Z	540
X position	125300
Y position	135100
Z position	5340
Z position (into)	5340
Spot-Area X	9500
Spot-Area Y	7200
Spot-Area No. X	1
Spot-Area Offset X	0
Spot-Area No. Y	1
Spot-Area Offset Y	0
Spot-Area Teach Corner	1

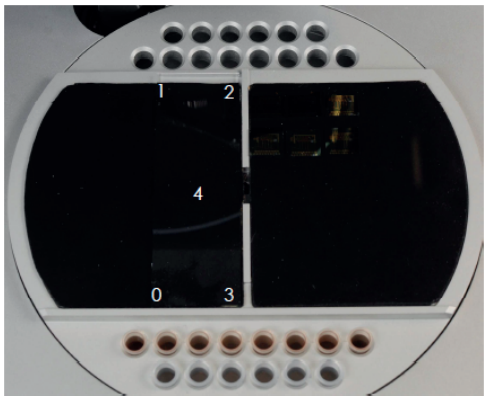

Figure 4.9: Spot area teach corner. Reprinted from *www.scienion.de*.

Fig. 4.8, which traces the area where spots are placed. The coordinates of the upper left corner of the spot area are given by *X, Y, and Z positions*, while *Spot-Area X* and *Spot-Area Y* are the dimension of that rectangle. It is also possible to replicate the same spot area in different part of the target substrate by moving the nozzle of a defined offset, indicated in *Spot-Area Offset X* and *Spot-Area Offset Y*. Finally, the definition of a new target requires also to indicate the reference corner to start the movements, called teach corners. This parameter is especially useful when the same spot area has to be replicated several times on the same target substrate. The teach corners are numbered according to Fig. 4.9.

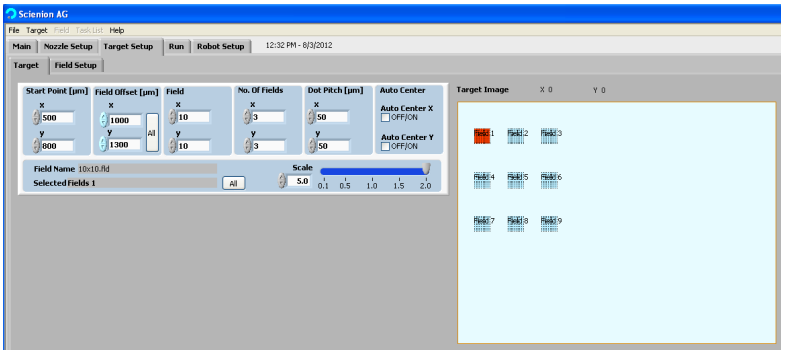

Figure 4.10: Patterned fields customized for our chip. Fields displayed in red are within the pre-selected target. Fields displayed in blue are not selected for editing in the Field Setup.

Spot area geometry

The geometry of the spot area is defined through the field layout, which determines the spotting procedure. The software allows us to define only rectangular fields with rows and columns within the spot area. In every field, then, it is possible to define the number of dot pitch (refer to Fig. 4.10). So, the user has to choose the following parameters:

- *start point*: X and Y coordinates of the upper left corner of the first field;
- *field offset*: the distances defined in X and Y between one field and the next one along the row or the column;
- *Field size*: the dimensions of the individual field have to be defined in X and Y-axes;
- *No. of fields*: it is possible to spot several fields using exactly the same parameters;
- *Dot pitch*: it is the distance between the spots. Every field can be filled with a certain number of dot pitches, which can be defined along the X and the Y-axes. The X and Y distances can either be equal or can be set to different values. For each dot spot corresponds one or more drops at the same coordinates. After positioning in correspondence of the dot pitch, the nozzle ejects the number of drops required by the procedure, and afterwards moves to the following dot pitch.

Every field spot, and even each dot pitch, can be individually programmed for the spotting. For each dot pitch it is possible to select the position of the vial from where aspirating the sample (for example when spotting in the same field different samples) and the number of

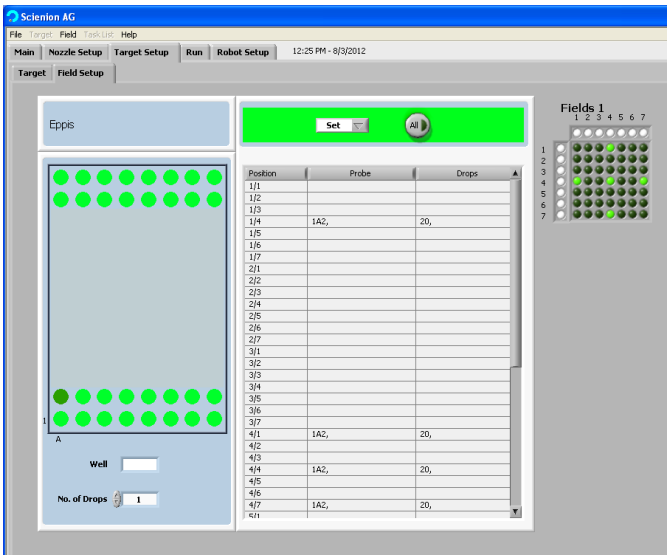

Figure 4.11: Software image of the Field Setup window. It is possible to graphically determine the correlation between the probe and the target. The light-green dot pitches are those where the tip will spot the indicated probe. Number of drops for each dot-pitch are specified in the table in the middle.

drops to dispense for each sample (when the purpose is to mix two different samples together at the same dot pitch). It is also possible to decide not to spot every dot pitch, by leaving some of them empty.
For our electrodes, since they cannot be modeled as a matrix of rectangles, we define three different layout fields, related to the three rows of electrodes. So, we have the layout field for the working electrodes 1 and 5 (1 x 2 field), the layout field for the working electrodes 2 and 4 (1 x 2 field), and the layout field for the working electrode 3 (1 x 1 field). Field offset are chosen according to the design of the chip. Since field layout can be just defined as rows and columns of dot pitches, we define 5 x 5 spots for each layout field as starting geometry (so we have 25 dot pitches for each field). Since the electrodes are round, we just spot the dot pitches highlighted in Fig. 4.11, trying to obtain a rounded spotting. Depending on the sample to spot, we set different numbers of drops per dot pitch. We dispense 20 drops of carbon nanotubes per dot pitch, so we have a total amount of 45 ng. We store carbon nanotubes in 200 μl vials, so the procedure for CNTs spotting has also to take into account the position of the vial. Enzymes, instead, are stored in 40 μl vials, and the spotted quantity is also different, depending on the initial concentration we have.

4.3.3 Spotting results

The automatic dispenser system allow us to precisely and selectively functionalize our working electrodes with CNTs and enzymes. However, due to the dimension of the nozzle and the hydrophobic nature of carbon nanotubes, we need to optimize CNT solution. Results obtained

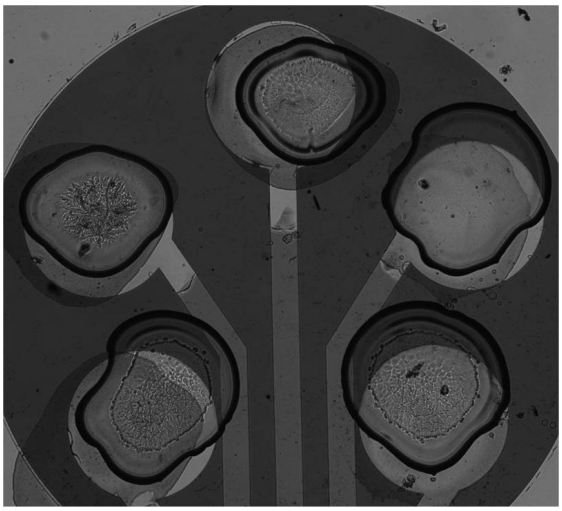

Figure 4.12: Optical image of the five working electrodes covered with CNT dissolved in Nafion solution (Microscope Nikon Eclipse LV100).

with screen-printed electrodes are obtained with CNTs dispersed in chloroform, according to the protocol reported in [158]. However, chloroform is a high-volatile solvent and may not be the right solution to disperse carbon nanotubes, due to the small volumes involved with the automatic dispenser. According to the promising results reported by Wang *et al.* [25], we dissolved CNTs in distilled water 50 vv%, ethanol 50 vv%, and Nafion 0.5 wt% solution. Carbon nanotubes are highly soluble in the Nafion-based solution and a well-dispersed mixture is obtained. By following this strategy, we avoid clogging of the nozzle orifice due to CNTs aggregation. The lyophilized powder of enzymes is instead dissolved in PBS. Enzyme solution is drop cast subsequently to CNTs deposition. Finally, glutaraldehyde is also dropped on top of the other layer, to cross-link the enzyme and the CNTs. Glutaraldehyde is not mixed with the enzyme to avoid a dense solution in the nozzle. Enzyme cross-linking is a fast process and we want to avoid that it takes place inside the spotting tip. An example of the resulting spotting on the five working electrodes is showed in Fig. 4.12.

4.4 Apparatus for continuous monitoring of cell culture

In Section 4.1 and in Section 4.2 we described the fabrication and the functionalization of the electrodes. It is now necessary to combine the integrated platform with the fluidic system to achieve the continuous monitoring. Our electrochemical measurements are based on chronoamperometry, which requires a flow to continuously renew the solution at the electrode interface. Continuous flow is typically achieved by magnetic stirring. However, this approach cannot be pursued in the case of the detection in cell cultures. Thus, it is necessary to refresh the solution close to the cell with another method. In this section we will discuss a possible strategy to accomplish chronoamperometries and performing the continuous monitoring of cell culture media.

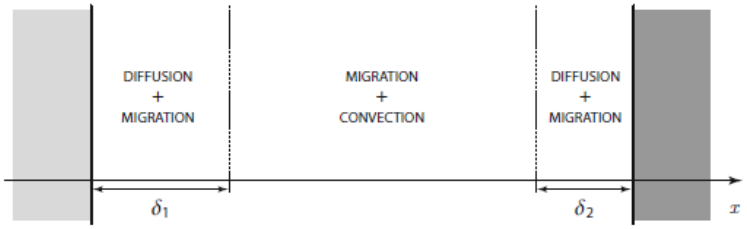

Figure 4.13: Distribution of the conduction modes in an unstirred electrolyte. Reprinted from [159].

4.4.1 Introduction to conduction phenomena at the electrode interface

The flow of current through the electrolyte involves microscopic conduction phenomena, and precisely it is the result of a movement of charges. However, charge movements always correspond also to macroscopic mass movements. The phenomena related to mass transport are generally classified in three categories:

- **migration**: it refers to the movement of charged species subjected to an electric field. Migration is generally characterized by the concentration and the molar conductivity of the charge carriers.
- **diffusion**: it is related to the movement of species submitted to a concentration gradient. The species diffuse from the most concentrated zone towards less concentrated zones. Diffusion is generally characterized by the diffusion coefficient of each species.
- **convection**: it concerns the overall movement of the medium when it is a fluid. The movement is characterized by the velocity and the concentration of the carriers. It can take the form of natural convection, caused by density gradients, or forced convection, corresponding to an homogeneous process caused by chemical agitation.

The distribution of mass transport processes in an quiescent electrolyte can by schematically represented as in Fig. 4.13. The thickness of the diffusion layer (δ) is typically in the order of few μm. When the electrolyte is not stirred, natural convection can be disregarded. When electrochemical phenomena take place, there is a depletion of the species at the electrode interface. However, the change in concentration does not immediately reach the electrolyte bulk from the interface. In between, the electrolyte has an homogeneous zone where only migration occurs. As the experiment progresses with time, the size of this non-perturbed zone decreases, while the thickness of the diffusion layers increases. These depletion zones at the electrode interface can affect the chronoamperometry, because species concentration in the bulk and at the interface are different. That is why it is important to force convection during the measurement. The distribution of conduction modes is depicted in Fig.4.14, related to the case when the electrolyte is stirred [159].
In the following section the apparatus for the continuous monitoring is discussed. The two

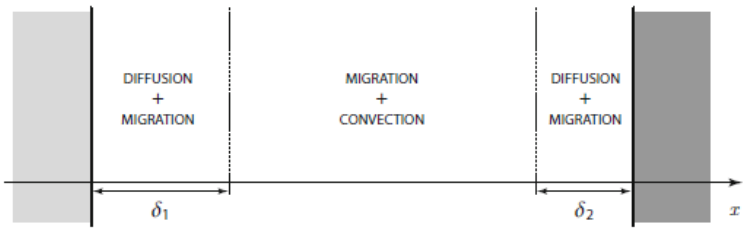

Figure 4.14: Distribution of the conduction modes in an electrolyte when submitted to forced convection, according to Nernst model. Reprinted from [159].

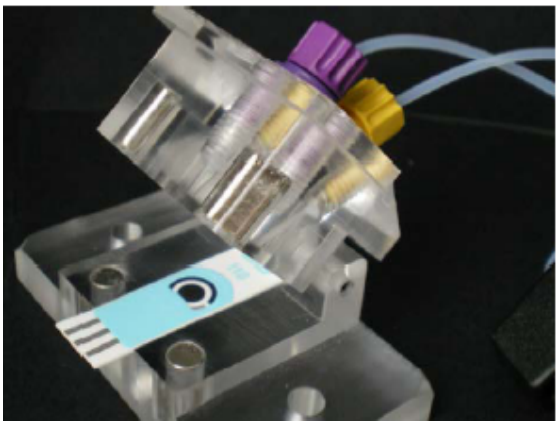

Figure 4.15: Flow-cell by Dropsens (Spain) for continuous measurements with screen-printed electrodes. Reprinted from *www.dropsens.com*.

main building blocks that will be presented are the fluidic chamber integrated on the top of the multi-sensor platform and the microdialysis probe for the *on-line* monitoring.

4.4.2 Solution for continuous monitoring

As already discussed in Section 2.2.1, flow-injection analysis is a possible strategy to perform measurements under flow conditions. However, FIA requires long channel to mix the carrier solution and the sample, due to the slow radial and convection diffusion phenomena. Thus, FIA systems are not easy to integrate in small devices.
The most straightforward solution to ensure a continuous flow next to the electrochemical cell is by means of a fluidic chamber. Such systems are also called flow-cells and can be purchased from the market. In Fig. 4.15 is showed an image of a flow-cell for screen-printed electrodes by Dropsens (Spain). The flow-cell is made of methacrylate, with a magnetic open-close system. The two screws on the top of the cell are the inlet and the outlet channels. Cell size and geometry are adapted for screen-printed electrodes produced by Dropsens. The flow is forced to pass through the cell and is confined next to the screen-printed electrodes by a rubber o-ring. O-rings ensure the hermetic enclosure of the system and no leakage. This first solution was used for the first set of experiments under continuous flow, as described later in

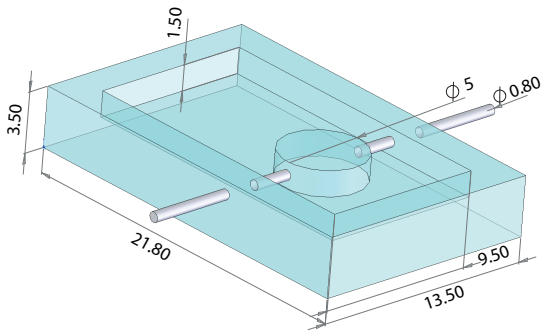

Figure 4.16: Milled master in PMMA for the PDMS chamber. All the dimensions are in mm.

Chapter 5. Commercial flow-cell works properly for our purposes, so we moved on trying to fabricate our own flow-cell that can be adapted to silicon chips.
Another solution to develop fluidic systems exploits the capability of PDMS to interact with silicon-based materials after plasma oxygen activation. PDMS is one of the most common polymers that has been used to develop microfluidics. Fabrication of channels in PDMS is particularly straightforward, since it can be purchased in liquid and then molded even at room temperature with sub-0.1 μm accuracy [160]. The latter strategy is suitable for our purposes. PDMS can be molded in a master and this technique is called soft lithography for rapid prototyping.

4.4.3 PDMS molding

PDMS molding can be obtained by soft lithography for rapid prototyping. Soft lithography starts with the production of the master in a material resistant to fairly high temperature (typically around 80 °C). The master can be obtained with several methods. When features are in the range of 10's of microns, a common method employs SU-8, an epoxy-based negative photoresist. SU-8 can be deposited by spin coating onto silicon or glass wafers with thickness up to 300 μm, and then processed by photolithographic methods. The features to replicate can be transferred onto the photoresist by exposing the SU-8 to UV light through a mask. The photoresist is then developed to remove the non-exposed portions and baked, to fix the SU-8. After that step, the master can be used to pour the PDMS on the top of it. The resolution of the SU-8 can go under 20 μm.
When features are bigger than 100 μm, the master can be directly milled from a block of *polymethylmethacrylate* (PMMA), for example. This is the case of the master we use in the following experiments. An image of the master is illustrated in Fig. 4.16. Chamber size is conceived to entirely contain the integrated electrodes of the electrochemical cell. The total volume of the chamber is around 118 μl and it has a metallic tube through the chamber for the inlet and outlet channels. The diameter of the passing tube is of 0.6 mm, even if the connectors used with the PDMS mold are of 0.8 mm. That solution aims to avoid leakage from

the chamber.
Silicon elastomer base and curing agent are purchased from Dow Corning GmbH (Germany). Silicon hydride groups present in the curing agent react with vinyl groups present in the base and form a cross-linked, elastomeric solid. Elastomeric base and curing agent are mixed in a rate of 10 to 1 and the solution is put in the desiccation chamber for about 30 minutes to pull out all the air bubbles. Then, the liquid pre-polymer is poured into the master and let dry in the oven at 80 °C for one hour. The liquid PDMS conforms to the shape of the master and replicates the features of the master with high fidelity. The low surface free energy and elasticity of PDMS allow it to release from the mold without any damage for neither the features of the PDMS and the mold.
PDMS is one of the most used elastomer, because it has several advantages. It is optically transparent, so it is possible to see through it. It is an electrical insulator, so it is possible to avoid short-circuits among the wires connecting the electrodes (in the case the passivation fails). As already mentioned, it has a low surface free energy, so an easy release from the mold is possible. It is impermeable to liquid water, but permeable to gases and non-polar organic solvents, which make it suitable for many applications where, for example, the permeability to oxygen and other gases is highly desirable. Finally, it is chemically inert, but can be functionalized by exposure to a plasma. This last characteristic is particularly interesting in our case. Indeed, PDMS can seal to itself or to Si-based surfaces. The sealing can be reversible or irreversible, depending on the intensity and the exposure time to the plasma. PDMS molded in contact with smooth surface can perfectly adhere with other smooth surfaces. Van der Waals contacts provide a reversible seal, which is watertight but cannot withstand pressures greater than 0.34 atm. To form an irreversible sealing, the PDMS can be exposed to an air plasma for 1 min. Some authors [160] believe that this treatment generates silanol groups (Si-OH) on the surface of the PDMS by the oxidation of methyl groups. Surface-oxidized PDMS can seal to itself, glass, silicon, and silicon oxide prior to expose also the substrate to the air plasma. In our experiments we do not use the irreversible sealing, because we cannot expose the silicon chip to plasma, due to its functionalization with enzymes. However, the exposure to air plasma confers hydrophilic properties to the PDMS, which is instead naturally hydrophobic. Contact with water or polar organic solvents maintains the hydrophilic nature of the surface indefinitely [160].

4.4.4 In-house chip holder

The developed PDMS chamber cannot be irreversibly sealed onto the silicon chip. Thus, we need another approach to fix the chip and the PDMS chamber together. We designed an in-house chip holder to strengthen the chip and the chamber together. In this way the PDMS chamber can perfectly adhere to the Si surface. The in-house chip holder is milled from a PMMA block. The holder is conceived with a base and a cover part, so the chip is hosted in a sandwich-like configuration. They are then fixed together by means of four screws. The two parts of the in-house holder and the chip are illustrated in Fig. 4.17. The PDMS chamber is then connected to a peristaltic pump, to ensure a flow rate of the surnatant of around

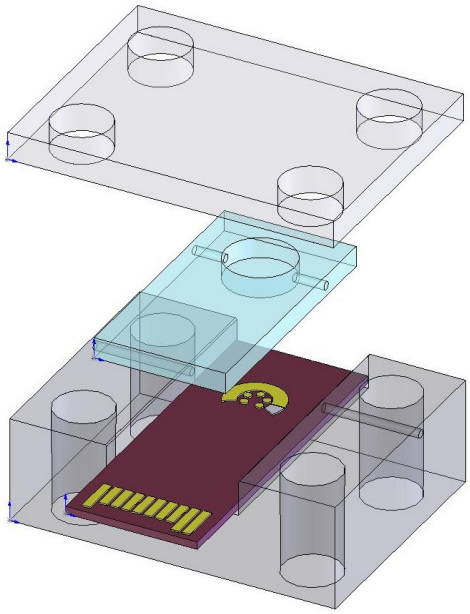

Figure 4.17: In-house chip holder, the PDMS chamber and the chip.

13 μl/min from the Petri dish to the electrochemical cell, as also reported in [161]. The inlet and the outlet of the chamber host a 0.8 mm diameter metal connector. The metal connectors are inserted in the in-house chip holder, so that the solution can flow towards the PDMS chamber. The transparency of the PMMA allows us to look through the cover and observe the chamber filling. The inlet and the outlet are then connected to the peristaltic pump by means of Tygon® tubes. Tygon® is a polymeric material that can be sterilized, so it is perfectly suitable for our application, since we need to keep sterility also when withdrawing metabolites from the Petri dish.

4.4.5 The microdialysis probe

The detection of electrochemical species cannot be performed in pure cell culture medium. Media are complex solutions enriched with nutrients, hormones, and antibiotics to ensure the proper proliferation and development of cells. However, due to the quantity of different compounds in the solution, this is not a proper electrolyte to perform electrochemical measurements. Microdialysis probes can help to overcome this problem, as already discussed in Section 2.2.2. Electrochemical biosensors have always an upper limit for the linear concentration range. This limit is directly related to the quantity and activity of the biological recognition element employed in the measurement. Enzymatic activity strictly depends on the protein itself, why quantity can be optimized according to the electrode surface. An empirical rule for the enzymatic concentration to use is to ensure 1 U/mm^2 on the working electrode. The upper limit of the linear range can be significantly extended by using an outer layer diffusion

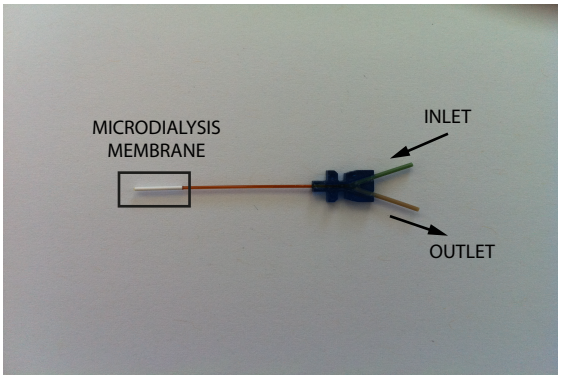

Figure 4.18: Schematic representation of a microdialysis probe, showing the spongious membrane matrix of the inner membrane.

barrier. Microdialysis probes hold this role, although the compromise for such an extension is the decrease of sensor sensitivity. Indeed, the local analyte concentration within the reaction layer can be at least two orders of magnitude lower than in the bulk solution. The outer layer diffusion barrier can be also useful to improve biosensor selectivity by choosing the proper cut-off of the membrane. We are mostly interested in detecting glucose, lactate, and glutamate. The atomic mass unit, which represents the "size" of the molecule, is typically measured in Dalton (Da), as the cut-off of the membrane. For example, glucose molecule ($C_6H_{12}O_6$) has a mass unit of 180 Da, lactate molecule ($C_3H_6O_3$) has 90 Da, and glutamate molecule ($C_5H_9NO_4$) has 147 Da. They are quite small molecules, so we need a microdialysis probe with low molecular weight cut-off. We chose a microdialysis probe by Microbiotech SA (Sweden) with cut-off of 6 kDa, to be selective to small molecules. It contains a PES (polyethersulfone) dry membrane. A further advantage of microdialysis probes is the possibility to sterilize them. In our experimental setup the probe is in direct contact with the cell culture, so it has to be sterile.
A picture of a microdialysis probe is depicted in 4.18. The probe is immersed in cell culture medium and connected with the fluidic system. The probe inlet is connected to the perfusate (in our case is PBS solution), which is flowed through the inner channel of the probe. When it reaches the end of the probe, it is pushed to pass outside in the outer channel. The pure medium and the outer channel are separated by the dialysis membrane, which allows the exchange of molecules between the perfusate and the medium under a concentration gradient. The solution is then sucked back toward the probe outlet and the enriched perfusate is flown next to the electrochemical cell.

4.5 Chapter contribution and summary

In this chapter we have described tools and methods for the development of the self-contained system for the *on-line* monitoring of cell cultures. The device is built through three main steps: the microfabrication of the integrated electrochemical cell, the structuring and the

functionalization of the electrodes by ultra-low volume dispensing, and the molding of a PDMS chamber on top of the chip to ensure a continuous flow at the electrode interface. Microfabrication technologies for MEMS can be successfully employed for the multi-working electrode manufacturing. Photolithography, thin film technologies, and etching methods are the main processing steps used to develop our platform. These facilities are available at the CMI in EPFL, where we performed the whole fabrication. We described the process flow followed for the most recent version of our platform, after having solved some issues of the previous versions. Once the integrated platform is ready, every electrode needs to be structured with carbon nanotubes and selectively functionalized with the corresponding enzyme. The dimension of the single electrodes does not allow us to manually spot the CNTs and proteins, so we can adapt technologies developed for DNA printing in favor of our purposes. No-one has shown so far the use of a non-contact piezo-electric spotting system for the selective functionalization of working electrodes developed for biosensing purposes. CNT solution has to be optimized for ultra-low volume handling, due to the hydrophobic nature of carbon nanotubes and the extremely small volumes involved. The automatic dispensing can be performed with a commercial spotter customized for our chip. After electrode functionalization, we also developed the fluidic system to carry out chronoamperometries under flow conditions. PDMS is chosen to develop the microfluidic chamber, because its use is straightforward and can be molded and polymerized even at room temperature. The molded chamber can be fixed on top of the chip by an in-house chip holder and chronoamperometries can be performed by means of a peristaltic pump connected to the inlet and outlet channels of the chamber. The chapter concludes with the description of the microdialysis probe, which is connected to the fluidic circuit and immersed in the cell culture media for the *on-line* detection of metabolic compounds.

5 Experimental measurements

In Chapter 4 we have described one possible strategy for the development of a self-contained device with multiple working electrodes for the real-time detection of metabolites in cell culture medium. The microfabrication of the integrated electrochemical cell, the selective functionalization of the working electrodes, and the fluidic system have been extensively described. In the current chapter we will show the results obtained while progressing in the development of the self-contained platform. We started the research by testing both bare graphite and carbon nanotube-based electrodes to prove the sensing enhancement due to CNTs and comparing the results with literature. An analysis of bare graphite and CNT-based electrode detection is presented in Section 5.1 for the sensing of pure hydrogen peroxide and in the case of enzyme-based sensors. Then, Section 5.2 will discuss about immobilization strategies of the enzyme, by comparing three different protein entrapments, according to biosensor performance and long-term stability. Once optimized the CNT quantity and the best enzyme immobilization strategy, Section 5.3 will present the detection of glucose and lactate in saline solution and in diluted cell culture media. Calibration lines for both glucose and lactate and biosensor performance are discussed. The *off-line* detection of a cholinergic cell culture is performed and the metabolic behavior of cells is extrapolated in different cultivation conditions. Once we will have successfully proved the feasibility of our method, we will move on with results related to the microfabricated electrochemical cell. In Section 5.4 we will present a characterization of the microfabricated electrodes from the electrochemical point-of-view and we will compare them with commercial screen-printed electrodes. Afterwards, we will calibrate the manufactured electrodes for the detection of glucose, lactate, and glutamate in saline solution. Finally, Section 5.5 will show the calibration of glucose and lactate in cell culture media by means of the fluidic system. The use of a microdialysis probe allow us to minimize the interactions with the cell culture and the sampling volume. The system is finally validated in a line of neuroblastoma cells in proliferative state. Glucose uptake and lactate production are evaluated in conditioned surnatant along three days of cultivation.

5.1 Characterization of graphite and CNT-based electrodes

The first part of the research was focused on the optimization of the several parameters involved when developing a biosensor. Such parameters include the material of the working electrode, the enzyme concentration required to sense a specific range of concentration, the identification of the solvent to disperse CNTs and the optimal concentration to achieve a proper electrochemistry. In this section, we will go through all these parameters and we will present some preliminary measurements obtained with our method. The obtained results encouraged us to pursue the development of a multi-working electrode platform for accomplishing the monitoring of different metabolites in cell cultures.

5.1.1 Electrode characterization with hydrogen peroxide

Since oxidases produce H_2O_2 in the enzymatic reaction, as already discussed in Section 2.4.1, we first investigate its electrochemical behavior by cyclic voltammetry and chronoamperometry [162]. Carbon paste SPEs are purchased from Dropsens (Spain). The electrodes are made of a graphite working electrode (area equal to about 13 mm^2), a graphite counter electrode and an Ag/AgCl reference electrode. The total area of the cell is 22 mm^2. H_2O_2 is purchased from Reactolab SA (Switzerland) and diluted in *Phosphate Buffer Saline* (PBS) solution 0.1 M at pH 7.4. MWCNTs are purchased in powder (90% purity) from Dropsens and diluted in chloroform to the concentration of 1 mg/ml, according to the protocol reported in [158]. CNT-solution is then sonicated in order to obtain an homogeneous mixture. Two sets of electrodes are prepared: the bare electrodes are tested as they are, while CNT-based electrodes are prepared by drop casting 60 μl of MWCNTs solution on the SPE surface. Drops of 5 μl are deposited each time and allowed to dry before a further deposition. All the electrodes are stored at room temperature when not used. The electrochemical response of the electrodes is acquired by Versastat 3 potentiostat (Princeton Applied Technologies, USA).

H_2O_2 cyclic voltammetry

We started with cyclic voltammetry, in order to identify the oxidation and reduction peaks in the absence and presence of CNT and the potential at which chronoamperometries should be carried out to detect hydrogen peroxide. The electrode under measurement is covered with 100 μl of PBS and hydrogen peroxide in different concentrations (from 0 to 50 mM with steps of 10 mM). The potential is swept in the range from -1 to +1 V vs Ag/AgCl, using a scan rate of 100 mV/s. Cyclic voltammetries related to bare and CNT-based electrodes are shown in Fig. 5.1a and 5.1b, respectively. Cyclic voltammetry related to bare electrode (refer to Fig. 5.1a) apparently shows just one peak around -500 mV, which is related to O_2 reduction, according to the following reaction:

$$O_2 + 4e^- + 2H_2O \rightarrow +4OH^-. \tag{5.1}$$

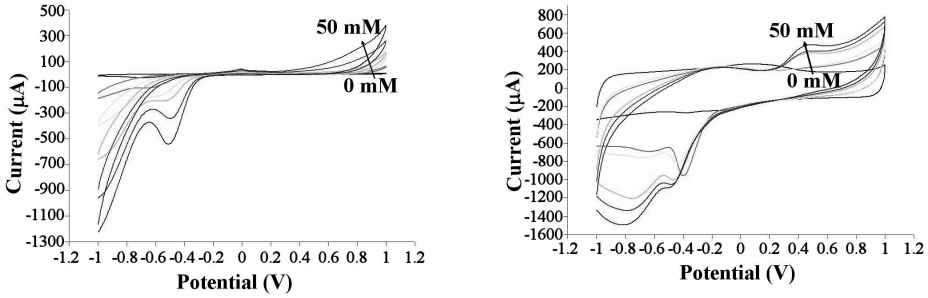

(a) Cyclic voltammetry of bare SPEs.

(b) Cyclic voltammetry of CNT-based SPEs.

Figure 5.1: Cyclic voltammetry are performed for concentration from 0 to 50 mM of H_2O_2 with steps of 10 mM. The scan rate is fixed to 100 mV/s. Reprinted from [162].

Moreover, with bare electrode it is not possible to observe the oxidation peak related to H_2O_2, which is typically around +700-750 mV. Instead, CNT-based electrodes show the oxidation peak of H_2O_2, as clearly visible from Fig. 5.1b. It starts to be well-shaped around +500 mV from 30 mM of H_2O_2, which is a lower potential with respect to those reported in literature for graphite electrodes [163]. The dicrease of the oxidation potential due to the presence of CNTs has been already observed in previous works [158]. Similarly, also the O_2 reduction peak shifts toward lower absolute potentials. Peak potential is a function of substrate concentration according to Nernst equation, as already discussed in Section 2.4.1. However, from Nernst equation it is not clear the parameters that can change adding carbon nanotubes onto the electrode. Thus, the hypothesis is that CNTs could modify the electrostatic attraction in the double layer that is formed onto the interface between the electrode and the solution. This layer effect changes the target molecule concentration close to the electrode and concentration ratio changes in Nernst equation. It follows that direct amperometric detection of H_2O_2 requires a higher potential at unmodified electrodes, which causes severe interference effects arising from easily electrooxidizable compounds, such as ascorbic and uric acid existing inherently in biological fluids. As a consequence, it is possible to overcome the influence due to other compounds by reducing the applied potential with the use of CNT-based electrodes.

H_2O_2 chronoamperometry

According to the results obtained from Cyclic voltammetries, chronoamperometries on bare and CNT-based electrodes are performed at the fixed potential of +650 mV in the range from 0 to 12 mM of H_2O_2. This is an useful range for glucose, lactate, and glutamate in cell monitoring. Calibration curves for bare and CNT-based electrodes are plotted in Fig. 5.2a. Bare electrodes show a sensitivity of 0.79 μA/mM cm^{-2}, while CNT-based electrodes have a sensitivity of 5.8 μA/mM cm^{-2}. CNTs confer a great improvement in sensitivity of about 7 fold compared with the case of H_2O_2 detected by bare electrodes. We also performe the chronoamperometry of H_2O_2 by just using CNT-based electrodes in a narrower range (from 0 to 1500 μM) and we get a sensitivity of 12.8 μA/mM cm^{-2} (refer to Fig. 5.2b). The system starts to respond to hydrogen

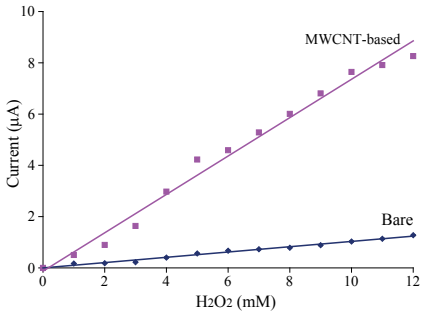

(a) Calibration curves obtained from chronoamperometry data analysis for the range from 0 to 12 mM of H_2O_2 with step of 1 mM in the case of bare and CNT-based electrodes.

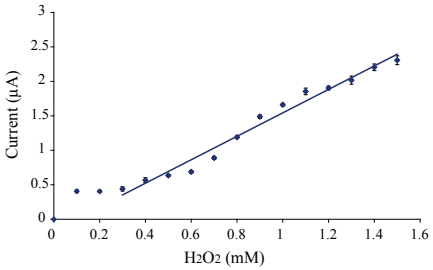

(b) Calibration curves obtained from chronoamperometry for the range from 0 to 1.5 mM of H_2O_2 in PBS by step of 0.1 mM for SPE with MWCNT.

Figure 5.2: Chronoamperometries performed with screen-printed electrodes for the detection of H_2O_2. Reprinted from [162].

peroxide from concentration higher than 300 μM. We can also compare the obtained results with previous works related to H_2O_2 detection by using carbon nanotubes. A comparison on the performance among our biosensor and other developed for hydrogen peroxide detection are summarized in Table 5.1. It could be observed that sensors without carbon nanotubes, such as the one described by Sung *et al.* [165], show a sensitivity of one order of magnitude lower than those based on CNTs. The sensitivity obtained by the present study is a little bit smaller compared to the one showed by *Cui et al.* [166], but it can be explained by the fact that they use oxidase in polymeric matrix, which can enhance the efficiency, despite of the cost and complexity of the sensor [162].

Table 5.1: Sensitivity values from literature. Reprinted from [162]

Methods	Sensitivity
Au-Nafion®- TNTs [164]	0.24 μA mM^{-1} cm^{-2}
Polypyrrole - polyanion/PEG [165]	0.15 μA mM^{-1} cm^{-2}
MWCNT-chitosan [95]	8.3 μA mM^{-1} cm^{-2}
chitosan/PVI-Os/CNT [166]	19.7 μA mM^{-1} cm^{-2}
casted MWCNT (Present study)	12.8 μA mM^{-1} cm^{-2}

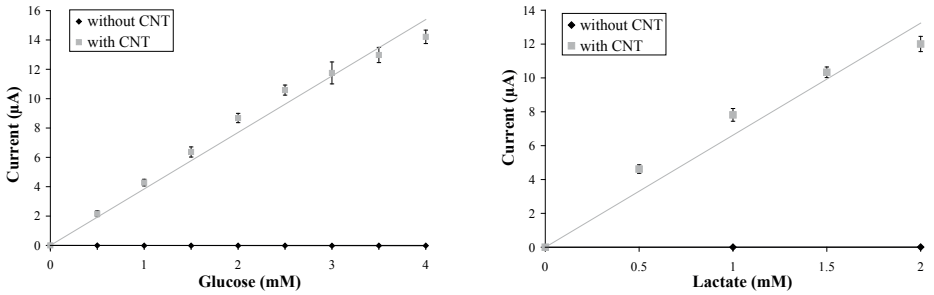

(a) Glucose detection for bare (black rhombus) and CNT-based (grey squares) electrodes.

(b) Lactate detection for bare (black rhombus) and CNT-based (grey squares) electrodes.

Figure 5.3: Comparison between bare and CNT-based screen-printed electrodes for glucose and lactate detection. Reprinted from [134].

5.1.2 Glucose and lactate detection with screen-printed electrodes

The improvements of CNT-based electrodes in H_2O_2 detection was already demonstrated in the previous section. The enhancement in terms of sensitivity between bare and CNT-based electrodes is about 7 fold, also suggesting a similar improvement in terms of performance for oxidase-based biosensors. Detection of glucose and lactate are performed with bare graphite and CNT-based electrodes to evaluate the performance of the two methods [134]. Calibration lines are extracted from chronoamperometries and glucose and lactate detection are depicted in Fig. 5.3a and 5.3b, respectively. Differently from the case of hydrogen peroxide detection, the oxidase selective for either glucose or lactate is drop cast on bare and CNT-based electrodes. Glucose oxidase from *Aspergillus Niger* (GOD, EC 1.1.3.4, 129.9 units/mg solid), lactate oxidase from *Pediococcus species* (LOD, EC 1.13.12.4, ≥20 units/mg solid), D-(+)-glucose, and lithium L-lactate are purchased from Sigma-Aldrich (Switzerland) in lyophilized powder. All the protein are dissolved in PBS 0.01 M at pH 7.4, while glucose and lactate are dissolved in double distilled water. For both the type of electrodes, 20 μl of glucose or lactate oxidase (15 mg/ml and 125 mg/ml, respectively) are deposited onto the working electrode with laboratory pipette and stored overnight at +4 °C, in order to allow the adsorption of the proteins onto the electrode surface. The drop is rinsed out with distilled water and the electrode is conditioned for 10 min at constant potential (+550 mV) before the first use. The electrodes are stored at +4 °C and covered with PBS, when not used.

For both glucose and lactate, bare electrodes do not respond or weakly responds within the range where electrodes are tested. For bare electrodes, the current is in the order of nA and signal-to-noise ratio is too high to sufficiently distinguish different concentrations of substrate. As an example, Fig. 5.4 shows the detection of lactate with bare electrodes: the signal is extremely weak, about three orders of magnitude lower than the case of CNT-based electrodes. Instead, CNT-based electrodes are sensitive to glucose and lactate injection and the recorded current is in the order of μA. From those results it is possible to infer that the electron transfer

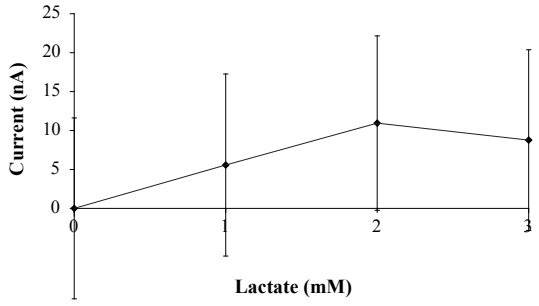

Figure 5.4: Calibration line for lactate detection with bare graphite electrodes.

between the oxidase and the surface is low for bare electrodes. Indeed, glucose oxidase, and more in general oxidases, does not directly transfer electrons to bare electrodes, because the FAD redox center is surrounded by a thick protein layer, creating an intrinsic barrier to direct electron transfer [84]. Second-generation biosensors overcome the difficulty by directly coupling the enzyme with the electrode by means of an artificial mediator, like prussian blue, for example [167]. The role of the mediator is shuttling electrons from the protein redox center to the electrode surface, while the mediator itself is oxidized or reduced. However, most of the *in vivo* devices are without mediators, due to their toxicity. From these results, it is possible to assert that nanomaterials, and in particular carbon nanotubes, are efficient candidates to replace the role of mediators. Moreover, chemical mediators are often bounded successively to the electrode surface, with problems related to mediator concentration and chemical bounding. On the contrary, nanomaterials can be simply drop cast in one step or even directly grown onto the electrode during the microfabrication process[168].

5.2 Enzyme immobilization on graphite electrodes

As already mentioned in the Introduction, electrodes have been structured with different strategies. Several researchers have reported the use of polymer membranes to entrap the enzyme onto the electrode [169], [170], [89]. Conductive polymers seem to be the best solution to develop amperometric biosensors, helping the exchange of charges. Polymers can be used either for entrapment and protective/selective layer. Other immobilization strategies involve fixative solutions, based on polymers, plasma proteins, and organic compounds. Chitosan, for example, is a natural polymer with excellent film-forming abilities, high surface energy for adhesion, and biocompatible properties, and it can be used as immobilization method for enzymes. However, it is a quite good insulator and is often used as selective layer rather than immobilizer [149]. Nafion is a perfluorinated sulfonated cation exchanger, which has been widely used in electrochemical biosensors, as already extensively discussed in Section 3.3.4, especially for its anti-fouling properties [70]. Bovine serum albumin is a plasma protein often coupled with enzymes to create closer physiological conditions for the proteins and

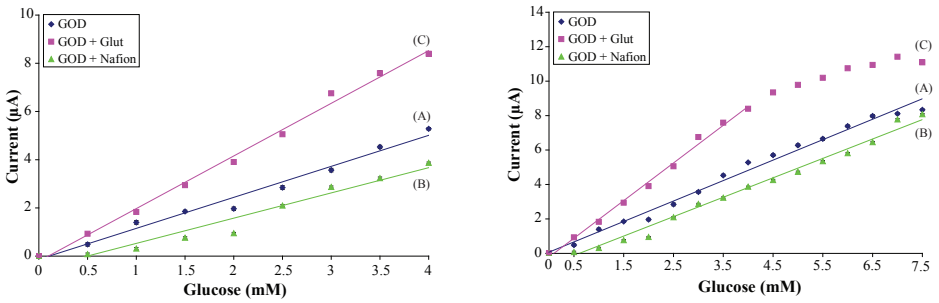

(a) Linear calibration between 0 and 4 mM.

(b) Measurements acquired for a range wider than the linear range.

Figure 5.5: Calibration lines: (A) adsorbed GOD; (B) GOD entrapped in Nafion; and (C) GOD cross-linked with glutaraldehyde. Reprinted from [171].

to improve the temporal stability of the electrodes. Unfortunately, BSA cannot promote the electron transfer, so it has to be coupled with other immobilization strategies. Among the organic compounds, glutaraldehyde is one of the most used cross-linker to fix the enzyme onto the electrode surface. All the aforementioned strategies have been presented together with different types of biosensors. In the next section we will choose three methods and we will compare them for enzyme immobilization by using CNT-based electrodes [171].

5.2.1 Immobilization strategies

The following evaluation is performed with glucose biosensors, but it can be obviously extended to other type of oxidases. CNT-based electrodes are prepared as described in Section 5.1.1, while the enzyme is entrapped with three different methods. For simple protein adsorption onto CNT-based electrodes, 20 μl of glucose oxidase (15 mg/ml) are cast onto the working electrode and stored overnight at +4 °C. For the electrode with Nafion (CNT/GOD/Nafion), Nafion is diluted at 0.5 wt% with a solution of 50% of ethanol and 50% of distilled water, according to the procedure reported in [25]. A drop of 2 μl of diluted Nafion is deposited onto the electrode and allowed to dry, forming a matrix of polymer which should protect the electrode from fouling and improving protein immobilization. For glutaraldehyde immobilization (CNT/GOD/glut), proteins are dispersed in PBS and glutaraldehyde 0.25% solution. Afterwards, 20 μl of the mixture is drop cast to cover the working electrode and stored overnight at +4 °C. Then, the drop is rinsed out with distilled water. All the three electrodes are conditioned for 10 minutes at constant potential (+550 mV) before the first use and stored at +4 °C in PBS when not used. Linear range, detection limit, sensitivity and lifetime are considered in order to evaluate the best immobilization strategy.

Comparison for different immobilization strategies

Calibration lines are derived from chronoamperometries within the concentration range from 0 to 4 mM of glucose with steps of 0.5 mM. The three electrodes are tested in the same

conditions and calibration curves are shown in Fig. 5.5a. GOD simply adsorbed onto CNT has a sensitivity of 10.24 μA/mM cm^{-2} in a range from 100 μM to 6.5 mM. Detection limit is calculated as 3 times of signal-to-noise ratio [37] and results in a value of 97 μM. The oxidase entrapped in Nafion shows a sensitivity of 8.18 μA/mM cm^{-2}, within a linear range from 500 μM to 7.5 mM and a detection limit of 59 μM. Finally, the enzyme cross-linked with glutaraldehyde has a sensitivity of 17.38 μA/mM cm^{-2} in a linear range from 25 μM to 5 mM and with a detection limit of 16 μM. The cross-linking shows the narrowest linear range, probably due to the fact that glutaraldehyde denaturates part of the enzyme during the cross-linking, leaving a smaller functioning amount on the CNTs. Regarding Nafion, these results are in accordance with what obtained by Rahman *et al.* [85]: they showed that electrodes modified with MWCNTs and Nafion exhibit wider range compared to unmodified electrodes. On the other hand, the same electrodes show a lower concentration limit: the sensor seems to be insensitive for values lower than 500 μM, due to its anti-fouling properties. Nafion films have been extensively used for their anti-interferent and anti-fouling properties in electrochemical sensing, since they work like an effective pre-selective barrier, eliminating anionic biological interferances due to ascorbic and uric acid [172]. However, Tsai *et al.* [70] showed that peak current decreases drastically if the glassy carbon electrode is coated with 0.5 wt% Nafion. Nafion film behaves like a barrier in diffusion on the surface of the electrode, as demonstrated by the detection limit.

Effect of Nafion volume on electrocatalytic properties of the biosensor

We also investigated Nafion volume cast onto the electrode, in order to determine its influence on the biosensor response. Nafion is cast in three different amounts (volumes of 1, 2, and 3 μl). Fig. 5.6 illustrates calibration lines for different polymer volumes. Sensitivity decreases with Nafion volume cast onto the surface, as also shown by Tang *et al.* [172]. The values of sensitivities for 1, 2, and 3 μl are 8.42 μA/mM cm^{-2}, 7.02 μA/mM cm^{-2}, and 5.33 μA/mM cm^{-2}, respectively. Note that sensitivity decreases drastically for higher volume of Nafion: the higher the volume, the thicker the matrix. Although Nafion is a cation exchanger, it obstructs glucose molecules to reach the electrode surface, and then glucose oxidase.

Sensor lifetime

Measurements of glucose are carried out for 38 days, in order to verify the stability of the different strategies for enzyme immobilization. The three electrodes are tested for a range of concentrations from 0.5 up to 4 mM every 2-3-4 days over 24 days. After a pause of 1 week, they are eventually tested to see the retained activity. Fig. 5.7, Fig. 5.8, and Fig. 5.9 illustrate the aging of the three immobilization strategies for 2.5 mM of glucose.

For the case of GOD cross-linking with glutaraldehyde, the 100% of the retained activity is considered the one related to the 3^{rd} day, because we observed a more evident increase of enzyme activity after some days from the electrode preparation, with respect to the other cases. Moreover, the measurement is unstable during the first ten days after the immobilization. It

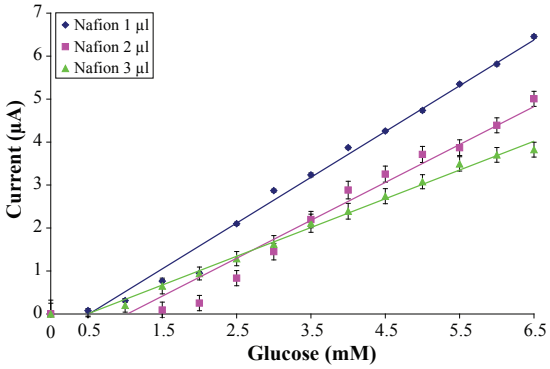

Figure 5.6: Calibration line for GOD entrapped in different quantities of Nafion. Reprinted from [171].

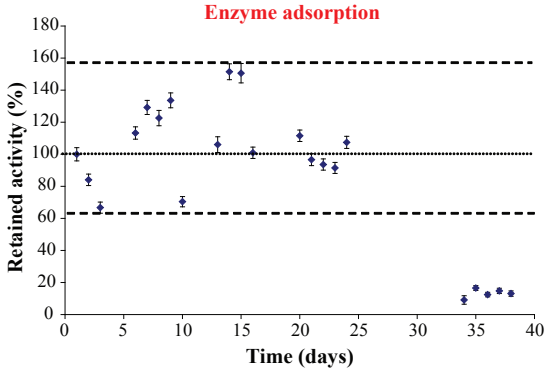

Figure 5.7: Stability of the adsorbed GOD onto the electrode surface for the detection of 2.5 mM of glucose. The applied potential is +550 mV. Reprinted from [171].

could be due to the fact that cross-linking process is still under development, and the enzyme needs more time to stabilize.
None of the three immobilization strategies highlights a specific trend over 25 days, but all the measurements oscillate around the 100% of the retained activity. The difference is really evident after 30 days, where GOD cross-linked with glutaraldehyde shows the highest lifetime. Indeed, the measurements are still around 100% after 35 days, without any identifiable decay over the time. On the contrary, for the other two strategies of immobilization there is a clear decay after 24 days, with a consequent retained activity of around 16% and 23% for adsorption and entrapment strategies, respectively.
The entrapment in Nafion (over the first 24 days) and the cross-linking (after the first 10 days) are the methods with highest reproducibility, with an error around 14%. GOD adsorbed on the electrode surface shows an error around 23%, denoting lower reproducibility. The values related to the retained activity are quite similar with what was previously found in literature. Regarding the adsorption of GOD onto MWCNT, Wang *et al.* [173] found that for the detection of 1 mM of glucose, the retained activity after 25 days was about 97%. Their sensor was quite

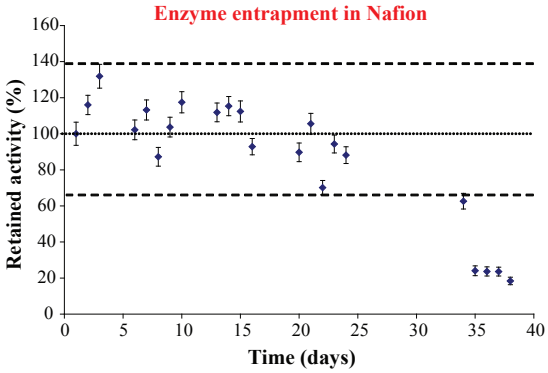

Figure 5.8: Stability of the entrapped GOD in Nafion matrix for the detection of 2.5 mM of glucose. The applied potential is +550 mV. Reprinted from [171].

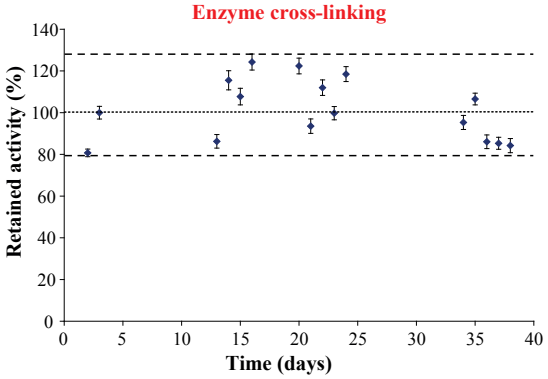

Figure 5.9: Stability of the cross-linked GOD with glutaraldehyde for the detection of 2.5 mM of glucose. The applied potential is +550 mV. Reprinted from [171].

similar to the one of the present work, since they just adsorbed GOD onto grown MWCNT. The best result for the case of adsorbed enzyme was obtained by Crounch *et al.* [174], where there was no apparent reduced activity of the sensor after 550 days. However, the immobilization strategy was quite different, since they developed a water-based carbon ink containing glucose oxidase and they stored the sensor in desiccated conditions, when not used. For the case of GOD entrapped in a Nafion membrane, Tang *et al.* [172] showed that the current response was still retaining the 73.5% of the initial value after 22 days, coherently with what was found in the present work. For the case of enzyme cross-linking, the work of Kang *et al.* [86] showed a retained activity of about 92% after 35 days and 85% after 50 days, in the case of 1 mM of glucose.
Table 5.2 reports the main features of biosensors developed with the three immobilization strategies. From the point-of-view of cell culture monitoring, the three presented techniques show an appropriate stability to be employed for this purpose. From the presented results we can conclude that glutaraldehyde cross-liking seems to be the most suitable method for cell culture monitoring, surviving for more than 40 days.

Table 5.2: Resume of the main features for the three immobilization strategies.

	Sensitivity (μA/mM cm^{-2})	Limit of detection (μM)	Linear range (mM)	Lifetime (days)
Adsorption	10.24	97	0.1 - 6.5	24
Entrapment	8.18	59	0.2 - 7.5	34
Cross-linking	17.38	16	0.025 - 5	>38

5.2.2 SEM images

To test the effective adsorption of the enzyme onto CNT-sidewalls we acquired *Scanning Electron Microscope* (SEM) pictures. SEM images of bare graphite, carbon nanotubes-based electrodes, and CNTs functionalized with oxidases are showed in Fig. 5.10. The morphology of nanostructured electrodes is clearly related to carbon nanotube properties, as demonstrated by the flatness of the bare electrode surface (Fig. 5.10A), where graphite nanoparticles can be clearly identified (Fig. 5.10B). Since nanotube walls are highly hydrophobic, as already discussed in Section 3.1, they tend to form bundles, as depicted in Fig. 5.10C, even if they consist of individual carbon fibers, as detailed in Fig. 5.10D. In the case of nanotubes functionalized with enzymes, the protein layer entirely covers the free-space within bundles (Fig. 5.10E), and wraps each carbon nanotube (Fig. 5.10F). The fiber size spans from 10.98± 1.64 nm, in the case of bare CNTs, up to 18.90± 2.09 nm, in the case of CNTs functionalized with GOD. Size variations are visually estimated by image analysis. The glucose oxidase from *Aspergillus Niger* is illustrated in Fig. 5.11, which structure has been obtained at 1.9 Å resolution [175]. It consists of two sub-units with individual size ranging from 2.6 up to 7.5 nm. Similarly, the lactate oxidase is a protein composed by four sub-units, which measure within 4.6 and 9.7 nm [176] (data not showed). Crystallographic models confirm that size enlargement measured in SEM images is compatible with a single layer of proteins around the nanotubes (refer to Fig. 5.11) [3].

5.3 *Off-line* measurements of glucose and lactate

In the previous section, we have shown that carbon nanotubes can significantly enhance the detection of metabolites and also offer an excellent immobilization surface. Glucose and lactate can successfully be detected by the developed biosensors. In this section, we will discuss about the calibration of glucose and lactate biosensors and we will show the validation of such biosensors in the detection of glucose and lactate in a cholinergic neuronal cell culture [3].

SN56 cell line is derived from the fusion of septal neurons of postnatal day 21 mice with N18TG2 murine neuroblastoma cells [177]. Proliferating cells are maintained in *Dulbecco's modified Eagle's medium* (DMEM), supplemented with 10% *Foetal Bovine Serum* (FBS), 2

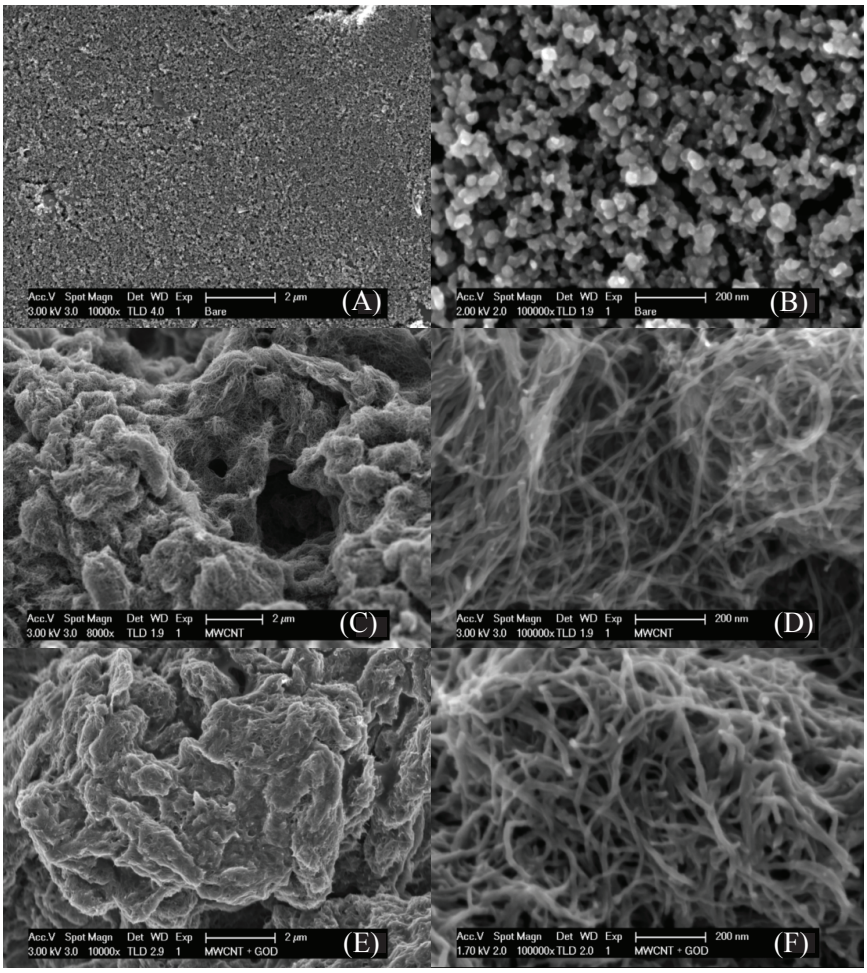

Figure 5.10: SEM images of multi-walled carbon nanotubes. (A) and (B) illustrate the surface of the screen-printed electrodes without MWCNT; (C) and (D) depict MWCNT drop-cast onto screen-printed electrodes from a chloroform solution of mono-dispersed tubes; (E) and (F) show MWCNT functionalized by using glucose oxidase. Reprinted from [3].

mM L-glutamine, and 40 U/ml penicillin/streptomycin in 25 cm^2 culture flask in a 5% CO_2 atmosphere at 37° C. Medium in the stock flasks is changed every 48 h and the cells are sub-cultured when they reach 80-90% of confluence. Cells are seeded at 5x10 ^{3}, 2.5x10 ^{4}, 2x10 ^{5} cell/cm^2, after four passages from thawing. Then, they are cultured onto uncoated wells in proliferating conditions for 48 h or onto poly-L-lysine coated wells when induced to differentiate, with or without cover lips, depending on the experiment. Differentiating cells are let adhere to coated substrates for further 48 h in the same, but serum free, growth medium; afterwards, they are supplemented with 1 μM *all-trans-retinoic acid* (RA) for 48 h [178]. Surnatant conditioned medium is collected for glucose and lactate level measurements at 4, 24, and 48 h after RA supply.

For glucose deprivation experiments, the differentiation by RA treatment is induced after 48 h of proliferation. Cells at 2.5x10^4 are subjected to glucose deprivation. Briefly, complete

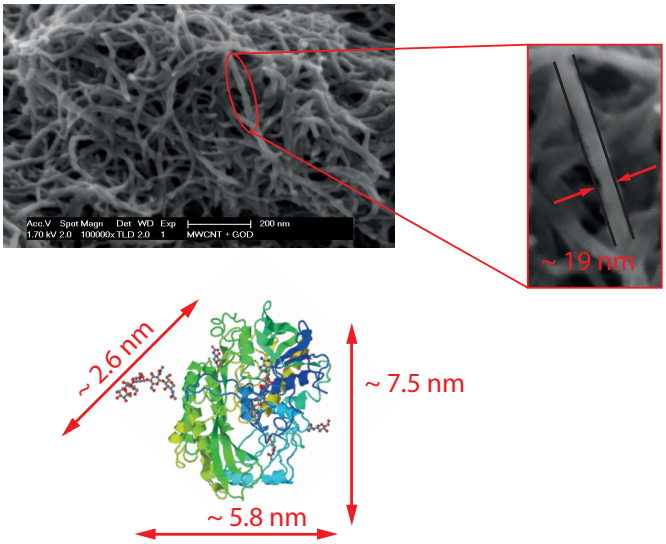

Figure 5.11: Magnified image of MWCNT functionalized with glucose oxidase. Carbon nanotube enlargement can be visually estimated by SEM images. Glucose oxidase structure is reprinted from *www.rcsb.org*.

medium (glucose 22.4 mM) is removed and cells are washed twice with glucose-free DMEM, 2 mM L-glutamine, 44 mM $NaHCO_3$, 40 U/ml penicillin/streptomycin, supplemented or not with FBS. Cells are glucose-deprived for 48 h by using the glucose-free medium described above.

5.3.1 Biosensor calibration

For calibration and investigation of the detection limits, the electrode is dipped into the PBS solution with a volume of 25 ml under stirring conditions. A volume of 25 μl per step of the target molecule is successively added into the solution with a time-step of 2 min. To perform measurements, we apply a potential of +550 mV vs Ag/AgCl, which corresponds to the oxidation potential of the hydrogen peroxide. For glucose biosensor, we obtain a sensitivity of 27.7 μA/mM cm^{-2}, a linear range within 0.5 and 4 mM, and a detection limit of 73 μM (considering a signal-to-noise ratio of 3). For lactate detection, we achieve a sensitivity of 40.1 μA/mM cm^{-2}, a linear range within 0.5 and 2.5 mM, and a detection limit of 28 μM. Calibration lines for both glucose and lactate are depicted in Fig. 5.12a, while the lower limit of detection was investigated for both the biosensors and it is reported in Fig. 5.12b.

The range of detection is chosen according to the fact that Hwang *et al.* [179] reported a mean value of 10.9 mM for lactate in the case of murine embryonic stem cells. For the case of glucose, instead, the maximum concentration in culture medium is roughly within 15 and 23 mM. Since it is not possible to perform measurements in pure medium, due to the fact that media are typically enriched with proteins, amino acids, growth factors, etc., the detection is performed in diluted medium (dilution 1:10 in PBS), so that the mean concentration of

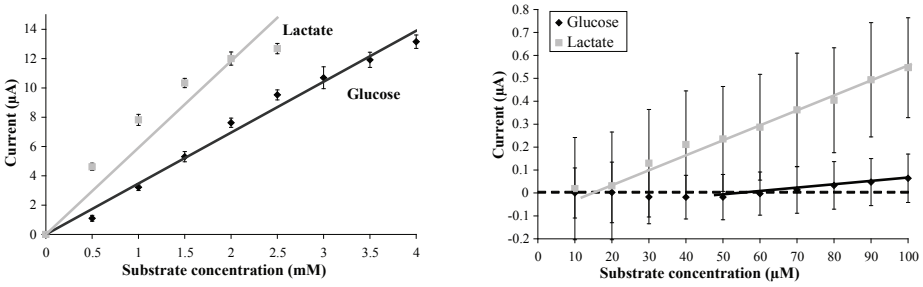

(a) Calibration lines for glucose and lactate in the concentration range of interest.

(b) Lower limit of the linear range for glucose and lactate biosensors.

Figure 5.12: Calibration lines and linear range for our glucose and lactate biosensors. Reprinted from [3].

interest is in the order of some mM for both glucose and lactate. By dilution step, we are able to detect the typical concentrations of glucose and lactate in cell culture with our biosensors. The range from 0.5 to 2.0 mM for lactate and from 0.5 to 4.0 mM for glucose are perfectly suitable for the objectives of the present research, by considering the dilution of the medium.

5.3.2 Metabolites in different cell densities

As mentioned above, DMEM is diluted with PBS in a rate of 1 to 10 to fall in the linear range of biosensors. Measurements are collected at the time of the seeding, and 4, 24 and 48 hours later. The same diluted medium is used for glucose and lactate detection: the probe enzyme onto the electrode is different, neither cross-talk nor interferences is noticed from other interfering compounds during measurements. The behavior of glucose uptake and lactate production is depicted in Fig. 5.13a and in Fig. 5.13b along 48 hours of cell culture for different densities of cells [3].

Note that glucose uptake and lactate production are different for various cell densities. It means that with the developed biosensors it is possible to distinguish metabolic variations according to cultivation conditions. Another important point is that glucose uptake and lactate production shapes are quite symmetric. The lack of feeding, i.e. glucose, induces the production of lactate, which is a mark of cell suffering. Consequently, the symmetry of trends is a further confirmation of this phenomena. On the other hand, in the lowest cell density the developed biosensor records an uptake of glucose in the first 4 hours, but afterwards the cells have enough feeding to survive more than 48 hours without changing the medium. It is also confirmed in two ways by the fact that lactate production is almost zero. On the contrary, for the highest cell density, glucose uptake increases along time, while lactate production reaches the maximum after 48 hours. Cells are still living, but the change of medium is required. From this perspective, the developed biosensors can be a useful instrument to investigate mechanisms, which occur during cell proliferation, while simultaneously provide information

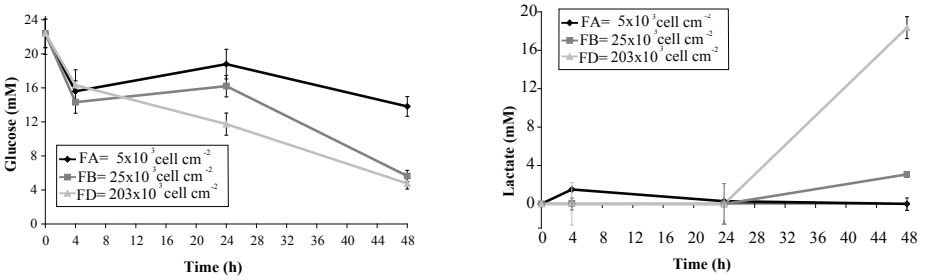

(a) Glucose uptake in cell line SN56 after 4, 24, and 48 hours.

(b) Lactate production in cell line SN56 after 4, 24, and 48 hours.

Figure 5.13: Glucose uptake and lactate production along 48 hours of cell culture for different densities of cells. Reprinted from [134].

to the operators about cell culture conditions and right timing for further cell feeding.

5.3.3 Metabolites in proliferation and differentiation states

With the aforementioned assumptions, we employ randomly distributed carbon nanotubes onto screen-printed electrodes to develop biosensors for glucose and lactate detection in cell culture medium. We validate and characterize our *in vitro* system by analyzing cell morphology, expression of neuronal and cholinergic markers, and cell viability both in proliferation and in differentiation phases, prior to identify their metabolic behavior.

Neuronal phenotype is induced by 48 h exposure to RA, as indicated by branched arborization (Fig. 5.14A and B, betaIII-Tubulin) and expression of neurochemical markers associated with mature cholinergic phenotype (Fig. 5.14C and D, ChAT-immunoreactivity; Fig. 5.14E and F, nerve growth factor low affinity receptor (p75)-immunoreactivity). To verify the effect of treatment with RA on cell number, cell viability is evaluated at a cell density of 2.5 x 10^4 cell/cm^2 by MTT (3-(4,5-Dimethylthiazol-2-yl)-2,5-diphenyltetrazolium bromide) assay. SN56 proliferation is confirmed by the progressive increase of viable cells over the culture time (superimposed bars on Fig. 5.16A and C), whereas RA exposure results in a decrease of viability over the culture time, confirming the interruption of proliferation (bars on Fig. 5.16B and D). These neurons uptake glucose from the medium, and partially convert it via anaerobic glycolysis into lactate. Assuming this metabolic mechanism, we plate the SN56 cells at different cell concentrations, collecting surnatants at 3 time points, to challenge our sensor with different glucose consumption (Fig. 5.16A and B) and lactate production rates (Fig. 5.16C and D). Therefore, we compare metabolite dynamics during proliferation (Fig. 5.16A and C) and differentiation (5.16B and D) conditions (obtained in the absence and in the presence of RA, respectively), to validate our sensors for neural cell monitoring. The expected metabolic behavior is depicted in Fig. 5.15, according to cell state.

Nanostructured sensors detect a progressive uptake of glucose in the media over the time,

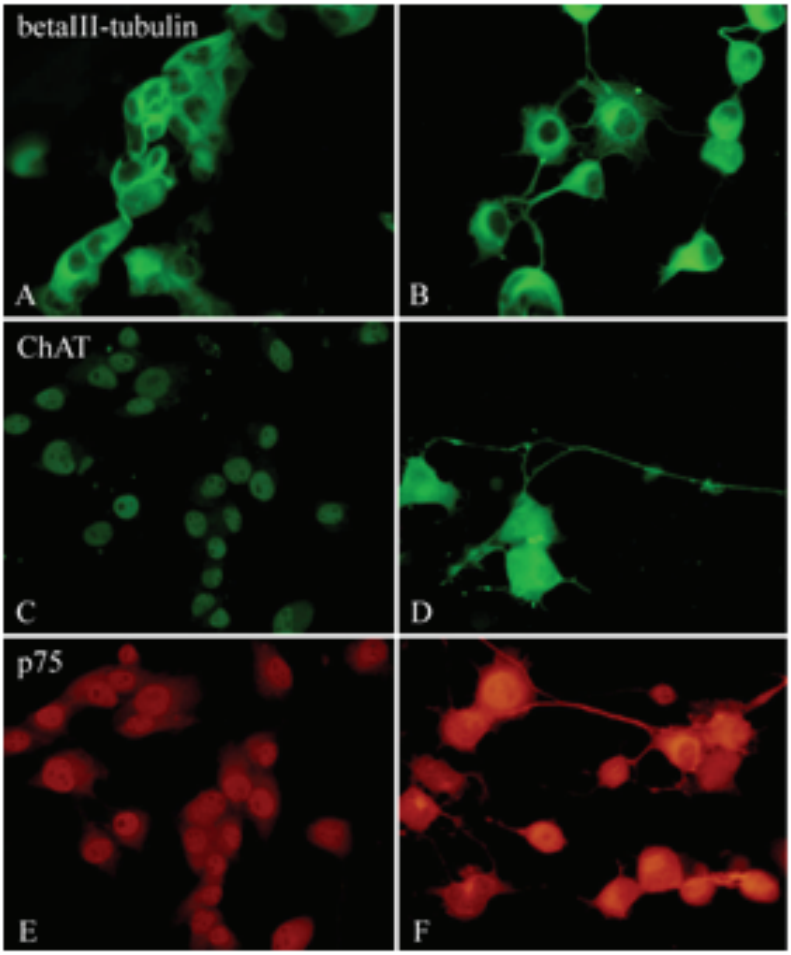

Figure 5.14: Images from optical microscopy of different cell culture experiments. Neuronal phenotype is induced by 48 hours exposure to RA, as indicated by morphology (A, B, Beta-tubulin), neurochemical marker expression (C, D, ChAT-immunoreactivity) and cholinergic marker expression (E , F, nerve growth factor low affinity receptor p75). Reprinted from [3].

depending on cell density and time in culture, as illustrated in Fig. 5.16A and B. Glucose uptake in mature neurons (Fig. 5.16B) occurs at a lower rate than in proliferating cells (Fig. 5.16A), with the exception of the lowest cell density. It can be also observed that glucose concentration changes extremely fast in the case of proliferating cells (Fig. 5.16A), while it shows more stable curves during differentiation (Fig. 5.16B).

Neuronal lactate production in proliferating and differentiating cells is demonstrated by Fig. 5.16C and D, respectively. Lactate levels progressively rise accordingly to cell number and proliferation/differentiation state, in a symmetrical manner with respect to glucose shapes. A sharp decrease in glucose concentration corresponds to an increase of the same extent in lactate levels, as obtained with higher cell density. Furthermore, lactate production is affected by cell state, occurring earlier and in a sharper manner in differentiating cells (Fig. 5.16D) than during proliferation (Fig. 5.16C). Note that in the case of 5 x 10^3 cell/cm^2, lactate amount

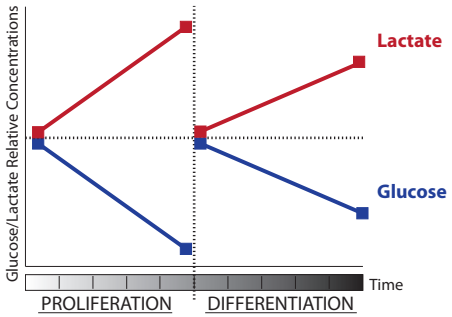

Figure 5.15: Expected metabolic behavior for glucose uptake and lactate production in SN56 cell line.

is below the detection limit of the sensor. Glucose and lactate behaviors identified with the developed biosensors are also confirmed by measurements performed with a commercially available spectrophotometer assay, as showed in Fig. 5.17.

5.3.4 Measurements in glucose deprivation

To further explore the effectiveness of our biosensors in monitoring cell state changes, we dramatically modified neuronal metabolism by removing glucose from the culture media, thereby inducing a metabolic stress. The glucose deprivation model is then applied to SN56 cell culture after 48 hours of proliferation or differentiation, and both glucose (Fig. 5.18A and B) and lactate (Fig. 5.18C and D) are measured in the surnatants.

Fig. 5.18A and B describe glucose levels in complete and glucose-free culture media in proliferating and differentiating cells, respectively. Glucose levels are low and stable at this time, independently of cell state (Fig. 5.18A and B, grey round dots), while values in deprived media are below the detection limit of the sensor (Fig. 5.18A and B, white square dots). Fig. 5.18C and D describe lactate levels in complete and glucose-free media, in proliferating and differentiating cells, respectively. Lactate levels are higher and more dynamic in the proliferating cultures (Fig. 5.18C and D, grey round dots) than in the differentiated ones (Fig. 5.18C and D, white square dots). The superimposed bars refer to cell viability measured by MTT assay in presence (grey bars) or absence (white bars) of glucose, and clearly indicate cell death in glucose-deprived cells, particularly in the case of differentiating cells.

Cell death induced by glucose deprivation was previously reported in SN56 cells [180], [181] and neurons in culture [182]. SN56 is a line of choligernic neurons which are highly sensitive to several stressors and to metabolic alterations. The interest about cholinergic neurons is connected to Alzheimer's disease, where their nearly loss is associated with a metabolic impairment in brain, whose extent is proportional to the severity of the cognitive deficits [182] [183]. Furthermore, RA treatment increases SN56 vulnerability to oxidative stress, as demonstrated by an increase of caspase-3 mediated cell death [184] [185] and lactate dehydrogenase

activity, which is responsible for lactate production and consumption [186]. From the detected responses we can infer that the amount of glucose is not enough for a correct cell feeding, as recorded just after 4 h. Coherently, in proliferating cells our biosensors measure a massive lactate production after 4 hours, followed by a dramatic decrease within 24 hours, and a sharp increase between 24 and 48 h. Furthermore, our results show that in actively proliferating cells, the lack of glucose for 24 h results in the consumption of neuronal lactate, dynamically released into the medium. These data confirm the idea that glucose consumption during increased neuronal activity might be non-oxidative [187] [188] [189] and results in lactate production. It has been hypothesized that astrocytes may produce lactate durig neuronal activation. Lactate is then oxidized by neurons to yield energy, playing a neuroprotective role after cerebral ischemia [190] [191]. According to other authors, oxidation of lactate by neurons would only be possible if the glycolytic consumption of glucose or its transport were inhibited [192]. The cellular system employed in this study contains uniquely neuronal cells [193]. Thus,

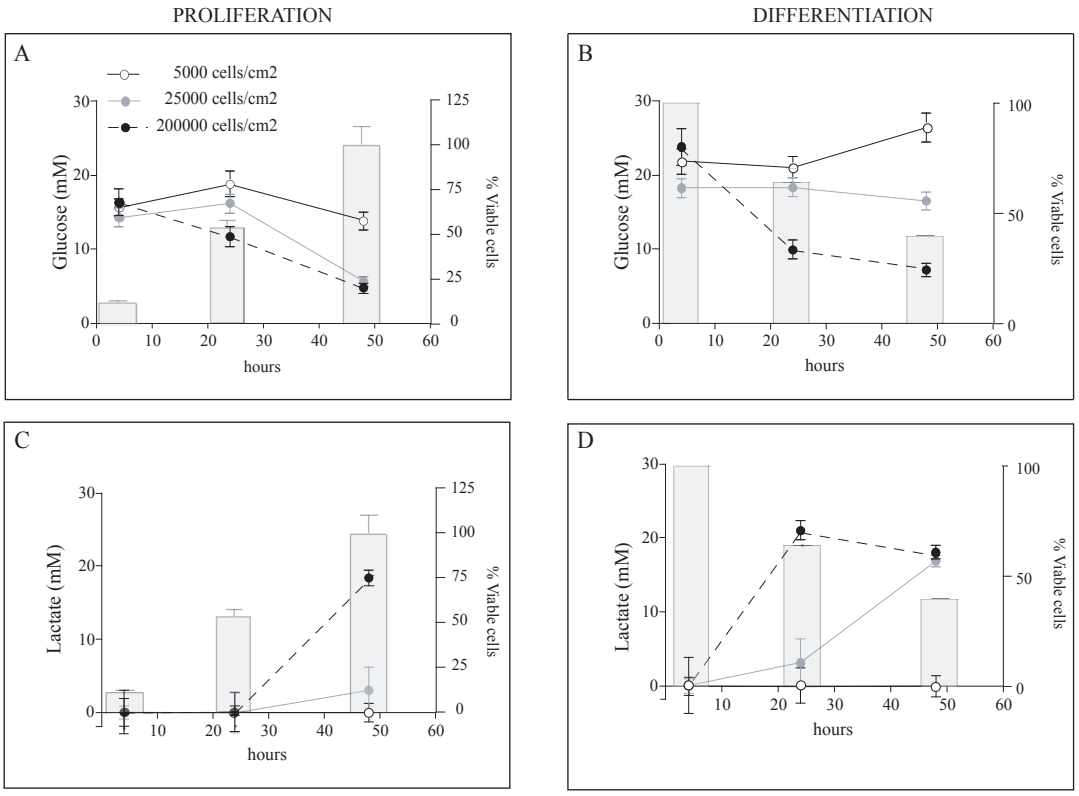

Figure 5.16: Effect of cell density and state on glucose and lactate levels in cell cultures. Dot-plots represent glucose (A) and (B) and lactate (C) and (D) concentrations (indicated on left y-axis) in SN56 supernatants collected from cell cultures at three different densities, at 4, 24, and 48 h (as indicated on the x-axis). The superimposed bar graphs point out the results of the cell viability assays in proliferation (A) and (C) and differentiation (B) and (D) media. The right y-axis indicates the percentages of viable cells respect to the control groups (100% of viable cells). Reprinted from [3].

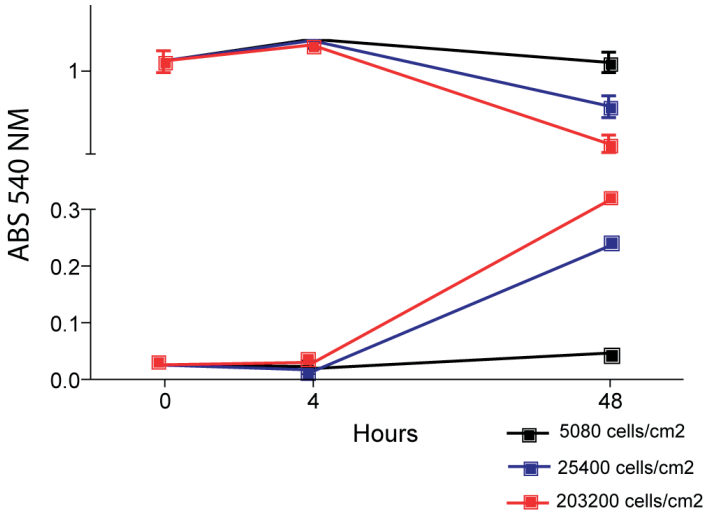

Figure 5.17: Spectrophotometric assay for glucose uptake and lactate production for differen cell densities. Relative absorbance respect to blank solution is measured at different cultivation time.

it offers the chance to make assumption about neuronal behavior.

5.4 Characterization of microfabricated electrodes

Following the experiments with screen-printed graphite electrodes and the encouraging results related to glucose and lactate detection in diluted cell culture media, we repeat a similar set of experiments with our microfabricated platform. First we carry out a comparison between commercial SPEs and our electrochemical cell. Instead of graphite electrodes, we purchase screen-printed electrodes from Dropsens, with gold working and counter electrodes, and platinum reference electrode, to perform a comparison with the same electrode materials. The only difference between the two electrochemical cells is the diameter of the working electrode: 2 mm^2 in the case of the screen-printed, while 0.2 mm^2 in the case of the microfabricated electrodes. The comparison can be performed prior a normalization respect to the working electrode area.

5.4.1 Electrode characterization with ferricyanide

Ferricyanide solutions are prepared in the range of 0 - 20 mM in PBS (ferricyanide is purchased in powder from Sigma-Aldrich, Switzerland). For cyclic voltammetry characterization, electrodes are kept in quiescent conditions, by casting a 100 μl drop of substrate to cover the whole electrochemical cell. We perform 10 cycles to obtain a stable voltammetry and we consider the last one for data analysis. We repeat the measurements for several concentrations of ferricyanide for all the five electrodes. Fig. 5.19 illustrates an example of cyclic voltammetry

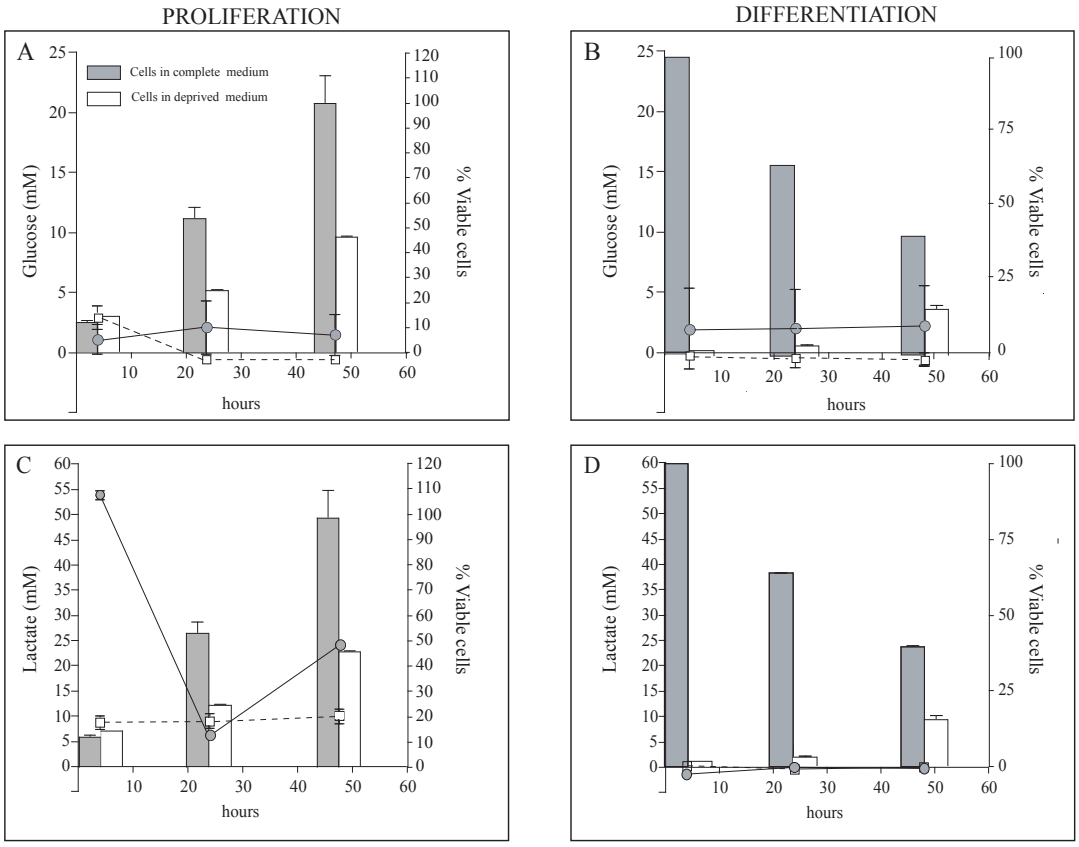

Figure 5.18: Effect of glucose deprivation on glucose and lactate levels in cell cultures. Dot-plots represent glucose (A) and (B) and lactate (C) and (D) concentrations (indicated on left y-axis) in SN56 supernatants collected from cell cultures at the time-points indicated on the x-axis). The superimposed bar graphs point out the results of the cell viability assays in complete and deprived media, both in proliferation (A) and (C) and differentiation (B) and (D) conditions. The right y-axis indicates the percentages of viable cells respect to the control groups (100% of viable cells). Glucose and lactate concentration have been calculated using the standard curve. Reprinted from [3].

performed on the five WEs for 10 mM of ferricyanide. The cyclic voltammetries overlap for different electrodes and the two peaks of ferricyanide are well shaped. The average potential for the oxidation peak is 229.4 ± 7.3 mV, while for reduction peak is 109.2 ± 8.7 mV. Therefore, the difference among the electrodes is lower than 10% (much lower in the case of oxidation peak, which is the one we use for the following measurements).
Peak height varies according to substrate concentration under cyclic voltammetry for both SPE and microfabricated electrodes. If we compare the two calibration lines, once they are normalized for the electrode area, we notice an almost perfect superimposition, as shown in the inset of Fig. 5.19. That result guarantees that microfabricated electrodes are suitable to be used as electrochemical biosensors.

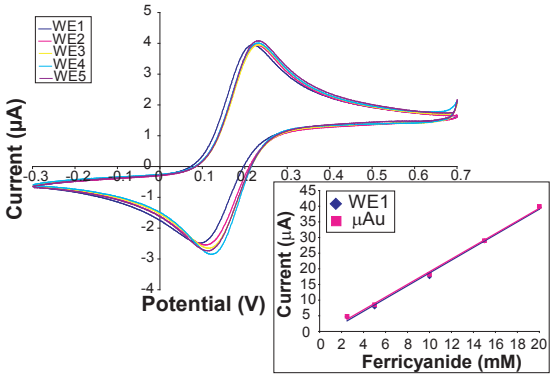

Figure 5.19: Cyclic voltammograms of 10 mM ferricyanide for the five working electrodes (scan rate 100 mV/s). Inset: comparison between commercial screen-printed and microfabricated electrodes for ferricyanide.

5.4.2 SEM images of the enzyme immobilization onto microfabricated electrodes

In Section 5.2.2 we have shown SEM images of graphite screen-printed electrode with CNT structuring and enzyme functionalization. We also acquired SEM images of our microfabricated electrodes in the same conditions, because we want to investigate the surface of the gold electrodes with CNT structuring and enzyme immobilization. Fig. 5.20a shows the gold surface of the electrode with cast MWCNTs and Nafion aggregates. Differently from the case of bare graphite, gold surface is completely flat and smooth. Surface discontinuity are given by the presence of CNT bundles and Nafion particles. Fig. 5.20b shows carbon nanotubes with an adsorbed layer of enzyme (lactate oxidase in this case). The morphology of modified electrodes is clearly related to carbon nanotube properties and their arrangement on the electrode surface. Carbon nanotubes are randomly dispersed, forming tangled bundles. Protein layer entirely wraps each carbon nanotube and results in diameter enlargement, as already discussed Section 5.2.2 for the case of screen-printed electrodes. Moreover, it is possible to distinguish also Nafion nanoparticles, which are solvent residues.

5.4.3 Calibration in PBS for different metabolites

We proved that H_2O_2 detection is possible with the developed biosensors. As already mentioned in Section 2.4.1, hydrogen peroxide is the common product of all reactions promoted by the oxidases. So, its detection is fundamental for the purpose of our research. Now, our sensors can be evaluated for glucose, lactate, and glutamate detection, so oxidases are spotted onto three different electrodes and performance of the biosensors are estimated. The three metabolites are detected in a range between 0 and 1000 μM with steps of 200 μM in PBS, to evaluate the sensitivity and the detection limit of the three biosensors. Calibration lines for glucose and lactate are depicted in Fig. 5.21a, while Fig. 5.21b shows the calibration line for glutamate. In particular, glutamate biosensor starts responding from 400 μM and the current range involved in the measurement is much lower, more than one order of magnitude, with

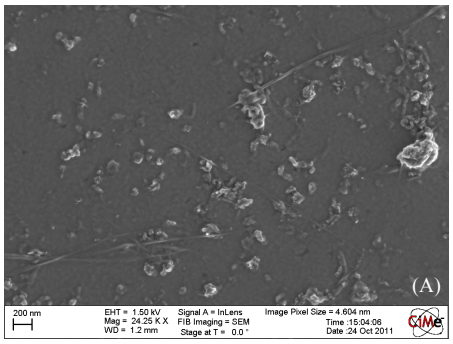

(a) SEM image of cast MWCNTs and Nafion aggregates onto microfabricated gold electrodes.

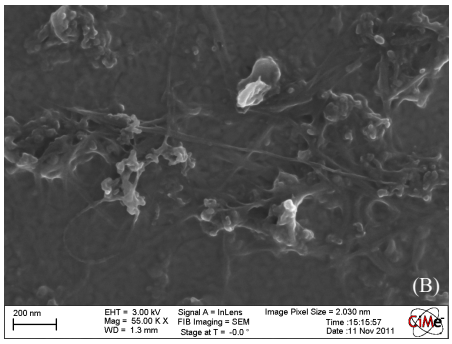

(b) SEM image of lactate oxidase immobilized onto MWCNTs.

Figure 5.20: SEM images of the microfabricated electrodes with CNTs and oxidases.

respect to the previous cases (refer to Fig. 5.21b). For glucose the sensitivity results in a value of 55.5 μA/mM cm^{-2} and a detection limit of 2 μM (S/N=3σ), for lactate in a value of 25.0 μA/mM cm^{-2} with a detection limit of 11 μM, and for glutamate in a value of 0.9 μA/mM cm^{-2} with a detection limit of 78 μM. Table 5.3 compares the state-of-the-art of CNT-based biosensors for glucose, lactate, and glutamate detection.

In the case of glucose monitoring, our biosensor shows the best performance for both sensitivity and detection limit, as illustrated in Table 5.3. All previous works reported in the comparison foresee to randomly drop cast CNTs solution onto the working electrode. Glucose oxidase can be directly mix with CNTs, as proposed by Tsai *et al.* [70], or CNTs can even be functionalized with butyric acid, for example, to increase their immobilization prior to deposition, as described in [91]. The latter approach obtains the best sensitivity, even if the value is half of what we achieve with our biosensor. Wang *et al.* [25] proposed to directly grow CNTs onto a silicon substrate and evaporate afterwards a thin gold film on the top. GOD was then drop cast on the top of carbon nanotubes after their detachment from the substrate. Also in this case the sensitivity of the biosensor results to be lower than in our case. Finally, an approach slightly different foresees to press synthesized MWCNTs to form a sheet-like structure. Then, GOD can be covalently bound to the CNTs of the so-formed "paper" [90]. Also this approach does not give sensitivity as high as in our case.

The literature on lactate biosensors is smaller as compared to the case of glucose detection. However, several modification and functionalization have been proposed as well. CNTs can be incorporated in mineral oil to form a paste [92] or into sol-gel film to form a matrix [93]. The obtained mixture can then be used as electrodes after the oxidase immobilization. However, the resulting sensitivities are lower than the value obtained from our biosensor of two and one orders of magnitude, respectively. Carbon nanotubes can be also doped with nitrogen to enhance sensor response, resulting in a really high sensitivity of 40.0 μA/mM cm^{-2}, although the detection range is indeed narrower (from 14 to 325 μM) [94]. Yang *et al.* [164] proposed titanate nanotubes for the detection of lactate. The obtained sensitivity is again two orders of magnitude lower than our case, suggesting that carbon gives better performance as material

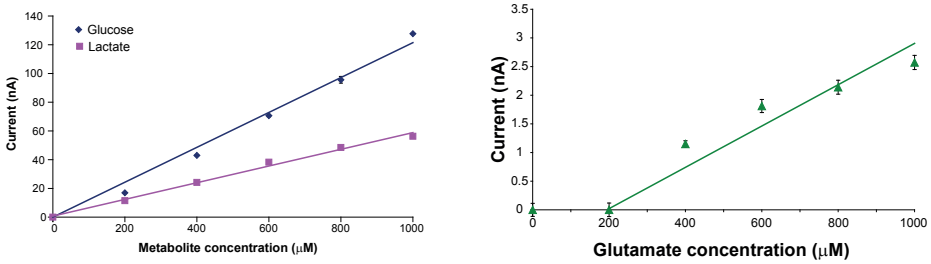

(a) Calibration lines for glucose and lactate detection in phosphate buffer solution.

(b) Calibration lines for glutamate detection in phosphate buffer solution.

Figure 5.21: Calibration lines in PBS for our microfabricated electrodes.

used for detection of hydrogen peroxide and not only for the structure in the nanoscale range. Glutamate microsensors have been extensively proposed to be implanted in the brain and most of them are not based on carbon nanotubes. Zhang *et al.* [98] described the entrapment of glutamate oxidase in chitosan with a sensitivity of 85.0 μA/mM cm^{-2} within 0 and 200 μM. Using Nafion as immobilization matrix, instead, Pan *et al.* [97] covered a Pt electrode with this polymer to entrap glutamate oxidase. The detection was carried out in a really narrow range within 1 and 13 μM, obtaining a sensitivity of 16.1 μA/mM cm^{-2}. Pt electrodes were also enhanced in terms of sensitivity (384 40.0 μA/mM cm^{-2}) with MWCNTs and polyurethane, while glutamate oxidase was dispersed in polypirrole [99]. All previous described sensitivities are higher (up to three orders of magnitude) than the one obtained by our sensors, as reported in Table 5.3. However, we exploited a wider linear range (from 0 to 2 mM), useful for cell culture monitoring. Indeed, we achieve a sensitivity of 0.9 μA/mM cm^{-2} and a detection limit of 78 μ. Sensitivities and detection limits of our biosensors are better as compared with previous results presented in literature. Thus, in the next section we proceed with their calibration in cell culture medium, with a particular attention in measuring the metabolites in the physiological range [194].

Table 5.3: Comparison of similar surface modification based on CNT and oxidases for the detection of glucose and lactate. Reprinted from [194].

	Modification	Sensitivity	Linear range	Limit of detection
GLUCOSE	CNT mat + GOD [90]	4.05 μA mM^{-1} cm^{-2}	0.2 - 2.18 mM	–
	MWCNT/Nafion + GOD [70]	4.7 μA mM^{-1} cm^{-2}	0.025 - 2 mM	4 μM
	MWCNT + GOD [25]	14.2 μA mM^{-1} cm^{-2}	0.05 - 13 mM	10 μM
	MWCNT-BA + GOD [91]	23.5 μA mM^{-1} cm^{-2}	0.01 - 2.5 mM	10 μM
	MWCNT/Nafion + GOD (present work)	55.5 μA mM^{-1} cm^{-2}	0 - 1 mM	2 μM
LACTATE	MWCNT/mineral oil + LOD [92]	0.204 μA mM^{-1} cm^{-2}	0 - 7 mM	300 μM
	Titanate NT + LOD [164]	0.24 μA mM^{-1} cm^{-2}	0.5 - 14 mM	200 μM
	MWCNT + sol-gel/LOD [93]	2.1 μA mM^{-1} cm^{-2}	0.3 - 1.5 mM	0.3 μM
	N-doped CNT/Nafion + LOD [94]	40.0 μA mM^{-1} cm^{-2}	0.014 - 0.325 mM	4 μM
	MWCNT/Nafion + LOD (present work)	25.0 μA mM^{-1} cm^{-2}	0 - 1 mM	11 μM
GLUTAMATE	Nafion + GlOD [97]	16.1 μA mM^{-1} cm^{-2}	0.001 - 0.013 mM	0.3 μM
	Chit + GlOD [98]	85.0 μA mM^{-1} cm^{-2}	0 - 0.2 mM	0.1 μM
	PU/MWCNT + GlOD/PP [99]	384 μA mM^{-1} cm^{-2}	0 - 0.14 mM	0.3 μM
	MWCNT/Nafion + GlOD (present work)	0.9 μA mM^{-1} cm^{-2}	0 - 2 mM	78 μM

5.5 On-line Monitoring of NG-108 Neuroblastoma Cells

NG-108 neuroblastoma cells belong to a neuronal cell line which exhibits two different morphologies according to the cell state. Cells are maintained in Dulbecco's modified Eagle's medium (DMEM/F12 + Glutamax, Gibco-Invitrogen, Switzerland), supplemented with 10% Foetal Bovine Serum (FBS, Gibco/BRL, Rockville, MD, USA) in 25 cm^2 culture flasks (Corning, New York, NY USA) in a 5% CO_2 atmosphere at 37 °C. When reaching 80-90% of confluence (normally after 48-72 hours of culture), cells are split with 0.05% Trypsin-EDTA (Gibco-Invitrogen, Switzerland) and seeded in new flasks, while surnatant conditioned medium is collected for glucose and lactate level measurements [195].

5.5.1 Biosensor calibration for glucose and lactate in cell culture medium

Cell culture medium contains several compounds for cell proliferation and growth. Therefore, pure medium is not suitable to perform electrochemical measurements, due to the numerous electroactive species that can interfere with the detection. Some works [196] overcome the problem by diluting the media prior to perform the detection. However, detection limit is affected by the dilution rate and sensor calibration has to be tuned according to the dilution step. Another approach alternative to dilution is the employment of dialysis membranes. Referring to the classification mentioned in Section 2.1, we perform an *ex situ* sampling for the *on-line* monitoring. The integration of the microdialysis probe in the fluidic system is described in Section 4.4. For glucose detection, we use glucose-free medium (D5030) and D5030 enriched with glucose in concentrations of 5, 10, 15, and 20 mM. The use of the membrane contained in the microdialysis probe allows to significantly extend the linear range of the biosensor playing the role of a diffusion barrier. In this way, we can easily measure glucose uptake in our cell culture medium without any dilution step. Nominal glucose concentration in commercial DMEM is of 3.15 g/l, equal to around 17.5 mM. We also prepare DMEM enriched with lactate, similarly to what we have done for glucose. Lactate concentration for calibration spans between 0 and 20 mM, as in the case of glucose. The range is chosen accordingly to data reported previously in literature for NG-108 neural cells [197] and murine embryonic cells [179]. Calibration lines for glucose and lactate detection in cell culture medium are depicted in Fig. 5.22. Glucose biosensor shows a sensitivity of 1.9 μA/mM cm^{-2} and a detection limit of 1 mM. Although the sensitivity is one order of magnitude lower than in the case of PBS, the linear range reaches up to 20 mM, which enables to measure glucose in cell culture medium. Lactate biosensor is also less sensitive with respect to the case of pure PBS, with a sensitivity of 0.4 μA/mM cm^{-2} and a detection limit of 1.1 mM. However, even in this case we fit the concentration range of interest. The system is now ready to be validated in conditioned cell culture medium.

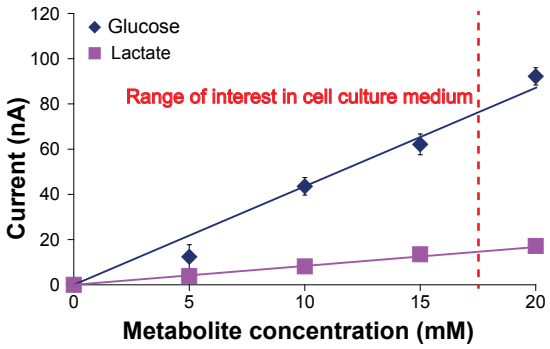

Figure 5.22: Calibration lines for glucose and lactate detection in cell culture medium. Measurements are acquired by using the commercial system.

5.5.2 Metabolic monitoring in a cell line: an example

Glucose and lactate biosensors have shown to be able to detect physiological concentrations of such metabolites in cell culture medium. Lactate production, in particular, is interesting from a biological point-of-view. Cells metabolize glucose mostly via the glycolytic pathway and they produce lactate, which is toxic to animal cells in high concentrations and can inhibit cellular metabolism. For this reason, monitoring lactate production enables a more efficient glucose metabolism and limits toxic accumulation in culture medium [62].

Neuroblastoma cells are derived from animal solid cancers. They can show an immature appearance, possessing a proliferative behavior, and then evolve in a differentiation state by elaborating long neurite-like processes. These properties make them also interesting from the metabolic point-of view.

We performed glucose and lactate detection in surnatant conditioned medium collected from two batches of neuroblastoma cells (NG-108 cell line), cultured in the same conditions. We first deep the microdialysis probe in fresh DMEM (without lactate) to measure the baseline. The fresh medium is then changed with medium containing a known glucose or lactate concentration (17.4 and 10 mM, respectively) without stopping the peristaltic pump and the electrochemical measurement. The current values related to the baseline and the nominal

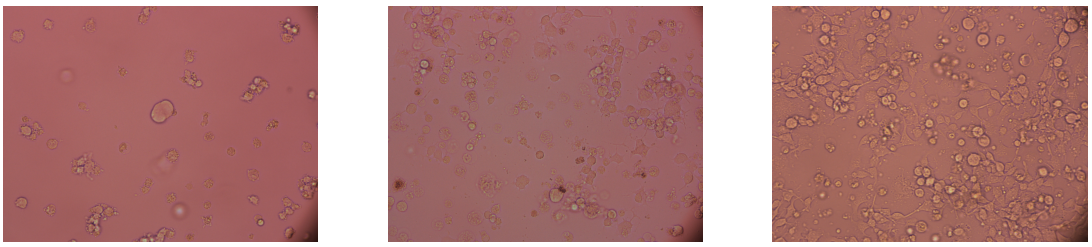

(a) Cells just seeded. (b) Cells after 1 day of cultivation. (c) Cells after 3 day of cultivation.

Figure 5.23: Neuroblastoma cells in three different days of cultivation.

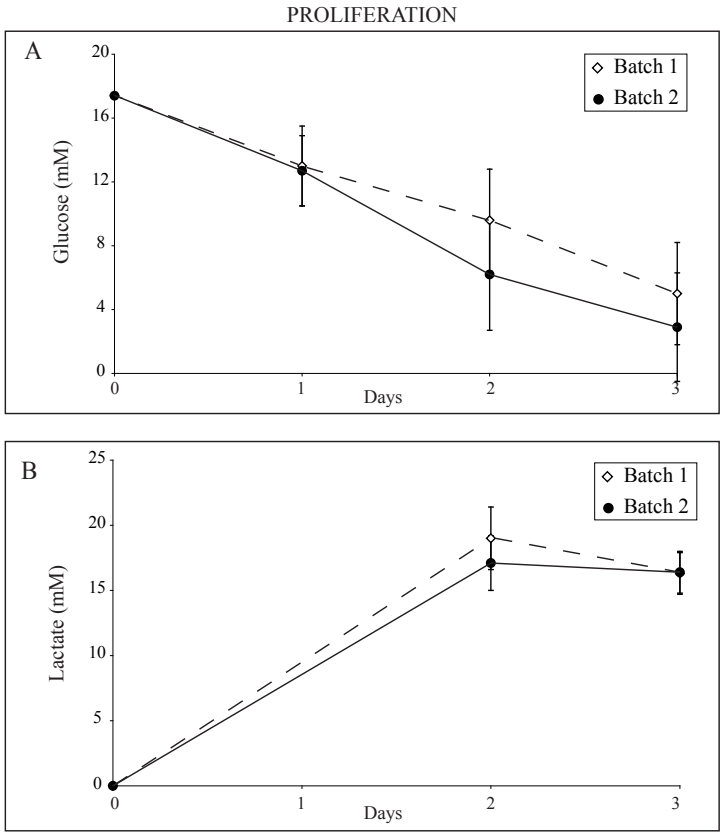

Figure 5.24: Glucose and lactate detection for the two batches of neuroblastoma cells over three days of cultivation.

concentration are used as a further check on the calibration of the biosensor. Successively, the surnatant of one of the two batches is measured for 5 minutes. Among measurements of different concentrations fresh medium deprived of the metabolite of interest is flown to rinse the electrode. Cell culture medium is not changed for three days and the conditioned surnatant is collected once per day from both the batches of neuroblastoma cells. Cell proliferation is visible by optical microscope analysis among different days of cultivation. Fig. 5.23a depicts neuroblastoma cells when seeded in the culture flask. After one day of cultivation they appear like in Fig. 5.23b, where it is possible to observe their rate of proliferation. After 3 days they typically cover the entire floor of the flask, as illustrated in Fig. 5.23c. It is possible to notice that some of the cells have already developed their processes as neurons, so they are at a cell state almost differentiated. However, others still show the characteristic round shape, that is typical for proliferative state. Since they are able to proliferate with quite high rate, we will consider them still in a proliferative state.
In Section 5.3.3 we described glucose uptake and lactate production in SN56 cell line. We performed similar measurements also in NG-108 cell line by monitoring glucose uptake and lactate production during three days of cultivation. Metabolite concentrations are showed in Fig. 5.24 and concentration value are resumed in Table 5.4. As already discussed in Section

Table 5.4: Glucose uptake and lactate production in surnatant conditioned medium.

GLUCOSE	Batch 1	Batch 2
Day 1	(13.0±2.5) mM	(12.7±2.2) mM
Day 2	(9.6±3.2) mM	(6.1±3.5) mM
Day 3	(5.0±3.2) mM	(2.9±3.4) mM
LACTATE	Batch 1	Batch 2
Day 1	—	—
Day 2	(19.0±2.4) mM	(17.1±2.1) mM
Day 3	(16.3±1.6) mM	(16.4±1.6) mM

5.3.3, also in this case we are expecting a metabolic behavior similar to the one in SN56 cells. Indeed, lactate levels increase in correspondence of a decrease of available glucose in the medium along the time. After three days of cultivation, cells have low quantities of available glucose. On the other hand, lactate concentration is already high after two days of cultivation (around 17 mM), and then it remains constant after the second day. Both the two batches of cells show a similar behavior, confirming this general trend for both glucose uptake and lactate production. The difference between the two batches is most probably due to different cell concentration. In the present experiment cells are always seeded with the same rate, but changes in the number of cells are intrinsically subjected to statistical fluctuation. However, lactate values measured in the samples are similar to those reported in [197] for NG-108 cell line. The increase of lactate levels from 0 mM (no lactate in the initial medium) to an average concentration of around 17 mM are a confirmation that cells proliferate. This evidence is fundamental to distinguish different cellular state, since proliferation and differentiation have different metabolic profiles [134], and their recognition can be automated.

5.6 Chapter contributions and summary

In this chapter we have presented the results obtained during our research work. We have started by evaluating the role of carbon nanotubes in biosensing, by comparing hydrogen peroxide detection performed with both bare graphite-electrodes and CNT graphite-based electrodes. Hydrogen peroxide is evaluated because is the common product of the reaction when working with oxidases. The sensitivity of CNT-based sensors results to be 7 times more than for bare sensors. CNTs show to be also the perfect candidates for enzyme immobilization. From SEM images it results that proteins spontaneously adsorb onto CNT sidewalls, forming an homogeneous layer of enzymes surrounding every single nanotube. Glucose and lactate biosensors are tested with CNT-based electrodes and biosensors characterization is performed in terms of sensitivity, linear range, and detection limit. We also evaluated different

immobilization strategies for the enzyme by comparing biosensor performance in the case of simple drop cast, entrapment in Nafion film, and enzyme cross-linking with glutaraldehyde. The last strategy results to be the best method for enzyme immobilization. CNT-based electrodes are then validated in cholinergic neural cell line for the detection of glucose and lactate. The obtained results show significantly different metabolic behaviors according to cell density and cultivation conditions. Moreover, observation of changes in the cell culture leads to develop skillful technologies for unknown cell systems. Biosensors developed in this study were tested and validated in a standard cell line, but such emerging devices can be applied to more complex cell lines, like stem cells, where there is a lack of knowledge about the mechanisms that unfold when cells switch from the stem state to the differentiate state.
Once we characterized commercial electrodes and we optimized CNT and oxidase deposition, we moved on the fabrication of our own integrated platform. We tested commercial gold electrodes and our platform and we compared ferrocyanide redox reactions on both the electrodes. The two electrochemical system did not show significant differences, so we characterized the manufactured electrodes in terms of sensitivity, linear range, and detection limit for glucose, lactate, and glutamate detection. Such characterizations are carried out both in PBS and cell culture media. A further characterization is performed with the fluidic system and the microdialysis probe and we showed that this strategy permits to expand the linear range of the sensor, while avoiding any sample handling for dilution. The complete self-contained system is finally validated for the detection of glucose and lactate in neuroblastoma cell line along the three days of cultivation. Trends for both glucose uptake and lactate production are correctly revealed from measurements performed with our biosensors.

6 Architecture for Electrochemical Measurements

Electrochemical sensors are widely used in many areas, from medicine and diagnostics to food industry, environmental monitoring, and biotechnology. The main reason of their success is that they lend themselves to be miniaturized and integrated in portable devices. In particular, amperometric biosensors require an electronic circuit for performing and transducing the electrical signal generated in the electrochemical cell. Depending on the electrochemical technique used to perform the measurement, the sensing element, the transduction mechanism, and the environment, different electronic features may be requested on board. Power source, transducer circuitry, control unit, wireless communication are some of the blocks that can be potentially used in biosensing systems.
In Chapter 5 we have shown and discussed all results obtained while progressing in the development of the self-contained platform. All reported measurements are obtained with commercial potentiostats for laboratory use. They are typically expensive and bulky, so not suitable for self-contained devices. Moreover, the electrochemical cell or the screen-printed electrodes are often connected to the potentiostat by coaxial and shielded cables, which are not compatible with a sterile environment. Therefore, an *ad hoc* electronics is highly desirable to perform the real-time detection of metabolites. The architecture has to be able to optimally record the current ranges involved in the electrochemical cell, while a wireless communication between the electronic system and a remote station ensures minimally invasiveness and high portability of the device.
Many works and reviews have described the circuits required for interfacing with amperometric sensors and they are available in literature [163], [198], [199]. The design of these circuits requires deep knowledge on both circuit design and redox mechanisms involved in the electrochemical cell. Moreover, system integration is a key-issue to develop smart and optimized biosensors. The development of the biochemical aspect of the sensor goes hand in hand with the design of the electronics. The detection procedure has to be carefully designed to be able to miniaturize and integrate the required circuitry for the chosen electrochemical technique together with the implantable biosensor into a single chip.
In the following chapter, we will describe a suitable architecture for electrochemical measurements in cell culture, taking into account requirements such as low-level noise and minimal

invasivity for *on-line* measurements. In Section 6.1, we will briefly discuss the working principles of the potentiostat. We will give an essential overview on the state-of-the-art of different configurations and we will briefly focus on some issues that can be encountered when realizing an integrated potentiostat. In Section 6.2 we will discuss system requirements and the general building blocks necessary to perform amperometric measurements, by detailing the constrains related to our particular application, such as the current range, the sampling frequency for real-time measurements, and the detection with multiple working electrodes. Section 6.3 will describe the main blocks and the chosen components for the realization of the prototype. Applied potentials, current ranges, microcontroller programming are described in detail. In Section 6.4 we will show the physical realization of the circuit and the user interface. Finally, some measurements related to H_2O_2 detection will be acquired with the developed system and shown in Section 6.5.

6.1 General considerations on the potentiostat

The potentiostat is the electronic instrument used in electrochemistry. Its main task lies in controlling the voltage difference between reference and working electrodes by sinking or furnishing electrons from or into an electrochemical cell through the counter electrode. Precise control of the applied potential is not generally possible with a two-electrode system, since the electrolyte has some resistance, which generates a potential drop across the solution when current flows through the cell. Moreover, the reference electrode becomes slightly polarized when current flows through it, causing some changes in the interfacial potential between the working and the reference electrode. Thus, since this potential cannot be precisely controlled by a two-electrode configuration, it is necessary to use a three-electrode system. The potential of the working electrode is controlled relatively to the reference electrode, while the current flows into the electrochemical cell by the counter electrode.

6.1.1 Architectural state-of-the-art

Different approaches can be exploited for the design of the voltage generator and the current detector. Regarding the application of the potential, it can be controlled in three configurations: *grounded working electrode* (GWE), *grounded reference electrode* (GRE), and *grounded counter electrode* (GCE). In the GWE configuration, the desired voltage (E_i) is applied to the positive input of an operational amplifier, called control amplifier, whereas the negative input is connected to the reference electrode. The output of the amplifier is then connected to the counter. The amplifier controls the current passing through the cell, such that the cell potential is kept at the desired voltage. A schematic of the grounded working electrode is depicted in Fig. 6.1a. The input bias current of the operational amplifier can affect the potential of the reference electrode, unless it is really small (in the range of pA or even less) and the input resistance of the operational amplifier is very high (in the range of GΩ). Usually another operational amplifier is connected at the reference, acting as voltage buffer, to minimize current flowing

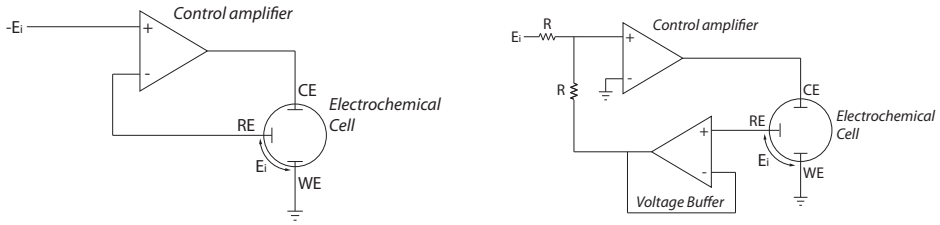

(a) Grounded working electrode configuration by using a single control amplifier.

(b) Grounded working electrode configuration by using a control amplifier and a voltage follower.

Figure 6.1: Schematic of two possible grounded working configurations. Reprinted from [163].

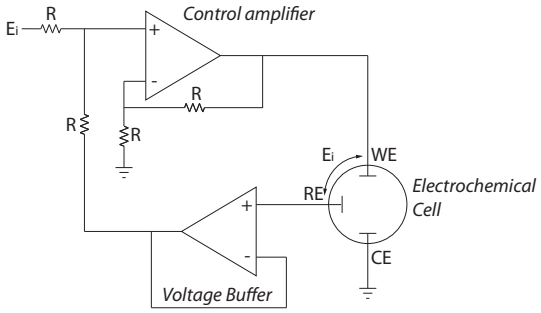

Figure 6.2: Schematic of a possible grounded counter configuration. Reprinted from [163].

in the reference electrode (refer to Fig. 6.1b). Working and reference electrodes can be also swapped, while maintaining all the other components unchanged (GRE configuration).
In the GCE configuration, two operational amplifiers are used to set the voltage between working and reference electrodes. The control amplifier is directly connected to the WE, configured as a summing amplifier. A voltage follower is instead connected to the RE. The output potential of the summing amplifier is added to the RE potential, so that the desired voltage can be applied between the WE and the RE. The voltage follower connected to the reference avoids current flowing through it. A schematic of this configuration is illustrated in Fig. 6.2.
Regarding the readout circuit, many strategies have been presented as well [163]. The most straightforward approach is to insert a resistor in the current path of the counter electrode and measure the voltage drop across the resistor. Thus, the voltage drop can be measured with an instrumentation amplifier. This configuration is less sensitive to noise and has better stability with respect to other configurations. However, it needs more components and suffers more from mismatches. Alternatively, current mirrors can be directly connected to the output of the electrochemical cell to “copy” the cell current into another branch, not to affect the current to

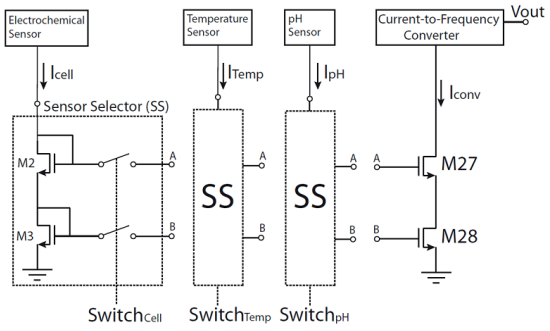

Figure 6.3: Current mirror used to multiplex signals from different sensors. Reprinted from [163].

be measured. They are often used downstream to a current-to-frequency converter [200] and when it is necessary to multiplex different signals into the same output reading [201]. Current mirrors with two *Metal-Oxide-semiconductor Field-Effect Transistors* (MOSFETs) per branch can be used to enhance the accuracy of current reading. An example of current mirrors used for molecular biosensing is reported in Fig. 6.3. Every sensor generates a current in its own mirror branch, while the branch connected to the current-to-frequency converter is common. A series of MOS switches, controlled by external output, multiplexes the signals coming from different sensors. In more complicated realizations, the current can be injected directly into a current-input A/D converter [202] or it can be converted to time [203]. Nevertheless, the use of transimpedance amplifier is by far the most common approach. In this case, the current flows through a resistor (R_M) placed between the output and the negative input of an operational amplifier, while the positive input is grounded (refer to Fig. 6.4). Ideally, no current is absorbed by the input pin of the operational amplifier and the counter is directly grounded, due to the virtual short-circuit at the inputs of the operational amplifier. However, this approach requires high values of resistance to measure low currents. Alternatively, high value resistors can be replaced by capacitors. Thus, the output voltage is proportional to the current charging the capacitors. According to these reasons, we choose to base our potentiostat on GCE configuration for the potential control and on the transimpedance amplifier configuration for the current detector.

6.1.2 Design issues for integrated biosensor realization

The scaling of semiconductor logic circuits decreases the feature size of the electronic devices, but also the oxide and junction breakdown voltages, requiring lower supply voltages for these processes. However, scaling the supply voltage may limit the range of chemical analysis, especially for general purpose potentiostats. Indeed, the drive voltages are defined by the reduction/oxidation potentials of the investigated analytes and some compounds, such as highly oxidizing radicals [204], are undetectable using a supply voltage (V_{dd}) of 1.8 V, which

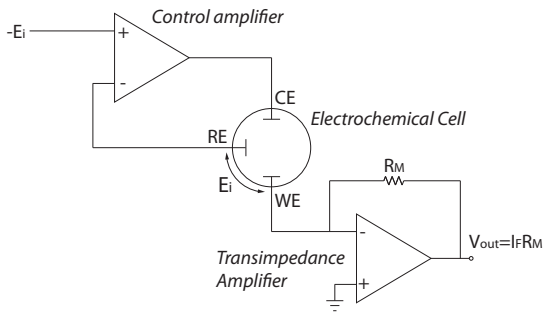

Figure 6.4: Current measurement using a transimpedance amplifier. Reprinted from [163].

is the standard for recent CMOS technologies, because they have higher standard potentials. Moreover, depending on the analyte to detect, the output voltage of the sensor current may work both with positive and negative voltages, which limits the working potential to $V_{dd}/2$ in the case of single-supply voltage circuits. Fully-differential potentiostat was developed by Martin *et al.* [198] to overcome this issue, based on the dynamic change of the working and the reference electrode potentials. In this way, the output swing potential can be doubled and the dynamic range is increased.
Another issue to take into account when designing integrated circuits is the direction of the current in the electrochemical cell. Especially for cyclic voltammetry, the direction of current and voltage do not necessarily match. Indeed, the direction of the current depends not only on the polarity of the applied voltage, but also on the sign of its derivative. A positive applied voltage can result in a negative current, if the voltage is decreasing in time. Likewise, an increasing negative voltage can result in a positive current. Consequently, several circuits and switches are needed to handle different voltage and current directions, which make the interface complicated, more noisy and power consuming. Smart designs are needed to integrate all different permutations of voltage-current in a single circuit.
Finally, the integration of very large resistors (> 1 MΩ) are difficult to implement in integrated circuit form. Thus, readout solutions involving large resistors to amplify very low currents with instrumentation amplifier are not possible. Moreover, also large capacitance values (> 100 pF) are difficult to realize, so transimpedance amplifiers should be realized with parallel switched capacitors. Our approach has been developed trying to take into account all these issues. The proposed solution is conceived with off-the-shelf components, but the design is also suitable for a further implementation in integrated circuit form. Indeed, previous works have already showed the integration of similar architectures implemented in 0.18 μm CMOS technology [205], [206].

6.2 System requirements

As already discussed in Section 2.4.1, hydrogen peroxide is an electrochemical species that can be optimally detected when a potential of 650 mV drops between working and reference elec-

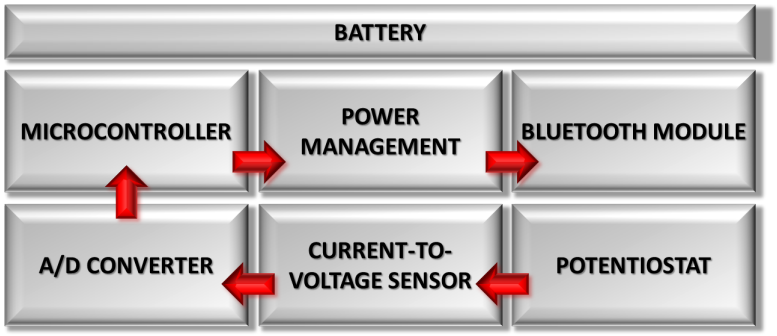

Figure 6.5: General building block diagram for a biosensor-based platform.

trodes. The current generated by the redox reaction strongly depends on the electron transfer efficiency of the transducer and on the area of the working electrode. The microfabricated electrodes have an area of 0.2 mm^2 and CNT structuring for each working electrode. Both these features affect the current intensity in the electrochemical cell. From measurements performed by the commercial potentiostat and reported in Section 5.5.1, we infer that the expected range of current goes from 1 nA up to around 100 nA in a first approximation. Due to such small ranges, we use a transimpedance amplifier based on switched capacitors. The current flowing through the cell charges the capacitors and the generated output voltage is proportional to the input current. Once the measurement is performed, the capacitors can be discharged by closing the switch, resetting the system for the successive measurement. For different current ranges, it is possible to switch *on* or *off* different capacitors in parallel to adjust the range of detectable currents.
Then, the analog voltage needs to be converted to digital, prior to be acquired by an *analog-to-digital converter* (ADC) with appropriate accuracy and transmitted to the remote station. Metabolic changes in cell cultures can be sampled slowly in the order of some Hz for the single continuous measurement, while each electrode can be sequentially activated every 10 minutes to detect one metabolite at the time.
The microcontroller coordinates all the blocks of the system, receiving and transmitting signals from/to the other blocks. The user can select a specific metabolite from the remote station or run a bench of sequential measurements scanning all the working electrodes. Indeed, the microcontroller can drive a multiplexer to select the proper WE. Once digitized, the current value is sent via the Bluetooth module. Bluetooth is chosen to simplify the communication between the system and the remote station, i.e. a laptop. Moreover, class-2 Bluetooth protocol can ensure a communication range up to 15 meters, compatible with the typical dimensions of a standard biological laboratory. Finally, the power management block supplies the voltages required by the other blocks. A schematic of the described building blocks is illustrated in Fig. 6.5.

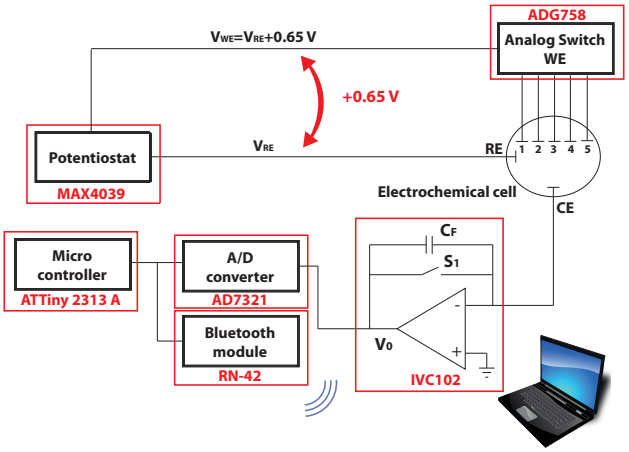

Figure 6.6: A schematic of the architecture conceived for the electrochemical measurements of metabolites in cell culture monitoring. The different blocks are detailed with the components used in our implementation.

6.3 Architectural solution

Based on the requirements discussed in the previous section, we now analyze the main building blocks of the system. The most important parts from the architectural point-of-view are definitely the potential control, the current-to-voltage converter, and the microcontroller. In the following section we will explain the architectural solution and the choice of the components. A schematic of the architecture presented in the following paragraphs is depicted in Fig. 6.6.

6.3.1 Potential control

For the potential control we adopted the grounded counter configuration. The potentiostat consists of two MAX4039 (Maxim). Each MAX4039 includes two operational amplifiers and has a buffered reference of 1.232 V. A zoom of the potential control is depicted in Fig. 6.7. The chosen ICs consume 800 nA of supply current per amplifier and have low input bias current (typically lower than 1 pA) to avoid reference polarization. The input offset voltage is generally below 200 μV. Referring to Fig. 6.6, amplifier O_1 acts as a voltage buffer to read the voltage at the reference electrode (V_{RE}) without polarizing it. Amplifier O_2 is configured as a control amplifier and it fixes the voltage of the working electrode (V_{WE}) to the value (V_{RE} + 0.65 V). Thus, a constant voltage of 0.65 V is set between the working and the reference electrodes. The rate between R_1 and R_2 is chosen so that at the output is set the desired voltage. It is possible to tune the output voltage of the control amplifier up to 1.232 V by changing the rate between the two resistors, in the case of different detected compounds.

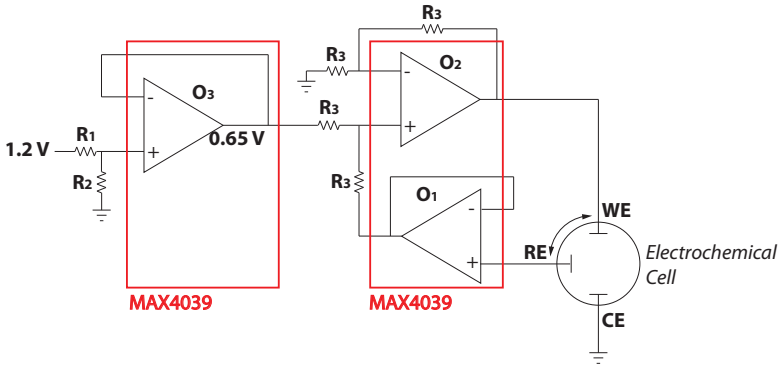

Figure 6.7: Schematic of the potential control, which is based on a grounded counter configuration.

6.3.2 Current-to-voltage sensor

The current generated in the electrochemical cell is read on the counter electrode by means of a current-to-voltage converter IVC102 (Burr-Brown). Current-to-voltage converters can use either feedback resistors (R_F) or feedback capacitors (C_F). When a feedback resistor is used, the sensor gain is directly determined by the value of R_F. This approach is not practical to sense low current values, requiring extremely high feedback resistance. This issue can be overcome by using a capacitance as feedback element. Indeed, the cell current is used to charge the capacitor C_F, while the switch S_1 is kept open (refer to Fig. 6.6). If the switch is opened at time t=0, the voltage difference ΔV_O across the capacitor between time t=t_1 and time t=t_2 is proportional to the charging current I:

$$I = -\frac{\Delta V_O C_F}{T_{INT}} , \tag{6.1}$$

where the integration time to charge the capacitor is T_{INT}=t_2-t_1. In Fig. 6.8 signals ΔV_O and S_1 are shown during a measurement. High gain can be achieved by using small capacitance values C_F and long integration time T_{INT}. In this design, C_F is chosen equal to 100 pF and T_{INT} is chosen equal to 8 ms (t_1 = 1 ms, t_2 = 9 ms). Thus, since the maximum output of the converter is $V_{SAT} = -9V$, the voltage ramp across the capacitor saturates at t_2 = 9 ms for a maximum current I_{MAX} equal to

$$I_{MAX} = -\frac{V_{SAT} C_F}{t_2} = 100nA . \tag{6.2}$$

The output voltage V_O of the current-to-voltage converter is digitized by a 12-bit plus sign serial ADC (AD7321 from Analog Devices). The input range is set to ± 10 V. By using that

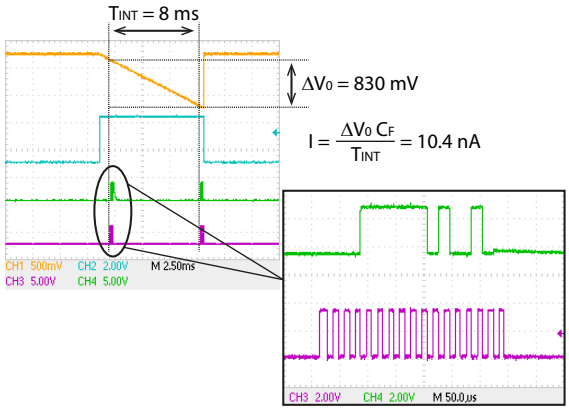

Figure 6.8: Clock signal of the ADC (SCLK) and the output of the ADC.

configuration, the *Least Significant Bit* (LSB) is equal to 2.441 mV.
The output voltage ΔV_O of the current-to-voltage converter is digitized by a 12-bit plus sign serial ADC (AD7321 from Analog Devices). The input range is set to ± 10 V. By using that configuration, the LSB is equal to 2.441 mV. The output voltage of the transimpedance amplifier is digitized by the analog-to-digital converter.

6.3.3 Microcontroller

A microcontroller is used to set the analog switch, drive the current-to-voltage converter, and read the ADC. We have chosen a low-power CMOS 8-bit microcontroller (ATTiny 2313A by Atmel) with 2 KBytes flash memory, 128 Bytes internal SRAM and EEPROM. The communication between the microcontroller and the user is achieved via Bluetooth module emulating the serial protocol RS232. The microcontroller communicates via Bluetooth with the LabVIEW interface, so that the user can set the parameters of the measurement, such as the working electrode, the integration time T_{INT} of the current-to-voltage converter, the sample rate, and the ADC input range. For every sample, the output of the ADC is read by the microcontroller and displayed at the remote station. Data are not stored in the internal memory of the microcontroller.
The flowchart of the microcontroller code is reported in Fig. 6.9. When powered, the microcontroller initializes the registers and the I/O ports; then, it waits for a request of measurement from the user. An interrupt is generated at microcontroller level when the user starts a new measurement; the parameters of the measurement are set by the microcontroller, according to the user request. Then, the current-to-voltage converter starts to acquire data from the electrochemical cell. Output values read by the ADC are immediately sent to the remote station via Bluetooth. The measurement goes on until the user stops the experiment. Afterwards, the microcontroller returns from the interrupt to the initial loop, waiting for a new measurement.

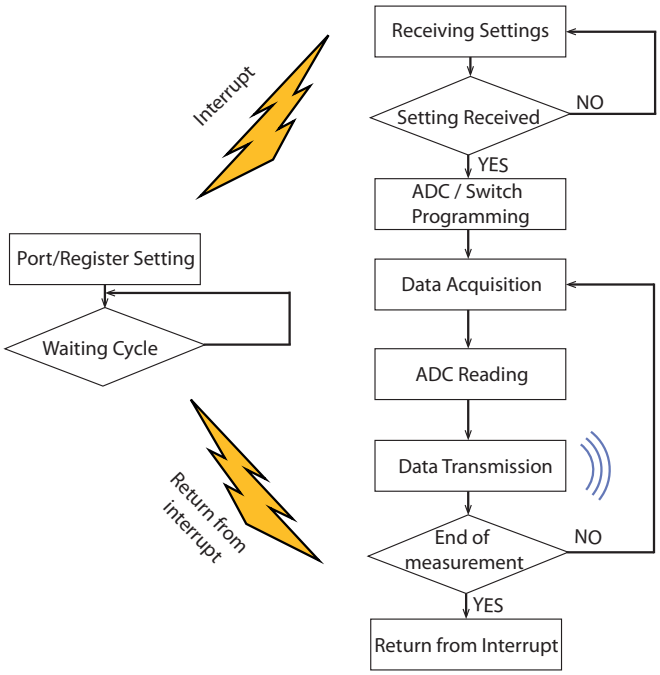

Figure 6.9: Flow chart of the microcontroller code.

6.3.4 Other components

The analog switch ADG758 (by Analog Devices) selects the physical electrode of the cell to be connected to V_{WE}. That switch has low ON resistance (typically 3 Ω) and low leakage current (100 pA). The Bluetooth module is an RN-42 by Roving Network with on board chip antenna, UART connection interface, 240 Kbps (slave mode) or 300 Kbps (master mode) of data rate, and a power consumption of 26 μA in sleep mode, 3 mA in connection mode, and 30 mA in transmission mode. Power supply is generated by using a single 9 V battery. Most components need stable voltage supply of different values. Several voltage values are generated on board for the different circuits: 3.3 V and 5 V by LP38693ADJ, +10 V by LMC7660IM, and -10 V by LM2662M.

6.4 Physical implementation

Once we have identified the commercial components with proper characteristics for our purposes (input and output voltages, bias currents, low-power consumption), we designed the PCB layout to host the ICs. This section will describe the physical layout on the PBC and the interface developed to remotely control the circuit.

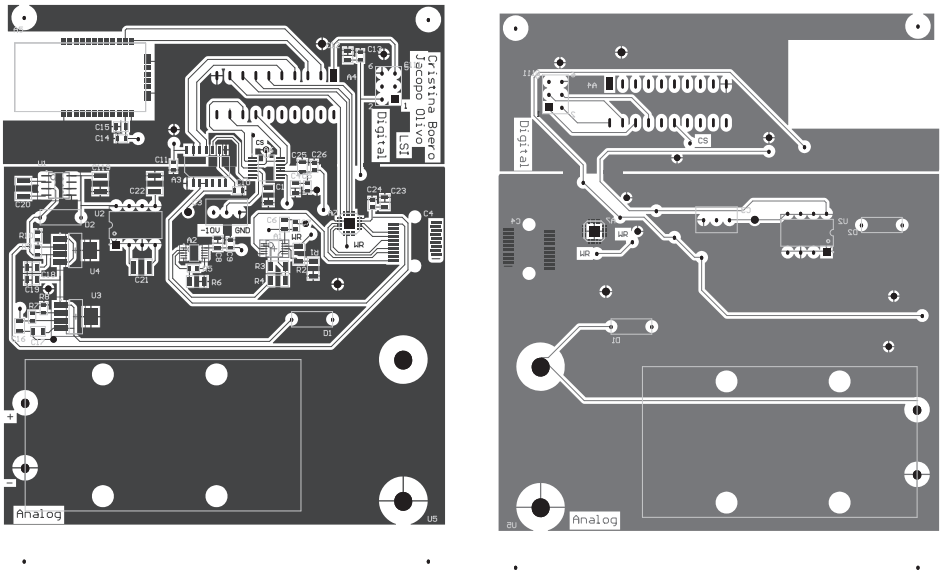

(a) PCB top layer.

(b) PCB bottom layer.

Figure 6.10: PCB layout.

6.4.1 Layout

The layout of the potentiostat is designed by using Altium Designer, an electronic design software for *Printed Circuit Board* (PCB) and *Field-Programmable Gate Array* (FPGA). The image of the developed layout is showed in Fig. 6.10. The PCB is conceived with a top and a bottom layer to facilitate the routing among the different components. This prototype hosts two power supply connections to give the possibility to both powering the PCB with an external supply or with a battery. The footprint for a battery holder is also included in the layout. The developed circuit involves both analog and digital signals, so it is important to prevent any interference between high-speed digital logic and low-level analog circuits. Thereby, digital ground currents should not flow in the analog section of the ground plane. Thus, a correct organization of the ground plane and a careful component placement are critical to an efficient layout. We decided to partition the PCB into a digital and an analog section and to place accordingly the different components. Analog signals have to be routed only in the analog section of the board, while digital signals in the digital section. Under these conditions the digital return currents will not flow in the analog section of the ground plane, but it will remain under the digital signal trace. Some of the components dealing with both analog and digital signals, instead, can then be positioned to straddle the partition, like the voltage-to-current sensor and the analog-to-digital converter. They are placed in the middle of the two planes, with analog pads on the analog side and digital pads on the digital side. The analog and digital planes are just connected together at one location, thus forming a bridge. Thus, the traces regarding mixed signals can cross at this bridge the two sides of the board. By routing all the traces in this way, the current return path is directly beneath each of the traces, thereby producing a small loop area.

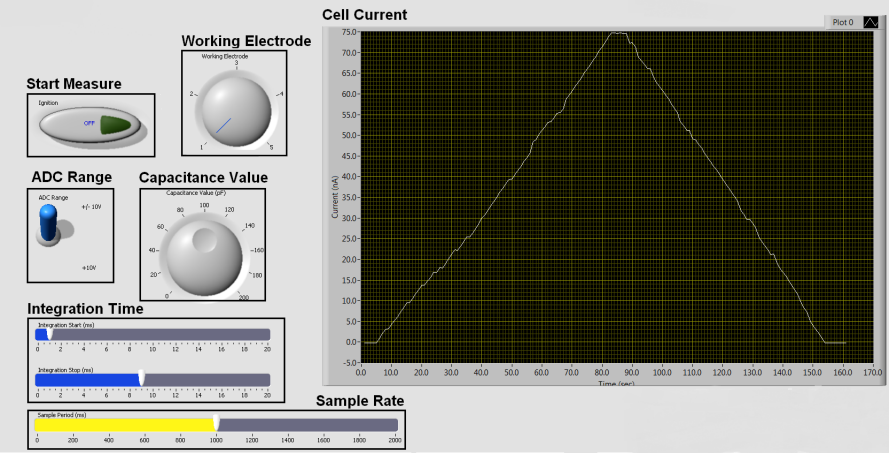

Figure 6.11: Labview interface to control the electronic circuit form a remote station.

6.4.2 LabVIEW interface

A user-friendly LabVIEW interface is designed to communicate with the microcontroller and plot the received data. A screen-shot of the interface is shown in Fig. 6.11. The user can directly set the parameters of the measurement from the main panel. At the end of the measurement, the cell current is directly plotted on the screen. Data collected from the measurement can be post-processed directly with LabVIEW or be exported and stored in other formats (such as a spreadsheet).

6.5 Measurements with the developed architecture

We initially test our potentiostat for the detection of H_2O_2, which is the by product of any chemical reaction based on oxidases. Then, we calibrate one of the microfabricated working electrodes for the detection of glucose. These two measurements have the purpose to demonstrate that our potentiostat is able to detect the current range involved in the metabolic monitoring.

6.5.1 H_2O_2 detection

We started testing our potentiostat for the detection of H_2O_2 with the microfabricated electrodes and we performed a comparison with analogous measurements acquired with the commercial potentiostat (Autolab by Metrohm). For all measurements the integrated platform is hosted in an in-house chip holder and connected to the peristaltic pump. The flow is adjusted at 13 μl/min and the measurement starts with PBS flowing through the camber. The signal recorded for PBS is considered as the baseline, so the successive values of currents are referred to the baseline value. Once the measurement is run, we change the solution at the inlet of the fluidic system every 3 minutes. For measurements with the commercial

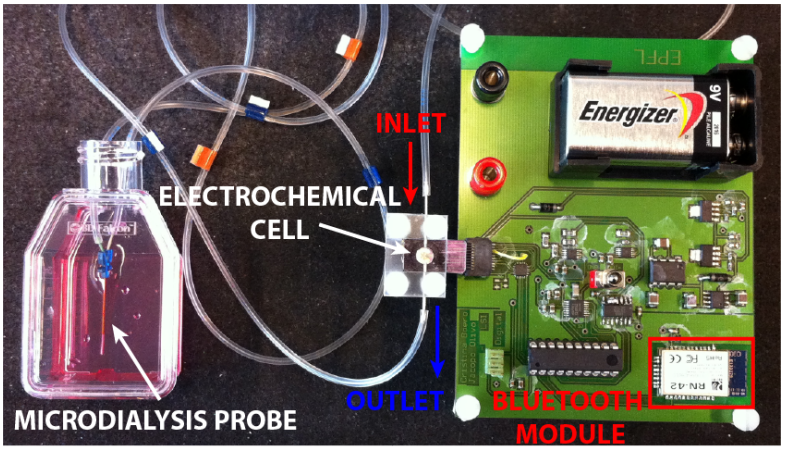

Figure 6.12: The developed potentiostat realized with off-the-shelf components. The potentiostat is connected to the biosensor, while the fluidic system enable the sampling in the medium.

potentiostat, a knob attached to a proper connector allows us to mechanically switch among the different working electrodes. In this case the platform is connected to the instrument through cables for working, counter, and reference electrodes. Such configuration is not suitable for the application of the system in cell culture monitoring. For this reason our circuit communicates with the remote laptop via Bluetooth, enabling measurements inside the flask and close to the incubator. An image of the experimental apparatus is shown in Fig. 6.12. The integrated platform is fixed in the in-house chip holder and connected to our potentiostat. The microdialysis probe is immersed in the culture medium and connected to the inlet of the PDMS chamber. The solution exits from the outlet channel and is then wasted away by the peristaltic pumps.

We acquire different concentrations of hydrogen peroxide (40, 80, 100, 150, and 200 μM) on one bare working electrode with both the commercial potentiostat and our circuit. The two recorded signals are superimposed and depicted in Fig. 6.13a. Even thought raw data show statistical fluctuations, after a moving average filtering the result compares well with the typical staircase of chronoamperometry and the signal recorded by the commercial potentiostat. Our potentiostat is able to follow the successive injections of more concentrated H_2O_2 and the current rise is proportional to concentration increase (for example between 100 and 150 μM current increases more than between 80 and 100 μM). Moreover, it fully meets the range of response without any saturation effect. Currents span from 1 nA up to about 65 nA and our circuit perfectly acquires the entire signal.

We also repeat the same measurements in the case of CNT-structured electrodes. The calibration curves obtained by the two instruments are depicted in Fig. 6.13b. Also in the case of CNT-based sensors, our circuit shows the typical staircase graph and records signals up to 80 μM. As in the previous case, to higher concentrations of hydrogen peroxide correspond higher currents and the stair amplitude is more marked for 150 and 200 μM.

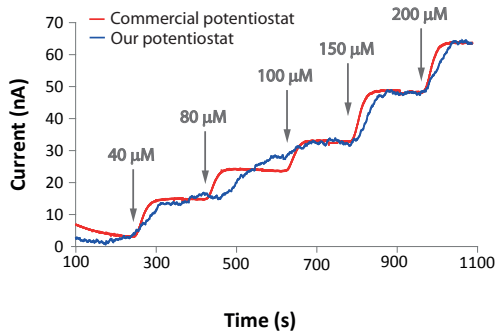

(a) Superimposed chronoamperometries acquired with the commercial potentiostat and our developed wireless system.

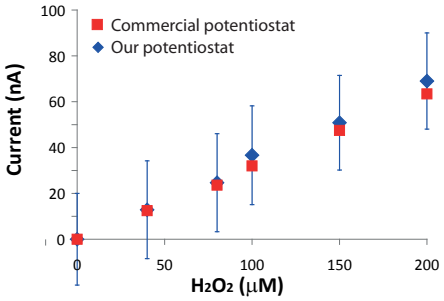

(b) Calibration lines for H_2O_2 detection measured with the developed circuit and a commercial potentiostat.

Figure 6.13: Detection of hydrogen peroxide (from 40 to 200 μ) on bare working electrode with both commercial potentiostat and our circuit.

6.5.2 Glucose detection with our potentiostat

Based on the results obtained for hydrogen peroxide detection, we also test our potentiostat with functionalized electrodes. As an example, Fig. 6.14 illustrates the calibration line in PBS for glucose biosensor acquired with our potentiostat. The inset shows the raw data of the real-time measurement. The acquired measurement is quite noisy, so post-processing filtering is required to extract data for the calibration (red line superimposed to raw data in the inset of Fig. **??**). However, our architecture is able to follow the increase of glucose concentration and the current perfectly fits the input range of the transimpedance amplifier without any saturation effect.

6.6 Chapter contributions and summary

The development of automated and portable instruments is crucial for the optimization and scale-up of bioprocesses. On the other hand , bulky and expensive machines can limit their use in daily laboratory life. Therefore, the integration of biosensors with electrical data acquisition chains and information systems opens new opportunities for cell analysis. In particular, integrated biosensors are key elements for portable and minimal invasive devices for metabolite monitoring, thus enabling possibly remote bioprocess controls. Most of the literature about biosensors is focused on the biochemical aspects of the sensor, while the development of the interface electronics is ignored. The circuit has to be carefully design and adapted for the used electrochemical techniques. The powerful and challenging approach to achieve these goals is the integration of the biosensor and the circuitry into a single chip.
In this chapter we were focused on the development of the architecture for amperometric measurements in cell cultures. Architectural design had to take into account some particular requirements due to the features of the integrated platform developed in Chapter 4, such as

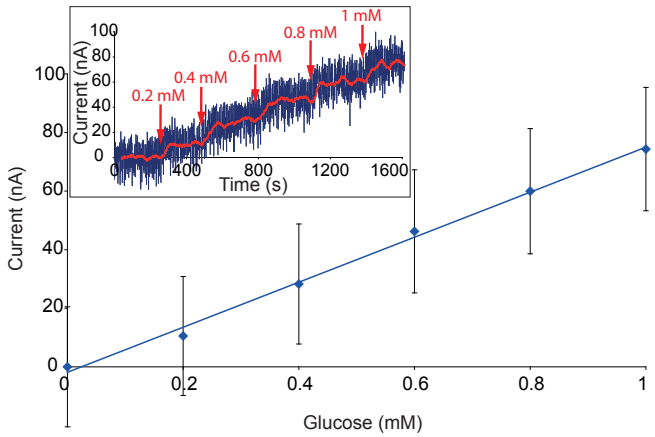

Figure 6.14: Calibration line for glucose in PBS in the range from 0 to 1 mM measured with our potentiostat. Inset: raw data of the real-time measurement. The red line is an average filtering of the raw data.

low-level noise and minimal invasivity. For this reason, we first discussed possible architectures that have been developed in literature and we chose the most suitable for our particular application, according to results obtained in 5. We also detailed system requirements, such as the applied potential, the expected current range, the sampling rate, and the management of multiple metabolite detection. Then, we proposed our architectural solution and we described the physical realization on a printed circuit board. We also conceived a user friendly interface to communicate with the device and to plot the measurement in a remote station. Finally, we showed a comparison of analogous measurements acquired with our architecture and with a commercial potentiostat. The comparison demonstrates that our system is able to follow current changes and the input range is suitable for recording currents generated in the electrochemical cell.

7 Conclusions and Future Work

This dissertation introduces new approaches for the development of amperometric biosensors to be dedicated to the monitoring of metabolites in biotechnology. Electrochemical detection of compounds has been extremely popular in the last two decades and a large number of commercial devices are based on enzyme-based biosensors. Monitoring systems have been developed for a wide range of applications and diverse strategies have been presented and tested for their development.
The novelties of our research work lie in the use of existing technologies and materials in an original manner towards the development of a non-invasive platform for the metabolic monitoring of cell cultures. In particular, a system developed for the detection of multiple compounds in cell culture media have never been presented before. Devices developed for these purposes and available in the market are often bulky and support the detection of a single metabolite. Moreover, we achieved the enhancement of biosensor performance and the robust immobilization of the enzymes by using carbon nanotubes. Previous researches have shown that these nanomaterials own excellent properties of electron transfer and they facilitate the exchange of electrons between the active site of the enzyme and the electrode surface. However, CNT handling often demands complicated and expensive instrumentation. We proposed a novel and systematic use of an existing technology, such as the ultra-low volume spotting for DNA and protein dispensing, for the drop cast of carbon nanotubes and the immobilization of different enzymes onto microfabricated electrodes.
In the following section, a summary of every chapter of the thesis is given. Then, improvements for the developed system and future work are also discussed.

7.1 Thesis summary and contributions

This thesis was organized as follows.

In **Chapter 2** we outlined the main biosensing strategies for the detection of biological analytes and physicochemical parameters in bioprocess monitoring. We proposed an essential classification according to the three main blocks characterizing a biosensor: the analyte, the sensing

element, and the transduction mechanism. We reported examples presented in literature for these three categories of biosensors. *Ex situ* and *in situ* measurements were also presented and the different strategies for their realization were discussed. We have also introduced some nanomaterials that have been recently used to successfully develop biosensors of new generation, with a particular focus on carbon nanotubes. We briefly discussed on the state-of-the-art of electrochemical biosensors, which are those used for our research. We explained the main principles of the measurement and the two electrochemical techniques typically used for amperometric biosensors. We particularly focused on carbon nanotube-based biosensors for the detection of glucose, lactate, and glutamate.

In **Chapter 3** we focused more on carbon nanotubes, detailing their physical, chemical, electrical, and electrocatalytic features. We discussed their excellent electron transfer properties and the fact that they are suitable for biosensing also because they are in the same scale as biological recognition elements. Especially metallic carbon nanotubes exhibit attractive properties suitable to be used as material for the development of electrochemical biosensors. We reported several strategies proposed in literature for the immobilization of carbon nanotubes onto the electrode surface and the development of CNT-based biosensors. We debated the field emission properties of sidewall and tips. We also showed the results from some simulation about their possible spatial arrangement when randomly drop cast on smooth surfaces and the total electron emission due to their random dispersion. We finally discussed the interaction between carbon nanotubes and proteins in redox reactions. Carbon nanotubes enhance the electron transfer between the active site of the enzyme and the electrode surface, allowing the development of non-mediated biosensors.

In **Chapter 4** we described the development of the self-contained platform in three main steps. The first step involved the microfabrication of the chip onto silicon substrate. Photolithography, thin film deposition and etching are the main processing steps used for the manufacturing of the integrated electrochemical cell. The second step concerned the structuring of the working electrodes with carbon nanotubes and the selective functionalization of the electrodes with different enzymes. To achieve this goal we exploited a spotting system developed for the automatic dispensing and printing of biological samples. We adapted system parameters to be able to dispense a solution of carbon nanotubes with high accuracy onto our working electrodes. We finally developed the apparatus for the continuous monitoring of cell culture. A PDMS chamber and channels were molded and fixed together with the platform in an in-house chip holder to have a continuous flow of solution in contact with the electrodes. A microdialysis probe was instead put in contact with the culture media to allow metabolite measurements, while reducing the invasivity and the sampling volume.

In **Chapter 5** we showed the main results obtained during all the research. Preliminary experiments were carried out on commercial graphite electrodes to test the efficacy of carbon

nanotubes in the detection of hydrogen peroxide. We also investigated the functionalization of such sensors with glucose and lactate oxidase and we acquired SEM images to verify the enzyme immobilization. *Off-line* detection of glucose and lactate in diluted media was performed in a cholinergic cell line and metabolic pathways were acquired in different experimental conditions. Afterwards, we characterized the microfabricated electrodes and we calibrated them for the detection of glucose, lactate, and glutamate in both PBS solution and cell culture media. We optimized also the fluidic system for the *on-line* detection of metabolites. We finally tested the system in a neural cell line for the detection of glucose and lactate over the cell culture time.

In **Chapter 6** we focused on the design of a suitable architecture to perform electrochemical measurements with our biosensors. We analyzed system requirements according to the particular application these biosensors are developed for. We debated the general building blocks required to perform amperometric measurements and we discussed the constrains related to our particular application. We described the architectural solution we adopted and the physical realization of the prototype. We also conceived a LabVIEW interface to allow the user to control the device from a remote station and to follow in real-time the trend of the metabolite levels. Finally, we showed some measurements acquired with our circuit and we compared them with those recorded by a commercial potentiostat. The comparison demonstrates that our system is able to follow current changes and the input range is suitable for recording currents generated in our electrochemical cell.

7.2 Future work

The system has been tested and validated and the results are promising for further work and experiments to perform. However, some improvements can be still implemented to enhance the portability and the performance of the system.
Regarding the microfabricated electrochemical cell, it has been conceived with five working electrodes. We have optimized the detection of glucose and lactate both in PBS solution and cell culture media, while glutamate has been just detected in PBS. As already discussed, glutamate is a neurotransmitter and can be interesting to sense in neural cell cultures. However, it is also involved in the detection of glutamine, which is a fundamental energy source for cells, and its monitoring can be crucial to describe the metabolic behavior of particular cell lines. The current design of the electrochemical cell allows us to host two other functionalizations. The synergic detection of glutamate and glutamine ca be achieved by functionalizing two of the available working electrodes with glutamine and glutamate oxidases. Cellular stress due to oxidative phenomena, such as free radicals that can damage the components of the cell, can be instead revealed by the monitoring of hydrogen peroxide, either with its direct reduction on CNT-based electrodes or by means of functionalized electrodes with peroxidase. Depending on the cell line to monitor, it is possible to envisage other metabolites particularly interesting to follow. The integrated platform may be enhanced with pH and temperature

sensors to also monitor the physicochemical parameters of the cell culture. The sensors can be microfabricated by thin film technologies directly on the platform and their readout can be electronically implemented and integrated with the rest of the developed circuit.
The electronic part can be also improved both at hardware and software levels. The readout circuit, and specifically the transimpedance amplifier, can be further optimized. More experiments will allow us to choose proper values of capacitance and integration time to accurately detect currents generated by the redox reactions. Noise can be also reduced by signal post-processing at software level, by considering that the signal of interest changes slowly and the noise contributes at more high frequencies. Moreover, the architecture chosen for the electronic circuit is suitable for a future integration, lending to further system miniaturization. Integration and miniaturization are two important issues for self-contained devices. To this purpose, the use of a peristaltic pump like the one we used for our experiment is not convenient. For instance, commercial miniaturized peristaltic pumps are available on the market and can be used in our case. Instead of moving the fluid mechanically, it is possible to envisage other smart and innovative solutions. Electro-osmotic pumps, for example, can move a fluid by applying an electric field. They can be fabricated by MEMS technologies and controlled by a simple electronic circuit.
Finally, further validation experiments can be carried out with the developed system. We may consider to monitor other cell lines and studying their metabolic behavior under particular conditions, as in the case of SN56 cell line under glucose deprivation conditions. The monitoring of stem cell metabolism at different cell states may be crucial to understand and model biological mechanisms involved in their proliferation and differentiation states.

Bibliography

[1] M.A. Selak, S.M. Armour, E.D. MacKenzie, H. Boulahbel, D.G. Watson, K.D. Mansfield, Y. Pan, M.C. Simon, C.B. Thompson, and E. Gottlieb. Succinate links tca cycle dysfunction to oncogenesis by inhibiting hif-α prolyl hydroxylase. *Cancer cell*, 7:77 – 85, 2005.

[2] G.D. Dakubo, R.L. Parr, L.C. Costello, R.B. Franklin, and R.E. Thayer. Altered metabolism and mitochondrial genome in prostate cancer. *Journal of Clinical Pathology*, 59:10 – 16, 2006.

[3] C. Boero, S. Carrara, G. Del Vecchio, L. Calzà, and G. De Micheli. Targeting of multiple metabolites in neural cells monitored by using protein-based carbon nanotubes. *Sensors and Actuators B*, 157:216 – 224, 2011.

[4] L. Pellerin and P.J. Magistretti. Glutamate uptake into astrocytes stinulates aerobic glycolysis: a mechanism coupling neuronal activity to glucose utilization. *PNAS*, 91:10625 – 10629, 1994.

[5] L. Zhu, G. Del Vecchio, G. De Micheli, Y. Liu, S. Carrara, L. Calzà, and C. Nardini. Biochips for regenerative medicine: real-time stem cell continuous monitoring as inferred by high-throughput gene analysis. *Bionanoscience*, 1:183 – 191, 2011.

[6] T. Stoll, P. Pugeaud, U. von Stockar, and I.W. Marison. A simple hplc technique for accurate monitoring of mammalian cell metabolism. *Cytotechnology*, 14:123 – 128, 1994.

[7] S.A. Arnold, J. Crowley, N. Woods, L.M. Harvey, and B. McNeil. *In situ* infrared spectroscopy to monitor key analytes in mammalian cell cultivation. *Biotechnology and Bioengineering*, 84:13 – 19, 2003.

[8] M. Rhiel, P. Ducommun, I. Bolzonella, I. Marison, and U. von Stockar. Real-time *in situ* monitoring of freely suspended and immobilized cell cultures based on mid-infrared spectroscopic measurements. *Biotechnology and Bioengineering*, 77:174 – 185, 2001.

[9] K.B. Male, J.H.T. Luong, R. Tom, and S. Mercille. Novel fia amperometric biosensor system for the determination of glutamine in cell culture systems. *Enzyme and Microbial Tehcnology*, 15:26 – 32, 1993.

[10] R. Renneberg, G. Trott-Kriegeskorte, M. Lietz, V. Jäger, M. Pawlowa, G. Kaiser, U. Wollenberger, F. Schubert, R. Wagner, R.D. Schmid, and F.W. Scheller. Enzyme sensor-fia-system for on-line monitoring of glucose, lactate, and glutamine in animal cell cultures. *Journal of Biotechnology*, 21:173 – 186, 1991.

[11] R.W. Min, V. Rajendran, N. Larsson, L. Gorton, J. Planas, and B. Hahn-Hägerdal. Simultaneous monitoring of glucose and l-lactic acid during a fermentation process in an aqueous two-phase system by on-line fia with microdialysis sampling and dual biosensor detection. *Analytica Chimica Acta*, 366:127 – 135, 1998.

[12] A. Weltin, J. Kieninger, G. Urban, I. Moser, G. Jobst, M. Wego, and R. Ehret. A novel multiparametric microphysiometry system for dynamic cell culture monitoring. In *Proceedings of IEEE Sensors Conference*, 2010.

[13] N.P. Rodrigues, Y. Sakai, and T. Fujii. Cell-based microfluidic biochip for the electrochemical real-time monitoring of glucose and oxygen. *Sensors and Actuators B*, 132:608 – 613, 2008.

[14] R.C. Nayak and I.M. Herman. Measurement of glucose consumption by hybridoma cells growing in hollow fiber cartridge bioreactors: use of blood glucose self-monitoring devices. *Journal of Immunological Methods*, 205:109 – 114, 1997.

[15] O. Frey, S. Talaei, P.D. van der Wal, M. Koudelka-Heo, and N.F. de Rooij. Continuous-flow multi-analyte biosensor cartridge with controllable linear response range. *Lab on Chip*, 10:2226 – 2234, 2010.

[16] K. Aravindalochanan, J. Kieninger, G.A. Urban, and G. Jobst. Simulation and design of a nitric oxide sensor array for cell cultures. *Proceedings of the IEEE Sensors Conference*, pages 325 – 328, 2009.

[17] M. Hämmerle, W. Schuhmann, and H.L. Schmidt. Amperometric polypyrrole enzyme electrodes: effect of permeability and enzyme location. *Sensors and Actuators B*, 6:106 – 112, 1992.

[18] G. Wang, J.J. Xu, H.Y. Chen, and Z.H. Lu. Amperometric hydrogen peroxide biosensor with sol-gel/chitosan network-like film as immobilization matrix. *Biosensors and Bioelectronics*, 18:335 – 343, 2003.

[19] V.K. Gade, D.J. Shirale, P.D. Gaikwad, P.A. Savale, K.P. Kakde, H.J. Kharat, and M.D. Shirsat. Immobilization of god on electrochemically synthesized ppy-pvs composite film by cross-linking via glutaraldehyde for determination of glucose. *Reactive and Functional Polymers*, 66:1420 – 1426, 2006.

[20] F. Ricci and G. Palleschi. Sensor and biosensor prepration, optimisation and applications of prussian blue modified electrodes. *Biosensors and Bioelectronics*, 21:389 – 407, 2005.

[21] T. Laaksonen, P. Ahonen, K. Kontturi, and L. Murtomäki. Charge transfer at an electrified liquid/liquid interface immobilised in fibre. *Journal of Electroanalytical Chemistry*, 575:75 – 80, 2005.

[22] V. Bavastrello, S. Carrara, M.K. Ram, and C. Nicolini. Optical and electrochemical properties of poly(o-toluidine) multiwalled carbon nanotubes composite langmuir-schaefer films. *Langmuir*, 20:969 – 973, 2004.

[23] V. Bavastrello, E. Stura, S. Carrara, V. Erokhin, and C. Nicolini. Poly(2,5-dimethyllaniline)-mwcnts nanocomposite: a new material for conductiometric acid vapours sensor. *Sensors and Actuators B*, 98:247 – 253, 2004.

[24] P.J. Britto, K.S.V. Santhanam, and P.M. Ajayan. Carbon nanotube electrode for oxidation of dopamine. *Bioelectrochemistry and Bioenergetics*, 41:121 – 125, 1996.

[25] J. Wang, M. Musameh, and Y. Lin. Solubilization of carbon nanotubes by nafion toward the preparation of amperometric biosensors. *Journal of the American Chemical Society*, 125(9):2408 – 2409, 2003.

[26] B. Sonnleitner. *Advances in Biochemical Engineering/Biotechnology, Vol. 66*. Springer-Verlag, 1999.

[27] M. Bäcker, L. Delle, A. Poghossian, M. Biselli, W. Zang, P. Wagner, and M.J. Schöning. Electrochemical sensor array for bioprocess monitoring. *Electrochimica Acta*, 56:9673 – 9678, 2011.

[28] G.A. Rivas et al. Carbon nanotubes for electrochemical biosensing. *Talanta*, 74(3):291 – 307, 2007.

[29] K. Balasubramanian and M. Burghard. Biosensors based on carbon nanotubes. *Analytical and Bioanalytical Chemistry*, 385:452 – 468, 2006.

[30] C. Stagni et al. (cmos dna) sensor array with integrated (a/d) conversion based on label-free capacitance measurement. *IEEE Journal of Solid-State Circuits*, 41:2956 – 2965, 2006.

[31] M. Schienle et al. A fully electronic (dna) sensor with 128 positions and in-pixel (a/d) conversion. *IEEE Journal of Solid-State Circuits*, 39:2438 – 2445, 2004.

[32] D.A. Gough, L.S. Kumosa, T.L. Routh, J.T. Lin, and J.Y. Lucisano. Function of an implanted tissue glucose sensor for more than 1 year in animals. *Nature Translational Medicine*, 2:42ra53, 2010.

[33] Y.C. Tsai et al. Fabrication process of integrated multi-analyte biochip system for implantable application. In *IEEE 22nd International Conference on Micro Electro Mechanical Systems*, 2009.

[34] A.R.A. Rahman et al. Fabrication and packaging of a dual sensing electrochemical biotransducer for glucose and lactate useful in intramuscular physiologic status monitoring. *IEEE Sensors Journal*, 9:1856 – 1863, 2009.

[35] A. Guiseppi-Elie et al. Design of a subcutaneous implantable biochip for monitoring of glucose and lactate. *IEEE Sensors Journal*, 5:345 – 355, 2005.

[36] F. Valgimigli et al. Evaluating the clinical accuracy of glucomen®day: a novel microdialysis-based continuous glucose monitoring. *Journal of Diabetes Science Technology*, 4:1182 – 1192, 2010.

[37] D.R. Thevenot et al. Electrochemical biosensors: recommended definitions and classification. Technical report, IUPAC, 1999.

[38] I. Moser, G. Jobst, and G.A. Urban. Biosensor arrays for simultaneous measurement of glucose, lactate, glutamate, and glutamine. *Biosensors and Bioelectronics*, 17:297 – 302, 2002.

[39] J.L. Romette and C.L. Cooney. L-glutamine enzyme electrode for on-line mammalian cell culture process control. *Analytical Letters*, 20:1069 – 1081, 1987.

[40] V. Vojinović, J.M.S. Cabral, and L.P. Fonseca. Real-time bioprocess monitoring. part i: In situ sensors. *Sensors and Actuators B*, 114:1083 – 1091, 2006.

[41] U. Bilitewski. *Comprehensive Analytical Chemistry*. Elsevier B.V., 2005.

[42] P. Sarkar, I.E. Tothill, S.J. Setford, and A.P.F. Turner. Screen-printed amperometric biosensors for the rapid measurement of l- and d- amino acids. *Analyst*, 124:865 – 870, 1999.

[43] R. M. Lequin. Enzyme immunoassay (eia)/enzyme-linked immunosorbent assay (elisa). *Clinical Chemistry*, 51(12):2415–2418, 2005.

[44] G. Marrazza, I. Chianella, and M. Mascini. Disposable dna electrochemical sensor for hybridization detection. *Biosensors and Bioelectronics*, 14:43 – 51, 1999.

[45] J. Wang. Towards genoelectronics: electrochemical biosensing of dna hybridization. *Chemistry - A European Journal*, 5:1681 – 1685, 1999.

[46] S. Marose, C. Lindemann, R. Ulber, and T. Scheper. Optical sensor systems for bioprocess monitoring. *Trends in Biotechnology*, 17:30 – 34, 1999.

[47] M.H. Rhiel, M.B. Cohen, M.A. Arnold, and D.W. Murhammer. On-line monitoring of human prostate cancer cells in a perfusion rotating wall vessel by near-infrared spectroscopy. *Biotechnology and Bioengineering*, 86:852 – 861, 2004.

[48] L. Brecker, H. Weber, H. Griengl, and D.W. Ribbons. In situ proton-nmr analyses of escherichia coli hb101 fermentations in h_2o and in d_2o. *Microbiology*, 145:3389 – 3397, 1999.

[49] L. Bernondini, S. Generelli, T. Kraus, O.T. Guenat, S. Koster, V. Linder, M. Koudelka-Hep, and N.F. de Rooij. Microfabricated platforms for the study of neuronal and cellular networks. *Journal of Physiscs: Conference Series*, 34:1 – 6, 2006.

[50] J.B. Christen and A.G. Andreou. Design, fabrication, and testing of a hybrid cmos/pdms microsystem for cell culture and incubation. *IEEE Transactions on Biomedical Circuits and Systems*, 1:3 – 18, 2007.

[51] P. Yáñez Sedeño and J.M. Pingarrón. Electrochemical sensing based on carbon nanotubes. *Trends in Analytical Chemistry*, 29:939 – 953, 2010.

[52] L. Lorenzelli, B. Margesin, S. Martinoia, M.T. Tedesco, and M. Valle. Bioelectrochemical signal monitoring of in-vitro cultured cells by means of an automated mycrosystem based on solid state sensor-array. *Biosensors and Bioelectronics*, 18:621 – 626, 2003.

[53] L.Jr. Clark and C. Lyons. Electrode systems for continuous monitoring in cardiovascular surgery. *Annals of the New York Academy of Science*, 102:29 – 45, 1962.

[54] M. Lehmann, W. Baumann, M. Brischwein, H.J. Gahle, I. Freund, R. Ehret, S. Drechsler, H. Palzer, M. Kleintges, U. Sieben, and B. Wolf. Simultaneous measurement of cellular respiration and acidification with a single cmos isfet. *Biosensors and Bioelectronics*, 16:195 – 203, 2001.

[55] J.S. Guez, J.P. Cassar, F. Wartelle, P. Dhulster, and H. Suhr. Real time in situ microscopy for animal cell-concentration monitoring during high density culture in bioreactor. *Journal of Biotechnology*, 111:335 – 343, 2004.

[56] I. Giaever and C.R. Keese. A morphological biosensor for mammalian cells. *Nature*, 366:591 – 592, 1993.

[57] S. Hauttmann and J. Müller. In-situ characterisation by impedance spectroscopy using a full-bridge circuit. *Bioprocess and Biosystems Engineering*, 24:137 – 141, 2001.

[58] U. von Stockar, P. Duboc, L. Menoud, and I.W. Marison. On-line calorimetry as a technique for process monitoring and control in biotechnology. *Thermochimica Acta*, 300:225 – 236, 1997.

[59] B.A.A. Dremel, S.Y. Li, and R.D. Schmid. On-line determination of glucose and lactate concentrations in animal cell culture based on fibre optic detection of oxygen in flow-injection analysis. *Biosensors and Bioelectronics*, 7:133 – 139, 1992.

[60] S. Benthin, J. Nielsen, and J. Villadsen. Flow-injection analysis of micromolar concentrations of glucose and lactate in fermentation media. *Analytica Chimica Acta*, 261:145 – 153, 1992.

[61] A. Hemmi, K. Yagiuda, N. Funazaki, S. Ito, Y. Asano, T. Imato, K. Hayashi, and I. Karube. Development of a chemiluminescence detector with photodiode detection for flow-injection analysis and its application to l-lactate analysis. *Analytica Chimica Acta*, 316:323 – 327, 1995.

[62] K.B. Male, P.O. Gartu, A.A. Kamen, and J.H.T. Luong. On-line monitoring of glucose in mammalian cell culture using a flow injection analysis (fia) mediated biosensor. *Biotechnology and Bioengineering*, 55:497 – 504, 2000.

[63] U. Bilitewski, W. Drewes, J. Neermann, J. Schrader, R. Surkow, R.D. Schmid, and J. Bradley. Comparison of differentbiosensor systems suitable for bioprocess monitoring. *Journal of Biotechnology*, 31:257, 1993.

[64] N. Torto, T. Laurell, L. Gorton, and G. Marko-Varga. Recent trends in the application of microdialysis in bioprocess. *Analytica Chimica Acta*, 374:111 – 135, 1998.

[65] N. Torto and L. Gorton. Technical issues of in vitro microdialysis sampling in bioprocess monitoring. *Trends in Analytical Chemistry*, 18:252 – 260, 1999.

[66] T. Hatfield and J.L. Spanis, C. McGaugh. Response of amygdalar norepinephrine to footshock and gabaergic drugs using in vivo microdialysis and hlpc. *Brain research*, 835:340 – 345, 1999.

[67] C. Liu, Q. Wu, A.C. Harms, and R.D. Smith. On-line microdialysis sample cleanup for electrospray ionization mass spectroscopy of nucleic acid samples. *Analytical Chemistry*, 68:3295 – 3299, 1996.

[68] I. Rohm, M. Genrich, W. Collier, and U. Bilitewski. Development of ultraviolet-polymerizable enzyme pastes: bioprocess applications of screen-printed l-lactate sensors. *Analyst*, 121:877 – 881, 1996.

[69] F.F. Zhang, C.X. Wan, Q. Li, X.L. Wang, Z.Q. Zhu, Y.Z. Xian, L.T. Jin, and K. Yamamoto. Simultaneous assay of glucose, lactate, l-glutamate and hypoxanthine levels in a rat striatum using enzyme electrodes based on neutral red-doped silica nanoparticles. *Microchimica Acta*, 121:31 – 40, 1995.

[70] Y.C. Tsai, S.C. Li, and J.M. Chen. Cast thin film biosensor design based on a nafion backbone, a multiwalled carbon nanotube conduit, and a glucose oxidase function. *Langmuir*, 21(8):3653–3658, 2005.

[71] J.J. Gooding. Nanostructuring electrodes with carbon nanotubes: A review on electrochemistry and applications for sensing. *Electrochimica Acta*, 50:3049 – 3060, 2005.

[72] J.J. Gooding, R. Wibowo, J. Liu, W. Yang, D. Losic, S. Orbons, F.J. Mearns, J.G. Shapter, and D.B. Hibbert. Protein electrochemistry using aligned carbon nanorube arrays. *Journal of the American Chemical Society*, 125:9006 – 9007, 2003.

[73] A. Mayer, N.M. Miskovsky, and P.H. Cutler. Theoretical comparison between field emission from single-wall and multi-wall carbon nanotubes. *Physics Review B*, 65:155420, 2002.

[74] T. Asefa, C.T. Duncan, and K.K. Sharma. Recent advances in nanostructured chemosensors and biosensors. *Analyst*, 134(10):1980–1990, 2009.

[75] J. Wang. Nanomaterial-based electrochemical biosensors. *Analyst*, 130:421 – 426, 2005.

[76] B. Pérez-López and A. Merkoçi. Nanoparticles for the development of improved (bio)sensing systems. *Analytical and Bioanalytical Chemistry*, 399:1577–1590, 2011.

[77] Q. Ma and X. Su. Recent advances and applications in qds-based sensors. *Analyst*, 136(23):4883–4893, 2011.

[78] N.S. Ramgir, Y. Yang, and M. Zacharias. Nanowire-based sensors. *Small*, 6(16):1705–1722, 2010.

[79] C. Li, M. Curreli, H. Lin, B. Lei, F.N. Ishikawa, R. Datar, R.J. Cote, M.E. Thmpson, and C. Zhou. Complementary detection of prostate-specific antigen using in_2o_3 nanowires and carbon nanotubes. *Journal of the American Chemical Society*, 127:12484 – 12485, 2005.

[80] H.J. Li, W.G. Lu, J.J. Li, X.D. Bai, and C.Z. Gu. Multichannel ballistic transport in multiwall carbon nanotubes. *Physical Review Letters*, 95:086601, 2005.

[81] C. Cai and J. Chen. Direct electron transfer of glucose oxidase promoted by carbon nanotubes. *Analytical Biochemistry*, 332:75–83, 2004.

[82] D. McClain et al. Effect of diameter on electron field emission of carbon nanotube bundles. In *Materials Research Society Symposium Proceedings*, volume 901E, 2006.

[83] AK. Wanekaya, W. Chen, N.V. Myung, and A. Mulchandani. Nanowire-based electrochemical biosensors. *Electroanalysis*, 18(6):533–550, 2006.

[84] J. Wang. Electrochemical glucose biosensors. *Chemical Reviews*, 108:814 – 825, 2008.

[85] M.M. Rahman, A. Umar, and K. Sawada. Development of amperometric glucose biosensor based on glucose oxidase co-immobilized with multi-walled carbon nanotubes at low potential. *Sensors and Actuators B*, 137:327 – 333, 2009.

[86] X. Kang, Z. Mai, X. Zou, P. Cai, and J. Mo. A novel glucose biosensor based on immobilization of glucose oxidase in chitosan on a glassy carbon electrode modified with gold-platinum alloy nanoparticles/multiwalled carbon nanotubes. *Analytical Biochemistry*, 369:71 – 79, 2007.

[87] G.D. Withey, A.D. Lazareck, M.B. Tzolov, A. Yin, P. Aich, J.J. Yeh, and J.M. Xu. Ultra-high enzyme signal transduction using highly ordered carbon nanotube array electrodes. *Biosensors and Bioelectronics*, 21:1560 – 1565, 2006.

[88] B.Y. Wu, S.H. Hou, F. Yin, Z.X. Zhao, Y.Y. Wang, X.S. Wang, and Q. Chen. Amperometric glucose biosensor based on multilayer films via layer-by-layer self-assembly of multi-wall carbon nanotubes, gold nanoparticles and glucose oxidase on the pt electrode. *Biosensors and Bioelectronics*, 22:2854 – 2860, 2007.

[89] A. Kausaite-Minkstimiene, V. Mazeiko, A. Ramanaviciene, and A. Ramanavicius. Evaluation of amperometric glucose biosensors based on glucose oxidase encapsulated within enzymatically synthesized polianiline and polypirrole. *Sensors and Actuators B*, 158:278 – 285, 2011.

[90] J. Ryu, H. Kim, S. Lee, H.T. Hahn, and D. Lashmore. Carbon nanotube mat as mediator-less glucose sensor. *Journal of Nanoscience and Nanotechnology*, 10:941 – 947, 2010.

[91] M.Y. Hua, Y.C. Lin, R.Y. Tsai, and C.C. Hsiao. Water dispersible 1-one-butyric acid-functionalised multi-walled carbon nanotubes for enzyme immobilisation and glucose sensing. *Journal of Materials Chemistry*, 22:2566 – 2574, 2012.

[92] M.D. Rubianes and G.A. Rivas. Enzymatic biosensors based on carbon nanotubes paste electrodes. *Electroanalysis*, 17(1):73–78, 2005.

[93] J. Huang et al. A highly-sensitive l-lactate biosensor based on sol-gel film combined with multi-walled carbon nanotubes (mwcnts) modified electrode. *Materials Science and Engineering C*, 27(1):29 – 34, 2007.

[94] J.M. Goran, J.L. Lyon, and K.J. Stevenson. Amperometric detection of l-lactate using nitrogen-doped carbon nanotubes modified with lactate oxidase. *Analytical Chemistry*, 83(21):8123–8129, 2011.

[95] Y.C. Tsai, S.Y. Chen, and H.W. Liaw. Immobilization of lactate dehydrogenase within multiwalled carbon nanotube-chitosan nanocomposite for application to lactate biosensors. *Sensors and Actuators B*, 125:474 – 481, 2007.

[96] H. Teymourian, A. Salimi, and R. Hallaj. Low potential detection of nadh based on fe_3o_4 nanoparticles/multiwalled carbon nanotubes composite: fabrication of integrated dehydrogenase-based lactate biosensor. *Biosensors and Bioelectronics*, 33:60 – 68, 2012.

[97] S. Pan and M.A. Arnold. Selectivity enhancement for glutamate with a nafion/glutamate oxidase biosensor. *Talanta*, 43(7):1157 – 1162, 1996.

[98] M. Zhang, C. Mullens, and W. Gorski. Amperometric glutamate biosensor based on chitosan enzyme film. *Electrochimica Acta*, 51:4528 – 4532, 2006.

[99] M. Ammam and J. Fransaer. Highly sensitive and selective glutamate microbiosensor based on cast polyurethane/ac-electrophoresis deposited multiwalled carbon nanotubes and then glutamate oxidase/electrosynthesized polypyrrole/pt electrode. *Biosensors and Bioelectronics*, 25(7):1597 – 1602, 2010.

[100] S. Iijima. Helical microtubules of graphitic carbon. *Nature*, 354(6348):56–58, 1991.

[101] Walt A. de Heer, A. Chatelain, and D. Ugarte. A carbon nanotube field-emission electron source. *Science*, 270(5239):pp. 1179–1180, 1995.

[102] H. Dai, J.H. Hafner, A.G. Rinzler, D.T. Colbert, and R.E. Smalley. Nanotubes as nanoprobes in scanning probe microscopy. *Nature*, 384(6605):147–150, 1996.

[103] M.H. Al-Saleh and U. Sundararaj. Review of the mechanical properties of carbon nanofiber/polymer composites. *Composites Part A: Applied Science and Manufacturing*, 42(12):2126 – 2142, 2011.

[104] S.J. Tans, A.R.M. Verschueren, and C. Dekker. Room-temperature transistor based on a single carbon nanotube. *Nature*, 393:49 – 52, 1998.

[105] A. Bachtold, P. Hadley, T. Nakanishi, and C. Dekker. Logic circuits with carbon nanotube transistors. *Science*, 294:1317 – 1320, 2001.

[106] V. Derycke, R. Martel, J. Appenzeller, and Ph. Avouris. Carbon nanotube inter- and intramolecular logic gates. *Nano Letters*, 1(9):453–456, 2001.

[107] H.W. Kroto, J.R. Heath, S.C. OḂrien, R.F. Curl, and R.E. Smalley. C_{60}: Buckminsterfullerene. *Nature*, 318:162, 1985.

[108] R. Krupke, F. Hennrich, H. von Löhneysen, and M.M. Kappes. Separation of metallic from semiconducting single-walled carbon nanotubes. *Science*, 301:344 – 347, 2003.

[109] D. Chattopadhyay, I. Galeska, and F. Papadimitrakopoulos. Route for bulk separation of semiconducting from metallic single-walled carbon nanotubes. *Journal of the American Chemical Society*, 125:3370 – 3375, 2003.

[110] K. Gong, Y. Yan, M. Zhang, L. Su, S. Xiong, and L. Mao. Electrochemistry and electroanalytical applications of carbon nanotubes: a review. *Analytical Sciences*, 21:1383 – 1393, 2005.

[111] Bharat Bhushan, editor. *Handbook of Nanotechnology*. Springer Berlin / Heidelberg, 2004.

[112] H.S.P. Wong and D. Akinwande. *Carbon nanotube and graphene device physics*. Cambridge University Press, 2011.

[113] H. Dai. Carbon nanotubes: synthesis, integration, and properties. *Accounts of Chemical Research*, 35:1035 – 1044, 2002.

[114] C. Crane, M. Wilson, and K. Kannangara. *Nanotechnology: basic science and emerging technologies*. 2002.

[115] A. Loiseau, P. Launois, P. Petit, S. Roche, and J.P. Salvetat. *Understanding carbon nanotubes. From basics to applications*. 2006.

[116] S.D. Bethune, C.H. Kiang, M.S. de Vries, G. Gorman, R. Savoy, J. Vazquez, and R. Beyers. Cobalt-catalysed growth of carbon nanotubes with single-atomic-layer walls. *Nature*, 363:605 – 607, 1993.

[117] S.B. Sinnot, R. Andrews, D. Qian, A.M. Rao, Z. Mao, E.C. Dickey, and F. Derbyshire. Model of carbon nanotube growth through chemical vapor deposition. *Chemical Physics Letters*, 315:25 – 30, 1999.

[118] A. Chou, T. Böcking, N.K. Singh, and J.J. Gooding. Demonstration of the importance of oxygenated species at the ends of carbon nanotubes for their favourable electrochemical properties. *Chemical communications*, pages 842 – 844, 2005.

[119] J. Chen, M.A. Hamon, H. Hu, Y. Chen, A.M. Rao, P.C. Eklund, and R.C. Haddon. Solution properties of single-walled carbon nanotubes. *Science*, 282:95 – 98, 1998.

[120] S. Niyogi, M.A. Hamon, H. Hu, B. Zhao, P. Bhowmik, R. Sen, M.E. Itkis, and R.C. Haddon. Chemistry of single-walled carbon nanotubes. *Accounts of Chemical Research*, 35:1105 – 1113, 2002.

[121] T. Ando. The electronic properties of graphene and carbon nanotubes. *NPG Asia Materials*, 1:17 – 21, 2009.

[122] J.M. Bonard, H. Kind, T. Stöckli, and L.O. Nilsson. Field emission from carbon nanotubes: the first five years. *Solid-State Electronics*, 45:893 – 914, 2001.

[123] D.M. Guldi and Martín. *Carbon nanotubes and related structures*. 2010.

[124] R. Saito, G. Dresselhaus, and M.S. Dresselhaus. *Physical properties of carbon nanotubes*. 1999.

[125] J. Li, A. Cassell, L. Delzeit, J. Han, and M. Meyyappan. Novel three-dimensional electrodes: electrochemical properties of carbon nanotube ensembles. *The Journal of Physical Chemistry B*, 106:9299 – 9305, 2002.

[126] B.R. Azamian, J.J. Davis, K.S. Coleman, C.B. Bagshaw, and M.L.H. Green. Bioelectrochemical single-walled carbon nanotubes. *Journal of the American Chemical Society*, 124:12664, 2002.

[127] I. Taurino, S. Carrara, M. Giorcelli, A. Tagliaferro, and G. De Micheli. Comparing sensitivities of differently oriented multi-walled carbon nanotubes integrated on silicon wafer for electrochemical biosensors. *Sensors and Actuators B*, 160:327 – 333, 2011.

[128] M. Musameh, J. Wang, A. Merkoci, and Y. Lin. Low-potential stable nadh detection at carbon-nanotube-modified glassy carbon electrodes. *Electrochemistry Communications*, 4:743 – 746, 2002.

[129] J. Wang, A.N. Kawde, and M. Musameh. Carbon-nanotube-modifed glassy carbon electrodes for amplified label-free electrochemical detection of dna hybridization. *The Analyst*, 128:912 – 916, 2003.

[130] K. Wu, Y. Sun, and S. Hu. Development of an amperometric indole-3-acetic acid sensor based on carbon nanotubes film coated glassy carbon electrode. *Sensors and Actuators B*, 96:658 – 662, 2003.

[131] J. Zhang and L. Gao. Dispersion of multiwall carbon nanotubes by sodium dodecyl sulfate for preparation of modified electrodes toward detecting hydrogen peroxide. *Materials Letters*, 61:3571 – 3574, 2007.

[132] R.R. Moore, C.E. Banks, and R.G. Compton. Basal plane pyrolytic graphite modified electrodes: comparison of carbon nanotubes and graphite powder as electrocatalysts. *Analytical Chemistry*, 76:2677 – 2682, 2004.

[133] J. Wang, M. Li, Z. Shi, N. Li, and Z. Gu. Direct electrochemistry of cytochrome *c* at a glassy carbon electrode modified with single-wall carbon nanotubes. *Analytical Chemistry*, 74:1993 – 1997, 2002.

[134] C. Boero, S. Carrara, G. Del Vecchio, L. Calzà, and G. De Micheli. Highly sensitive carbon nanotube-based sensing for lactate and glucose monitoring in cell culture. *IEEE Transactions on Nanobioscience*, 10:59 – 66, 2011.

[135] Z. Liu, Z. Shen, T. Zhu, S. Hou, and L. Ying. Organizing single-walled carbon nanotubes on gold using a wet chemical self-assembling technique. *Langmuir*, 16:3569 – 3573, 2000.

[136] F. Valentini, A. Amine, S. Orlanducci, M.L. Terranova, and G. Palleschi. Carbon nanotube purification: prepararion and characterization of carbon nanotube paste electrodes. *Analytical Chemistry*, 75:5413 – 5421, 2003.

[137] J. Wang and M. Musameh. Carbon nanotube screen-printed electrochemical sensors. *Analyst*, 129:1–2, 2004.

[138] M. Gao, L. Dai, and G.G. Wallace. Glucose sensors based on glucose-oxidase-containing polypirrole/aligned carbon nanotube coaxial nanowire electrodes. *Synthetic Metals*, 137:1393 – 1394, 2003.

[139] C. Dhand, S.K. Arya, M. Datta, and B.D. Malhotra. Polyaniline-carbon nanotube composite film for cholesterol biosensor. *Analytical Biochemistry*, 383:194 – 199, 2008.

[140] A. Cavallini, G. De Micheli, and S. Carrara. Comparison of three methods of biocompatible multi-walled carbon nanotubes confinement for the development of implantable amperometric adenosine-5′-triphosphate biosensors. *Sensor Letters*, 9:1838 – 1844, 2011.

[141] C. Deng, J. Chen, Z. Nie, and S. Si. A sensitive and stable biosensor based on the direct electrochemistry of glucose oxidase assembled layer-by-layer at the multiwall carbon nanotube-modified electrode. *Biosensors and Bioelectronics*, 26:213 – 219, 2010.

[142] Y. Wang, X. Wang, B. Wu, Z. Zhao, F. Yin, S. Li, X. Qin, and Q Chen. Dispersion of single walled carbon nanotubes in poly(diallylmethylammonium chloride) for preparation of a glucose biosensor. *Sensors and Actuators B*, 130:809 – 815, 2008.

[143] A. Mayer, N.M. Miskovsky, and P.H. Cutler. Three-dimensional calculation of field electron energy distributions from open hydrogen-saturated and capped metallic (5, 5) carbon nanotubes. *Applied Physics Letters*, 79:3338, 2001.

[144] C. Adessi and M. Devel. Theoretical study of field emission by single-wall carbon nanotubes. *Physical Review B*, 62:13314 – 13317, 2000.

[145] M. Pumera, T. Sasaki, and H. Iwai. Relationship between carbon nanotube structure and electrochemical behavior: heterogeneous electron transfer at electrochemically activated carbon nanotubes. *Chemistry - An Asian Journal*, 3:2046 – 2055, 2008.

[146] Y. Chen, D.T. Shaw, and L. Guo. Field emission of different oriented carbon nanotubes. *Applied Physics Letters*, 76:2469 – 2471, 2000.

[147] L. Qiao, W.T. Zheng, Q.B. Wen, and Q. Jiang. First-principles density-functional investigation of the effect of water on the field emission of carbon nanotubes. *Nanotechnology*, 18:155707, 2007.

[148] D. Moscone, M. Pasini, and M. Mascini. Subcutaneous microdialysis probe coupled with glucose biosensor for *in vivo* continuous monitoring. *Talanta*, 39:1039 – 1044, 1992.

[149] M. Yang, Y. Yang, B. Liu, G. Shen, and R. Yu. Amperometric glucose biosensor based on chitosan with improved selectivity and stability. *Sensors and Actuators B*, 101:269 – 276, 2004.

[150] A. Noorbakhsh, A. Salimi, and E. Sharifi. Fabrication of glucose biosensor based on encapsulation of glucose-oxidase on sol-gel composite at the surface of glassy carbon electrode modified with carbon nanotubes and celestine blue. *Electroanalysis*, 20:1788 – 1797, 2008.

[151] M.M. Musameh, R.T. Kachoosangi, L. Xiao, A. Russell, and R.G. Compton. Ionic liquid-carbon composite glucose biosensor. *Biosensors and Bioelectronics*, 24:87 – 92, 2008.

[152] Y. Liu, Z. Chu, Y. Zhang, and W. Jin. Amperometric glucose biosensor with high sensitivity based on self-assembled prussina blue modified electrode. *Electrochimica Acta*, 54:7490 – 7494, 2009.

[153] K. Habermüller, M. Mosbach, and W. Schuhmann. Electron-transfer mechanisms in amperometric biosensors. *FreseniusJournal of Analytical Chemistry*, 366:560 – 568, 2000.

[154] C. Taylor, G. Kenausis, I. Katakis, and A. Heller. "wiring" of glucose oxidase within a hydrogel made with polyvinyl imidazole complexed with [(os-4,4'-dimethoxy-2,2'-bipyridine) c1]$^{+/2+1}$. *Journal of Electroanalytical Chemistry*, 396:511 – 515, 1995.

[155] C. Danilowicz, E. Corton, F. Battaglini, and E.J. Calvo. An os(byp)$_2$clpych$_2$nhpoly(allylamine) hydrogel mediator for enzyme wiring at electrodes. *Electrochimica Acta*, 43:3525 – 3531, 1998.

[156] W. Schuhmann. Conducting polymer based amperometric enzyme electrodes. *Mikrochimica Acta*, 121, 1995.

[157] R. Ghodssi and P. Lin, editors. *MEMS Materials and Processes Handbook*. Springer Science + Business Media, 2011.

[158] S. Carrara, V. Shumyantseva, A.I. Archakov, and B. Samorí. Screen-printed electrodes based on carbon nanotubes and cytochrome p450scc for highly sensitive cholesterol biosensors. *Biosensors and Bioelectronics*, 24:148 – 150, 2008.

[159] C. Lefrou, P. Fabry, and J.C. Poignet. *Electrochemistry: The Basics, with Examples*. Springer Berlin Heidelberg, 2012.

[160] J.C. Mc Donald and G.M. Whitesides. Poly(dimethylsiloxane) as a material for fabricating microfluidic devices. *Accounts of Chemical Research*, 35:491 – 499, 2002.

[161] A. Poscia, D. Messeri, D. Moscone, F. Ricci, and F. Valgimigli. A novel continuous subcutaneous lactate monitoring system. *Biosensors and Bioelectronics*, 20:2244 – 2250, 2005.

[162] C. Boero, S. Carrara, and G. De Micheli. Sensitivity enhancement by carbon nanotubes: Applications to stem cell cultures monitoring. In *Research in Microelectronics and Electronics, PRIME Conference*, pages 72 –75, 2009.

[163] B. R. Eggins. *Chemical sensors and biosensors*. John Wiley & sons. pp. 125-169.

[164] M. Yang, J. Wang, H. Li, J. Zheng, and N. Wu. A lactate electrochemical biosensor with a titanate nanotubes as direct electron transfer promoter. *Nanotechnology*, 19:075502 (6pp), 2008.

[165] W. Sung and Y Bae. Glucose oxidase, lactate oxidase, and galactose oxidase enzyme electrode based on polypirrole with polyanion/peg/enzyme conjugate dopant. *Sensors and Actuators B*, 114:164 – 169, 2006.

[166] X. Cui, C. Li, J. Zang, and S. Yu. Highly sesnitive lactate biosensor by engineering chitosan/pvi-os/cnt/lod network nanocomposite. *Biosensors and Bioelectronics*, 22:3288 – 3292, 2007.

[167] R. Garjonyte, Y. Yigzaw, R. Meskys, A. Malinauskas, and L. Gorton. Prussina blue- and lactate oxidase-based amperometric biosensor for lactic acid. *Sensors and Actuators B*, 79:33 – 38, 2001.

[168] C. Wisitsoraat, C. Karuwan, K. Wong-ek, D. Phokharatkul, P. Sritongkham, and A. Tuantranont. High sensitivity electrochemical cholesterol sensor utilizing a vertically aligned carbon nanotube electrode with electropolymerized enzyme immobilization. *Sensors*, 9:8658 – 8668, 2009.

[169] E. Al-Jawadi, S. Pöller, R. Haddad, and W. Schuhmann. Nadh oxidation using modified electrodes based on lactate and glucose dehydrogenase entrapped between an electrocatalyst film and redox catalyst-modified polymers. *Microchimica Acta*, 177:405 – 410, 2012.

[170] S.D. Psoma, P.D. van der Wal, O. Frey, and N.F. de Rooij. A novel enzyme entrapment in su-8 microfabricated films for glucose micro-biosensors. *Biosensors and Bioelectronics*, 26:1582 – 1587, 2010.

[171] C. Boero, S. Carrara, and G. De Micheli. Long-term biosensors for metabolite monitoring by using carbon nanotubes. *Sensors & Transducers*, 125:229 – 237, 2011.

[172] H. Tang, J. Chen, S. Yao, L. Nie, G. Deng, and Y. Kuang. Amperometric glucose biosensor based on adsoprtion of glucose oxidase at platinum nanoparticle-modified carbon nanotube electrode. *Analytical Biochemistry*, 331:89 – 97, 2004.

[173] S. Wang, Q. Zhang, R. Wang, and S. Yoon. A novel multi-walled carbon nanotube-based biosensor for glucose detection. *Biomedical and Biophysical Research Communication*, 311:572 – 576, 2003.

[174] E. Crounch, D. Cowell, S. Hoskins, R Pittson, and J. Hart. A novel, disposable, screen-printed amperometric biosensor for glucose in serum fabricated using a water-based carbon ink. *Biosensors and Bioelectronics*, 21:712 – 718, 2005.

[175] G. Wohlfahrt, S. Witt, D. Hendle, D. Schomburg, H.M. Kalisz, and H.J. Hecht. 1.8 and 1.9 a resolution structures of the penicillium amagasakiense and aspergillus niger glucose oxidases as a basis for modelling substrate complexes. *Acta Crystallographica Section D*, 55:969 – 977, 1999.

[176] S.J. Li, Y. Umena, K. Yorita, T. Matsuoka, A. Kita, K. Fukui, and Y. Morimoto. Crystallographic study on the interaction of l-lactate oxidase with pyruvate at 1.9 a resolution. *Biochemical and Biophysical Research Communications*, 358:1002 – 1007, 2007.

[177] H. Lee, D. Hammond, T. Large, and B. Wainer. Immortalized young adult neurons from the septal region: generation and characterization. *Developmental Brain Research*, 52:219 – 228, 1990.

[178] M. Malik, C. Greenwood, J. Blusztajin, and B. Berse. Cholinergic differentiation triggered by blocking cell proliferation and treatment with all-trans-retinoic acid. *Brain Research*, 874:178 – 185, 2000.

[179] Y. Hwang, J. Cho, F. Tay, J. Heng, R. Ho, S. Kazarian, D. Williams, A. Boccaccini, J. Polak, and A. Mantalaris. The use of murine embryonic stem cells, alginate encapsulation, and rotary microgravity bioreactor in bone tissue engineering. *Biomaterials*, 30:499 – 507, 2009.

[180] L. Colom, M. Diaz, D. Beers, A. Neely, W. Xie, and S. Appel. Role of potassium channels in amyloid-induced cell death. *Journal of Neurochemistry*, 70:1925 – 1934, 1998.

[181] A. Pinheiro, R. Gomez, A. Massensini, M. Cordeiro, M. Richardson, M. Romano-Silva, M. Prado, L. Marco, and M. Gomez. Neuroprotective effect on brain injury by neurotoxins from the spider *Phoneutria nigriventer*. *Neurochemistry International*, 49:543 – 547, 2006.

[182] G. Gibson, L. Park, K. Sheu, J. Blass, and N. Calingasan. The [alpha]-ketoglutarate dehydrogenase complex in neurodegeneration. *Neurochemistry International*, 36:97 – 112, 1999.

[183] T. Sawamura, K. Shimizu, M. Nibuya, T. Wazikono, G. Suzuki, T. Tsunoda, Y. Takahashi, and S. Nomura. Effect of paroxetine on a model of post-traumatic stress disorder in rats. *Neuroscience Letters*, 357:37 – 40, 2004.

[184] U. Fass, K. Panickar, D. Personett, D. Bryan, K. Williams, J. Gonzales, K. Sugaya, and M. McKinney. Differential vulnerability of primary cultured cholinergic neurons to nitric oxide excess. *Neuroreport*, 11:931 – 936, 2000.

[185] D. Personett, U. Fass, K. Panickar, and M. McKinney. Retinoic acid-mediated enhancement of the cholinergic/neuronal nitric oxide synthase phenotype of the medial septal sn56 clone. *Journal of Neurochemistry International*, 74:2412 – 2424, 2000.

[186] A. Szutowicz, A. Jankowska, J. Blusztajin, and M. Tomaszewicz. Acetylcholine and acetyl-coa metabolism in differentiating sn56 septal cell line. *Journal of Neuroscience Research*, 57:131 – 136, 1999.

[187] T. Bolwing and B. Quistorff. *In vivo* concentration of lactate in the brain of conscious rats before and during seizures: a new ultra-rapid technique for the freeze-sampling of brain tissue. *Journal of Neurochemistry*, 21:1345 – 1348, 1973.

[188] P. Fox and M. Raichle. Focal physiological uncoupling of cerebral blood flow and oxidative metabolism during somatosensory stimulation in human subjects. *Proceedings of the National Academy of Sciences of the united States of America*, 83:1140 – 1144, 1986.

[189] P. Fox, M. Raichle, M. Mintun, and C. Dence. Nonoxidative glucose consumption during focal physiologic neural activity. *Science*, 241:462 – 464, 1988.

[190] A. Bouzier-Sore, P. Voisin, P. Canioni, P. Magistretti, and L. Pellerin. Lactate is a preferential oxidative energy substrate over glucose for neurons in culture. *Journal of Cerebral Blood Flow & Metabolism*, 23:1298 – 1306, 2003.

[191] C. Berthet, H. Lei, J. Thevenet, R. Gruetter, P. Magistretti, and L. Hirt. Neuroprotective role of lactate after cerebral ischemia. *Journal of Cerebral Blood Flow & Metabolism*, 29:1780 – 1789, 2009.

[192] M. Castro, Beltrán, S. Brauchi, and I. Concha. A metabolic switch in brain: glucose and lactate metabolism modulation by ascorbic acid. *Journal of Neurochemistry*, 110:423 – 440, 2009.

[193] D. Hammond, H. Lee, J. Tonsgard, and B. Wainer. Development and characterization of clonal cell lines derived from septal cholinergic neurons. *Brain Research*, 512:190 – 200, 1990.

[194] G. De Micheli, C. Boero, C. Caj-Rossi, I. Taurino, and S. Carrara. Integrated biosensors for personalized medicine. In *DAC Conference Proceedings*, 2012.

[195] W.A. Klee and M. Nirenberg. A neuroblastoma x glioma hybrid cell line with morphine receptors. *Proceedings of the National Academy of Sciences*, 71:3474 – 3477, 1974.

[196] R.M. Pemberton, J. Xu, R. Pittson, N. Biddle, G.A. Drago, S.K. Jackson, and J.P. Hart. Application of screen-printed microband biosensors to end-point measurements of glucose and cell numbers in hepg2 cell culture. *Analytical Biochemistry*, 385:334 – 341, 2009.

[197] G. Leegsma-Vogt, K. Venema, N. Brouwer, J.B. Gramsbergen, S. Copray, and J. Korf. Quantitative on-line monitoring of cellular glucose and lactate metabolism in vitro with slow perfuzion. *Analytical Chemistry*, 76:5431 – 5435, 2004.

[198] S.M. Martin, F.H. Gebara, T.D. Strong, and R.B. Brown. A low-voltage, chemical sensor interface for systems-on-chip: the fully-differential potentiostat. In *Proceedings of the International Symposium on Circuits and Systems (ISCAS)*, volume 4, pages IV – 892–5 Vol.4, may 2004.

[199] M. Carminati, G. Ferrari, and M. Sampietro. Attofarad resolution potentiostat for electrochemical measurements on nanoscale biomolecular interfacial systems. *Review of Scientific Instruments*, 80:124701, 2009.

[200] D. De Venuto, M.D. Torre, C. Boero, S. Carrara, and G. De Micheli. A novel multi-working electrode potentiostat for electochemical detection of metabolites. *IEEE Sensors Conference*, pages 1572 – 1577, 2010.

[201] S. Carrara, M.D. Torre, A. Cavallini, D. De Venuto, and G. De Micheli. Multiplexing ph and temperature in a molecular biosensor. In *IEEE Biomedical Circuits and Systems Conference (BioCAS)*, pages 146 –149, nov. 2010.

[202] R. Reay, S. Kounaves, and G. Kovacs. An integrated cmos potentiostat for miniaturized electroanalytical instrumentation. *Proceedings of the IEEE International Solid-State Circuits Conference (ISSCC)*, pages 162 – 163, 1994.

[203] H.S. Narula and J.G. Harris. A time-based vlsi potentiostat for ion current measurements. *IEEE Sensors Journal*, 6:239 – 247, 2006.

[204] M. Kirsch and H. De Groot. Nad(p)h, a directly operating antioxidant? *The FASEB Journal*, 15:1569 – 1574, 2001.

[205] S.S. Ghoreishizadeh, S. Carrara, and G. De Micheli. Circuit design for human metabolites biochip. In *IEEE Biomedical Circuits and Systems Conference (BioCAS)*, pages 357 –360, nov. 2011.

[206] S. Carrara, S.S. Ghoreishizadeh, J. Olivo, I. Taurino, C. Baj-Rossi, M.O. Cavallini, de Beeck, C. Dehollain, W. Burleson, F.G. Moussy, A. Guiseppi-Elie, and G. De Micheli. Fully integrated biochip platforms for advanced healthcare. *Sensors*, 12:11013 – 11060, 2012.

Curriculum Vitae

Personal Information

First Name / Surname: Cristina Boero

Address: Avenue des Figuiers, 20
1007 – Lausanne - Switzerland

Telephones: 0041 78 9031778 / 0039 339 1143154

E-mail: cristina.boero@epfl.ch, cristina.boero@gmail.com

Nationality: Italian

Date of birth: 18/03/1983

Work experience

January 2009 – October 2012

PhD candidate - Ecole Polytechnique Fédérale de Lausanne

Design, fabrication, characterization, and validation of multiple amperometric biosensors based on enzymes immobilized onto carbon nanotubes for the on-line and real-time monitoring of different metabolites in cell culture media.

Employer: Prof. Giovanni De Micheli
(EPFL IC ISIM LSI1
INF 341 (Bâtiment INF) - Station 14 - 1015 Lausanne - Switzerland
giovanni.demicheli@epfl.ch)

December 2007 – May 2008

Assistant - Université de Genève and Ecole Polytechnique Fédérale de Lausanne

Design of a wireless implantable device for EEG recording. Development of the circuit concerning the detection of biomedical signals; design of transmitter and receiver for RF communication; microcontroller programming for interfacing the system with a computer.

Employer: Prof. Daniel Bertrand
(Dept of Neuroscience CMU
1, rue Michel Servet - 1211 Geneva 4 - Switzerland
Daniel.Bertrand@medecine.unige.ch)

March 2007 – August 2007

Master project - Ecole Polytechnique Fédérale de Lausanne

Design of a totally implantable device for induction and suppression of epileptic seizures. Analysis of possible approaches for wireless transmission; development of an infrared communication system; microcontroller programming.

Prof. Adrian Ionescu
(EPFL STI IEL LEG2
ELB 335 Bâtiment ELB Station 11 - 1015 Lausanne – Switzerland
adrian.ionescu@epfl.ch)

Education and training

2005 – 2007

Master's degree in Biomedical Engineering

Institute: Politecnico di Torino (Italy)

2002 – 2005

Bachelor's degree in Biomedical Engineering

Institute: Politecnico di Torino (Italy)

Languages	
Italian	Mother tongue
English	Proficient (level C2 of the common European framework)
French	Upper intermediate (level B2 of the common European)

Publications

Journals

- C. Boero, J. Olivo, S. Carrara, G. De Micheli. "A self-contained system with CNTs-based biosensors for cell culture monitoring", accepted in *IEEE Journal on Emerging and Selected Topics in Circuits and Systems.*
- C. Boero, J. Olivo, G. De Micheli, S. Carrara. "New approaches for carbon nanotubes-based biosensors and their application to cell culture monitoring", accepted in *IEEE Transactions on Biomedical Circuits and Systems.*
- C. Boero, S. Carrara, G. Del Vecchio, L. Calzà, G. De Micheli. "Targeting of multiple metabolites in neural cells monitored by using protein-based carbon-nanotubes", *Sensors & Actuators B*, vol. 157, Issue 1, September 2011, pp. 216 – 224.
- C. Boero, S. Carrara, G. Del Vecchio, L. Calzà, G. De Micheli. "Highly sensitive carbon nanotube-based sensing for lactate and glucose monitoring in cell culture", *IEEE Transactions on Nanobioscience*, vol. 10, No. 1, March 2011, pp. 59 – 67.
- C. Boero, S. Carrara, G. De Micheli. "Long-term biosensors for metabolite monitoring by using carbon nanotubes", *Sensors & Transducers Journal*, vol. 125, Issue 2, February 2011, pp. 229 – 237.

Conferences

- G. De Micheli, C. Boero, C. Baj-Rossi, I. Taurino, S. Carrara. "Integrated biosensors for personalized medicine", *DAC*, June 2012, San Francisco CA, USA
- C. Boero, S. Carrara, G. De Micheli. "Carbon nanotubes-based biosensors for metabolite monitoring in cell culture medium", *Biosensors*, May 2012, Cancun, Mexico.
- C. Boero, S. Carrara, G. De Micheli. "New technologies for Nanobiosensing and their applications to real-time monitoring", *BioCAS*, November 2011, San Diego CA, USA.
- S. Carrara, L. Bolomey, C. Boero, A. Cavallini, E. Meurville, G. De Micheli, T. Rezzonico, M. Proietti, F. Grassi. "Single-metabolite bio-nano-sensors and system for remote monitoring in animal models", *IEEE Sensors Conference*, October 2011, Limerick, Ireland.
- G. De Micheli, S.S. Ghoreishizadeh, C. Boero, F. Valgimigli. "An integrated platform for advanced diagnostics", *DATE*, November 2011, Grenoble, France
- D. De Venuto, M.D. Torre, C. Boero, S. Carrara, G. De Micheli. "A novel multi-working electrode potentiostat for electrochemical detection of metabolites", *IEEE Sensors Conference*, November 2010, Waikoloa, Hawaii
- C. Boero, S. Carrara, G. Del Vecchio, G.D. Albini, L. Calzà, G. De Micheli. "Carbon nanotubes-based electrochemical sensing for cell culture monitoring", *IEEE ICME*, July 2010, Gold Coast, Australia
- C. Boero, S. Carrara, G. De Micheli. "Amperometric biosensor with nanostructured electrodes by using multi-walled carbon nanotubes for glucose detection in cell culture medium", *NanoTech*, November 2009, Montreux, Switzerland
- S. Carrara, C. Boero, G. De Micheli. "Quantum dots and wires to improve enzymes-based electrochemical bio-sensing", *Nano-Net*, October 2009, Luzern, Switzerland
- C. Boero, S. Carrara, G. De Micheli. "Sensitivity enhancement by carbon nanotubes: applications to stem cell cultures monitoring", *IEEE PRIME*, July 2009, Cork, Ireland
- C. Boero, S. Carrara, G. De Micheli. "Design and optimization of a lactate amperometric biosensor based on lactate oxidase and multi walled-carbon nanotubes", *NanoTech*, November 2008, Montreux, Switzerland

Publications not related to the thesis

- C. Boero, M. Mazza, A.M. Ionescu, D. Bertrand. "Implantable brain stimulator for epilepsy seizure inhibitor", published in the *Proceedings of Smart System Integration* 2008, ISBN 978-3-8007-3081-0.